1989

Application of impact fragmentation to rock trenching

Hilary Inyang Inyang
Iowa State University

Order Number 8920146

Application of impact fragmentation to rock trenching

Inyang, Hilary Inyang, Ph.D.

Iowa State University, 1989

U·M·I
300 N. Zeeb Rd.
Ann Arbor, MI 48106

Application of impact fragmentation to rock trenching

by

Hilary Inyang Inyang

A Dissertation Submitted to the
Graduate Faculty in Partial Fulfillment of the
Requirements for the Degree of
DOCTOR OF PHILOSOPHY

Department: Civil and Construction Engineering

Co-majors: Geotechnical Engineering
Civil Engineering Materials

Approved:

Signature was redacted for privacy.

In Charge of Major Work

Signature was redacted for privacy.

For the Major Department

Signature was redacted for privacy.

For the Graduate College

Iowa State University
Ames, Iowa
1989

TABLE OF CONTENTS

ACKNOWLEDGEMENT

This work was supported (in part) by the Iowa State Mining and Mineral Resources Research Institute through the U.S. Department of the Interior's Mineral Institutes program administered by the U.S. Bureau of Mines under Allotment Grants G1164119, G1174119, and G1184119. I am grateful to my major professor, Dr. John Pitt, and to my doctoral committee members, Professors R. L. Handy, D. Y. Lee, J. Lemish, and N. Dietrich, for their guidance during this work.

I express my thanks to Mr. Todd Olsen, of Cold Springs Research Establishment, who provided most of the rocks used in this research, to Mr. Giraud of the ERI Machine Shop at Iowa State University, and to Mr. John Abing of the Machine Shop, University of Wisconsin, Platteville. To John Vu, David Robson, and other colleagues at the Spangler Geotechnical Laboratory, I express my thanks.

I acknowledge the support of my parents, Chief and Mrs. I. A. Inyang; of my guardians, Dr. and Mrs. Kermit DeGraffenreidt of New York; of my friends Bumi Salami, Sonie Braih, and Sam Otong; of Dr. Emeh Ekpo at St. Louis; and of my devoted and loving wife, Robin Ann. Above all, I humbly thank God for protecting me and providing me with the ability, luck, and confidence to come this far.

I. INTRODUCTION

A. Problem

Mechanical excavators have applications in tunnel boring, undercutting in mines and excavation of utility trenches in rock. Existing trenching machines apply the action of drag bits across a rock surface. Unfortunately, this mechanism is inadequate for cutting hard, abrasive rocks. Many rocks require greater penetrating and cutting forces than can be exerted by existing machines. Trenching with existing machines in such rocks often results in grinding rather than chip removal. Coupled with increased bit wear rate, this situation often culminates in slow, uneconomic trenching. Thus, there is a need for methods which reduce the required cutting forces for hard, abrasive rocks. This investigation attempts a solution to this problem.

The objectives of this research are as follows:

(a) development of a theory relevant to a more efficient mode of operation for mechanical excavators in hard rock,

(b) simulation of this operational mechanism in the laboratory and experimental verification of the theory,

(c) proposition of a rational design for a trencher in which this new mechanism would be used based on experimental results.

B. Approach and Scope

Hard rocks, despite their high compressive strengths are relatively weak in tension. Their engineering behavior falls within the brittle regime, in which negligible plastic deformation occurs before catastrophic failure. The presence of flaws causes brittleness.

Utility trenches are usually excavated within a few feet of the ground surface, and therefore involve surficial rocks. Surficial rocks contain flaws which may originate from differential expansion of minerals, differential volumetric changes due to erosion unloading, chemical attack by weathering solutions and exsolution of gases. Weak grain boundaries can also be regarded as flaws. The low temperatures and relatively low confining pressures of the surficial environment cause these flaws to remain open. Consequently, a large proportion of rocks existing close to the ground surface exhibit brittle behavior. Depending on the trencher operational mode and scale of excavation, the flaws that are significant to trenching may range in size from a few millimeters (i.e., microcracks) to a few meters (i.e., macrocracks). Some microcracks are too small to aid in trenching but can be brought within a significant size range (i.e., one in which they will aid trenching) by selecting a suitable mode of operation for the trencher.

Impulse loads promote the growth of cracks in rocks. Stress waves of short duration travel through the rock within the vicinity of the impact point and propagate fractures from microflaws. The resistance of hard rocks to drag bit action may be reduced by prefracturing. This is a potentially effective loading mode which may make trenchable a previously untrenchable or marginally trenchable rock.

To incorporate this mode of loading in trenchers requires analyses of the degree of damage at various levels of impulse loads. Choice of a suitable physical behavior model is important. Ideally, the model should relate impact loads to the number, orientations and sizes of the resulting cracks. However, since rocks are composed of various minerals, it should be noted that each mineral in the rock has its own intrinsic properties; individually and collectively, these affect the properties of the rock. Regardless of the size of the rock mass considered, the properties vary from point to point and with direction.

The tiny flaws which are capitalized upon during impulse loading are distributed within most rocks in an unpredictable manner. Classical models assuming isotropy, homogeneity and continuity of materials have limited practical application to this problem. Furthermore, the

randomness of cracks resulting from impulse loads on brittle materials excludes the use of approaches from fracture mechanics, which describe single cracks of particular orientations.

This investigation attempts to develop a theory for percussive impacts based on the law of conservation of energy. The goal was to design, build and use a device that simulates impact action on rocks. Empiricism is incorporated in estimating the required impact energy for permanent rock deformation.

II. LITERATURE REVIEW

A. Previous Improvement Schemes

Research on novel techniques of improving the efficiency of rotary drills assumed importance in the early 1950s. The addition of percussive impacts to the rotary action of drag bits increased drilling rates in hard rocks significantly. For medium hard sandstones, Jahn (1954) reported up to a 320 percent increase in drilling rate subsequent to the addition of percussive impacts to rotary drill bit action. Similar increases in trenching rate and efficiency may be expected with the addition of percussive impact mechanism to available rotary trenchers.

No practical use has been made of drag bit cutting, but the potential for using the effects of chemically active agents to reduce rock strength has been investigated (Street and Wang, 1966). The reduction in strength of solids due to the adsorption of chemical agents is called the `Rebinder effect'. Its effectiveness is promoted by the presence of microflaws in the rock. Engelmann et al. (1987), Westwood (1975) and Appl et al. (1981) suggest that the application of this technique is possible. However, problems with handling chemicals and contamination of excavated fragments could impose limitations in rock trenching.

The use of water jets in drag bit cutting has been investigated by various workers among whom are Styler and Thimons (1987), Dubugnon (1981), Hood (1976), Fowell et al. (1985), Geier and Hood (1987), and Straughn (1985). Their experiments indicate that water jets can be used to weaken rocks.

B. Percussive Drill Energetics

Two methods for applying impact energy on rocks are as follows:

(a) an arrangement where a hammer or a projectile hits a rock surface directly, or

(b) an arrangement in which a hammer or a projectile hits a rod which transfers energy to a bit at the rock surface.

In determining impact energy, impact stress and proportion of impact energy transferred to rock, method (a) is more amenable to straightforward treatment and experimental rebound measurements. Method (b) is commonly used in percussive drilling. Its analytical treatment is complex, even with simplifying assumptions. This is especially true when the rod (or drill stem) is short and of variable cross-section. Reflection and refraction of compressive waves and gradual changes in bit end conditions make analytical treatment difficult.

Transfer of impulse-induced energy from a drill bit to rock is an important measure of drilling efficiency. Various drill stem-hammer-bit configurations were investigated by Goldsmith and Wu (1981), Long (1966), Hustrulid (1968), Hustrulid and Fairhurst (1971a, 1971b), Dutta (1968), Lundberg (1987), Furby (1974), Fairhurst (1961), and Fischer (1961). Researchers agree that the maximum stress does not develop instantaneously. Stress decays exponentially with time. Also, changing sectional area of the drill stem or bit complicates the wave form. Empirical transmission factors are required to estimate the fraction of energy that reaches the rock.

Bit penetration into rock causes a gradual change in end conditions from "free" to "fixed." This further complicates the stress wave form. Experimental results by Fairhurst (1961) indicated that in spite of these complications, maximum stress resulting from impact for a particular hammer-drill rod-bit configuration can be approximated by the relationship

$$\sigma_m = V(E/C)(D^2/(D^2 + d^2)) \qquad (1)$$

where σ_m = maximum stress

V = velocity of piston impact

E = elastic modulus of drill rod and piston

C = velocity of stress waves in drill rod and piston

d = diameter of drill rod

D = diameter of piston

It is possible to modify this relationship for drop hammers as is done in the Appendix. The final impact velocity can be computed for any drop height from dynamics. For equation (1), it was assumed that only longitudinal or compressive waves are generated. This assumption requires that both the hammer and the drill rod axes be colinear and that contact surfaces remain parallel. If impact conditions deviate from the assumed conditions, shear waves may be generated. Furby (1974) postulates that shear waves absorb impact energy and do not contribute significantly to rock deformation since they travel normal to the drill rod axis.

Expressions for transmission factors for rods with circular cross-sections were developed by Dutta (1968). This is given by the equation:

$$T_{1-2} = 2p/(p + 1) \tag{2}$$

$$p = A_2/A_1 = D_2^2/D_1^2 \tag{3}$$

where T_{1-2} = transmission factor for the passage of waves from section area 1 to section area 2 (see Figure 6 for arrangement)

A_1 = cross-sectional area of rod region 1

A_2 = cross-sectional area of rod region 2

D_1 = diameter corresponding to A_1

D_2 = diameter corresponding to A_2

$$T_{1-2} = 2D_2^2/(D_1^2 + D_2^2) \tag{4}$$

Equation (4) is the general relationship which can be used in determining new stress levels resulting from the passage of waves through boundaries in cylindrical rods, across which the diameter changes. A similar transmission factor is applied in the determination of impact stress for the Rock Fracture Hammer (RFH), which was developed and used for this investigation.

C. Rock Deformation due to Impulse Loads

In drilling investigations, much attention has been focused on depth of penetration of percussive drill bits (Hustrulid 1968, Goldsmith and Wu 1981). Some of the concepts and assumptions used in percussive drilling apply indirectly the current proposition on hard rock percussion trenching. However, in percussion trenching,

the fracture depth resulting from impact may be more important than bit penetration. Depending on the level of brittle behavior exhibited by the rock, the fracture depth can far exceed the bit penetration depth.

As shown in Figure 1, Gnirk and Cheatham (1965) contrasted idealized deformation patterns for brittle vs. ductile rock. The brittle rock exhibits fractures penetrating well beyond the bit penetration depth. The ductile rock does not fracture extensively, but material piles up on the rock surface around the perimeter of the bit. These differing behaviors are also reflected in the shape of force-penetration curves. For ductile rock, the plot is linear; for brittle rock, the plot is jagged. The jaggedness corresponds in time to fragmentation events as the bit penetrates the rock.

The locus of the peaks in the plot can be described by the relationship

$$p = kd^n \tag{5}$$

where p = indentation force

n = a constant depending on the shape of the bit

d = bit penetration depth

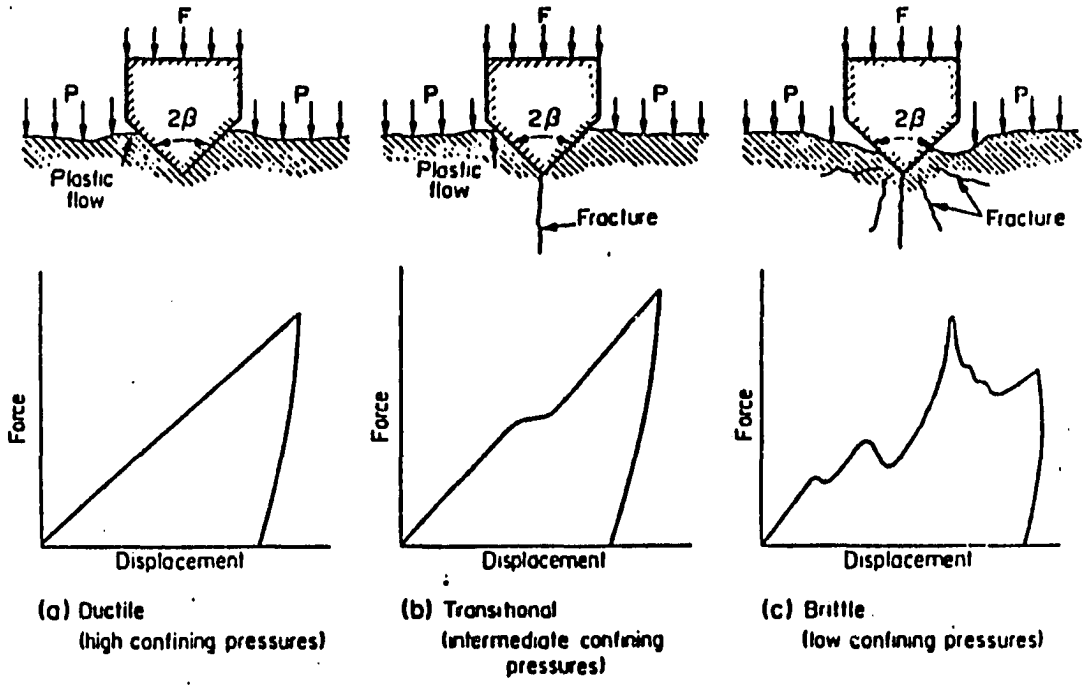

Figure 1. Rock failure pattern under a sharp wedge (Gnirk and Cheatham, 1965)

k = a constant depending on the properties of the rock; e.g., friction angle, cohesion, and modulus of elasticity. Bit geometry is also a factor in k.

For two-dimensional bits like wedges and chisels, n is approximately equal to 1. This implies that the relationship between force applied and bit penetration is approximately linear as confirmed by experimental results (Paul and Sikarskie 1965, Larson et al. 1987). Experimental results (Miller and Sikarskie 1968, Lundberg 1987, Cherepanov and Sokolinsky 1972, and Dutta 1972) also indicated that for three-dimensional bits like cones and pyramids, n varies from 1.5 to 2. Most of these investigations were conducted under static loading conditions. Minus a change in force thresholds for breakage, discussed later in this subsection, the same pattern may be expected for dynamic cases.

Kumano and Goldsmith (1982a, 1982b) conducted impact experiments on rocks with projectiles of various shapes; their experimental arrangement conformed to method (a) previously described. Such factors as energy partition, effects of rock texture, and the effects of projectile shape on fracture patterns in rocks were investigated. Generally, an impact crater and a severely fractured region beneath the crater resulted. Rocks with larger

grain sizes tended to fracture more randomly. Kabo et al. (1977) estimated that 70% to 80% of a projectile's initial kinetic energy is used for cratering and fracturing.

Analysis of stress resulting from impact of an object on a surface is complicated by the influences of a rock's response on the magnitude of stress developed. This response depends on the modulus of elasticity and Poisson's ratio. A theory proposed by Heinrich Hertz (1896) as presented in Timoshenko and Gooddier (1954) for a hemispherical bit allows estimation of fracture impact stress from Poisson's ratio and static strength according to the following:

$$\sigma_{mc}/\sigma_o = 1/n(1-2v) \qquad (6)$$

where σ_{mc} = critical impact stress

σ_o = compressive strength of rock

n = ratio of compressive strength to tensile strength of rock

v = Poisson's ratio of rock

Modifications of Hertz's original theory for other bit geometries were made by Ladanyi (1968).

Response of rock to imposed force or stress depends on the strain rate. Strength is directly proportional to

loading rate. Impulse or impact loading is high rate loading. For the same rock, dynamic strength is greater than the static strength values often quoted. This behavior implies that compressive strength must be empirically modified for dynamic loading as follows:

$$\sigma_c' = X\sigma_o \tag{7}$$

where σ_c' = compressive strength of rock under impulse loading

X = impulse loading factor which equals the ratio of impact strength to static strength of rock

σ_o = static compressive strength of rock

Rinehart's (1966) experiments indicate that X ranges from 6.5 to 13.0, as shown in Table 1. Birkimer (1970) conducted similar tests on portland cement concrete; his results indicate a range of X from 0.9 to 5.1.

D. Empirical Approaches

Specific energy is the energy per unit volume of an excavation. A measure of excavation efficiency, it has units of stress. It is often assumed to approximate the compressive strength of rock. Specific energy is inversely proportional to the surface area of fragments produced. Energy is wasted in producing dusts, whereas

Table 1. Ratio of dynamic to static tensile strength for a variety of rocks (Rinehart, 1966)

	Strengh (psi)		
Rock	Static	Dynamic	Ratio
Bedford Limestone	600	3900	6.5
Yule Marble (perpendicular to bedding)	300	2700	9.0
Yule Marble (parallel to bedding)	900	700	7.8
Granite	1000	5700	5.7
Taconite	700-1000	13200	13.0

larger fragments imply efficient operation. In drilling, empirical and analyticalrelationships have been developed among specific energy, rock strength, and drilling rate. Examples are those of Hustrulid and Fairhurst (1971a, 1971b), Paone et al. (1969), Hustrulid (1971), Unger and Fumanti (1972), Schmidt (1972), Reichmuth (1963), and Rabia (1982). However, it is emphasized that specific energy is not an intrinsic rock property but also depends on such factors as bit type, fragment size, and mode of rock breakage. Figure 2 summarizes results of investigations by Tutluoglu et al. (1983) on the relative efficiencies of various methods of excavation in hard rock. The impact-driven wedge, owing to its creation of large fragments utilizes very little energy. A scheme in which impact is combined with drag bit action has potential for effectiveness.

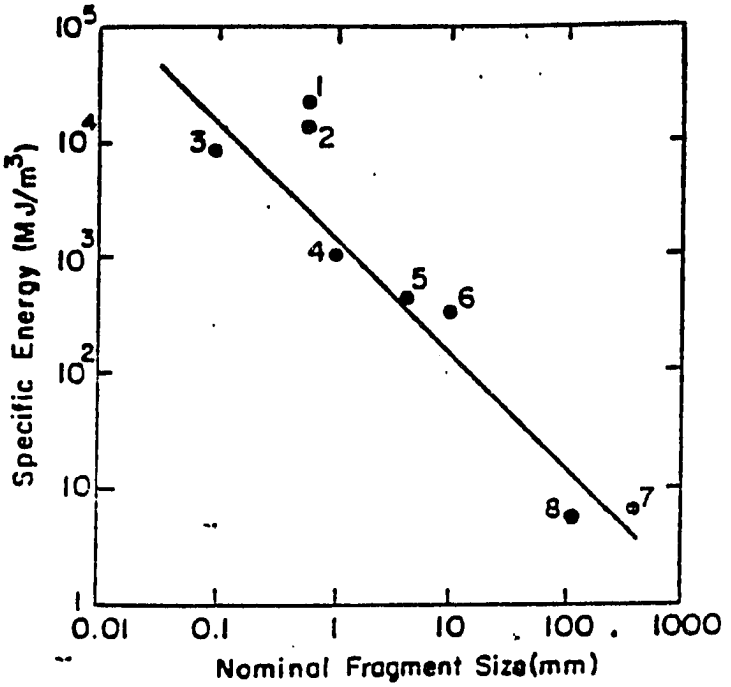

1. Flame jet piercing
2. Water erosion jet
3. Diamond drilling
4. Percussive drilling
5. Drag bit cutting
6. Gyratory crusher
7. Impact driven wedge
8. Explosive blasting

Figure 2. Specific energies of various excavation methods in hard rock with a compressive strength of 200 MPa (Tutluoglu et al., 1983)

III. THEORY AND EXPERIMENTATION

A. Theoretical Considerations of Impact Loading

An impact is a phenomenon in which the velocities of various points on the travelling body undergo a finite change over a negligible interval of time as a result of contacting another body.

In a perfectly elastic impact, neither the hammer nor the target (rock) is permanently deformed. In this case, the law of conservation of mechanical energy is satisfied largely by the rebound of the hammer. The ratio of the rebound velocity to the impact velocity of the hammer is called the coefficient of restitution, r. For a perfectly elastic impact, r has a value of 1. In a perfectly plastic impact, the law of energy conservation is satisfied solely by the deformation of either the hammer or the rock. The hammer used in this investigation terminates in a carbide-tipped bit. Since the hammer tip has a much greater modulus of elasticity than the rock, in non-elastic impact, it is assumed that all deformation occurs in the rock. Impact on rock is both plastic and elastic, the proportions of which depend on the magnitude of impact energy and stress relative to the dynamic strength of the impacted rock.

Only a fraction of the total impact energy, E_o , will be utilized in rock deformation. Wave transmission energy through the rock is considered as a part of this fraction. Mathematically, this energy partition can be expressed as:

$$E_o = E_u + E_r \tag{8}$$

where E_o = total kinetic energy of impact hammer

E_u = energy utilized in rock deformation processed and wave movement

E_r = hammer rebound energy

The ratio E_u/E_r can be denoted by K_1 , which represents the fraction of the initial kinetic energy which goes into rock deformation.

$$E_u = K_1 E_o \tag{9}$$

Similarly, E_r/E_o represents the fraction of the initial kinetic energy which goes into hammer rebound and is denoted by K_2. Hence,

$$E_r = K_2 E_o \tag{10}$$

From equation (8), (9), and (10) it follows that

$$K_1 + K_2 = 1 \tag{11}$$

and

$$E_u = K_1 E_o = (1-K_2)E_o \tag{12}$$

$$E_u = K_1 E_o = (1-(E_r/E_o))E_o \tag{13}$$

$$K_1 = 1-(E_r/E_o) \tag{14}$$

E_r and E_o can be computed using basic principles of dynamics. Hence

$$E_o = 0.5mV_f^2 \tag{15}$$

$$E_r = 0.5mV_r^2 \tag{16}$$

where m = mass of the impact hammer

V_f = final pre-impact velocity of impact hammer

V_r = rebound velocity of the impact hammer

Substituting equations (15) and (16) into equation (14), the following relationship results

$$K_1 = 1-(V_r/V_f)^2 \tag{17}$$

The coefficient of restitution of the impact hammer is defined as follows

$$r = V_r/V_f = (h'/h)^{0.5} \tag{18}$$

where h = hammer drop height

h' = hammer rebound height

Substituting equation (18) into equation (17), the K_1 relationship becomes

$$K_1 = 1-(h'/h) \tag{19}$$

$$E_u = (1-(h'/h))E_o \tag{20}$$

This research proposes the existence of a critical impact energy, E_{oc}, at which the rock deforms extensively. Below the critical impact energy, E_{oc}, impact is predominantly elastic; above it, impact becomes predominantly plastic. Figure 3 shows that at the critical impact energy, a jump occurs in the energy transferred from the impact bit to the rock. This jump should be manifested as a sharp decrease in the rebound ratio, h'/h. Equation (19) indicates that the energy transfer coefficient, K_1 approaches unity if the rebound ratio, h'/h, decreases significantly. This implies that the utilized energy, E_u, would approach the impact energy, E_o, in magnitude.

Below the critical impact energy, minimal and local crushing should occur; the rebound ratio, h'/h, should be high (as required by the law of conservation of energy). At critical impact energy, flaws within a brittle rock should extend (causing cracking) but should cause minimal crushing (because crushing requires more energy than

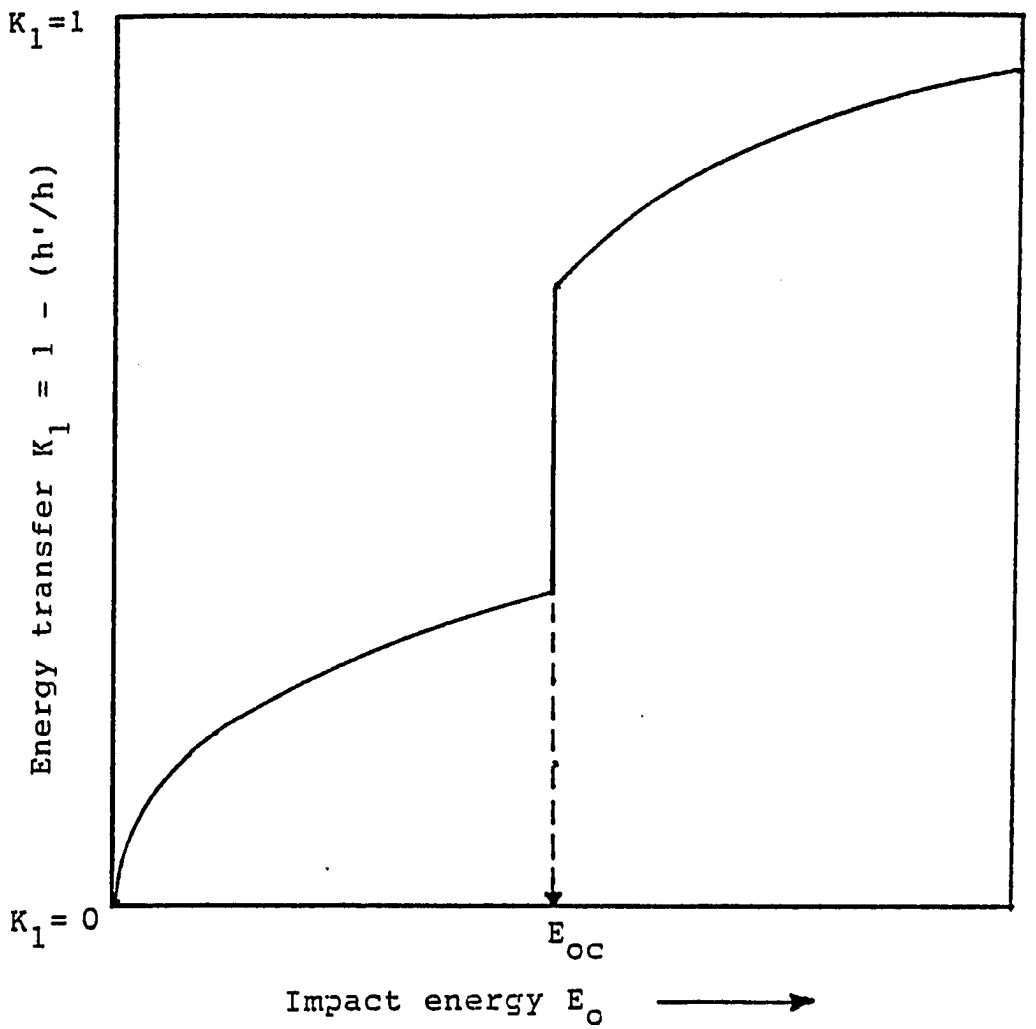

Figure 3. Theoretical relationship between energy transfer and impact energy for a semi-elastic rock; critical impact energy is shown by dotted line

cracking). Beyond the critical impact energy, crushing should become an important part of the deformation process (although some cracking may occur as well). This is illustrated in Figure 4.

Applying impact mechanics to rock excavation requires estimating the critical impact energy for each rock. Impacts at subcritical energy levels would be ineffective because the flaws would not extend (i.e, the rock would retain its strength). Impacts at critical energy level should cause a sharp decrease in strength (implying a similar decrease in rebound ratio). Impacts far exceeding the critical energy level are expected to cause excessive crack frequency (i.e., crushing). The latter situation may be due to the entrapment of stress waves in the cracked rock surrounding the impact point. Excessive super-critical impact energies may result in the removal of small fragments (i.e., grinding); this would reduce efficiency.

B. Design of the Rock Fracture Hammer (RFH)

Part of this investigation involved the development of the Rock Fracture Hammer (RFH). This is a simple impact hammer with an impact activated friction that simulates impact loading for a proposed percussion trencher; it can be used in the field to determine the

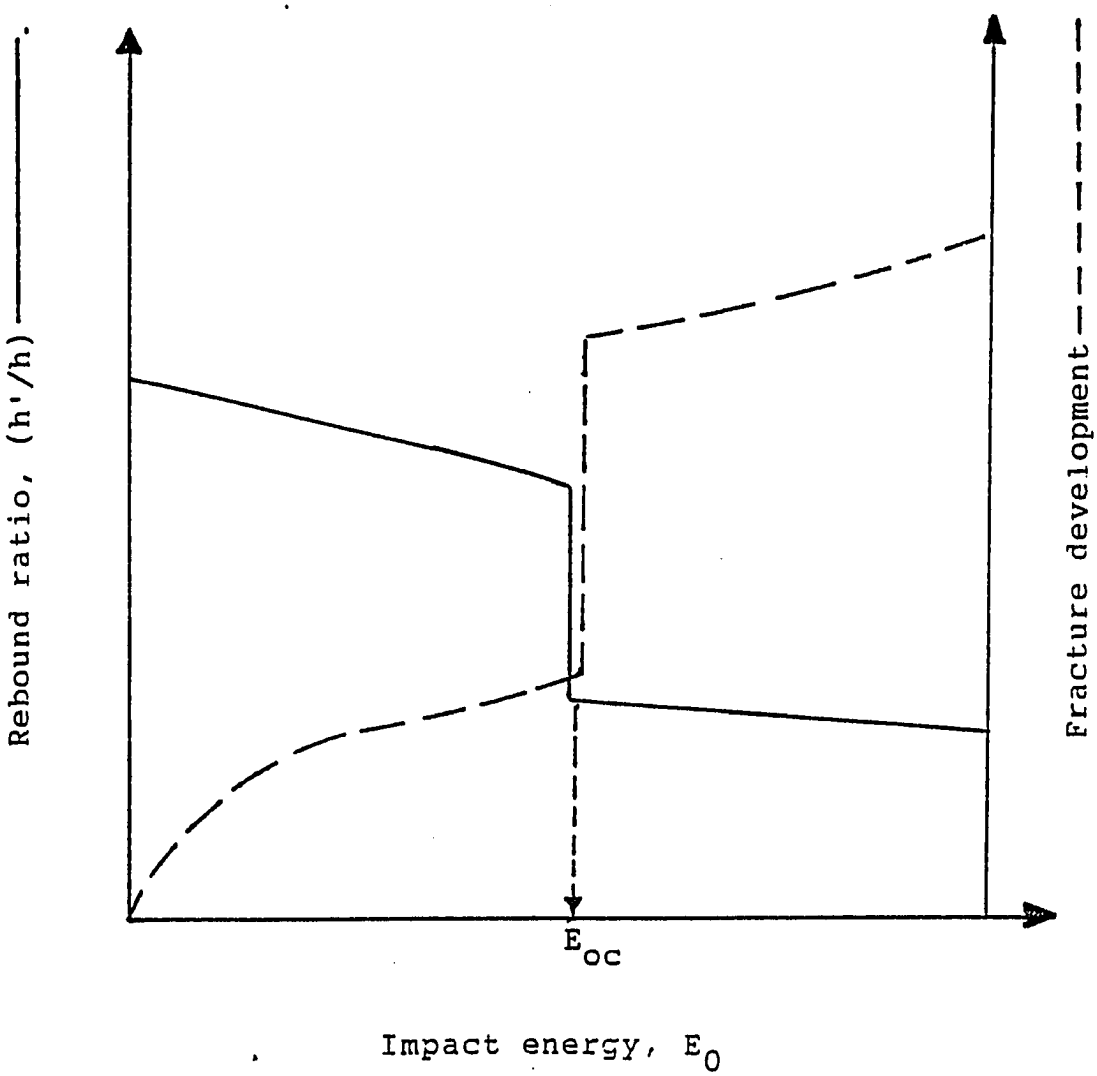

Figure 4. Theoretical relationship between impact energy, rebound ratio, and fracture development for brittle rock

critical impact energy for a variety of rocks. The RFH is basically a 25-pound (11.34 kg) cylindrical steel block that slides on a 3/4 inch (1.9 cm) diameter steel rod (see Figure 5). Figure 6 shows that the RFH terminates at a conical bit having a spherical carbide tip. With a trip mechanism, the RFH can register maximum rebound resulting from various levels of energy input.

The rebound height indicator rides with the hammer and can be released by impact-induced pressure on the trigger. This pressure unhooks the indicator such that it can be pushed up to any terminal rebound height by the upward-moving hammer. Hammer rotation is inhibited by a slender rod attached to the indicator. Acceleration tests with a Stratham 814 TC bi-directional linear accelerometer scaled to a free-fall acceleration of 9.81 m/sec^2 indicate that friction is negligible. Figure 7 shows comparisons of recorder print-outs of free-fall acceleration and sliding acceleration of the hammer.

By varying the hammer drop height, h, various levels of impact energy and resulting stress can be produced. If impact energy for a selected drop height is not adequate to fracture rock, rebound of the hammer occurs and the indicator is left clamped on the guide rod at the maximum rebound height, h'. In this case, the impact energy, E_o, is

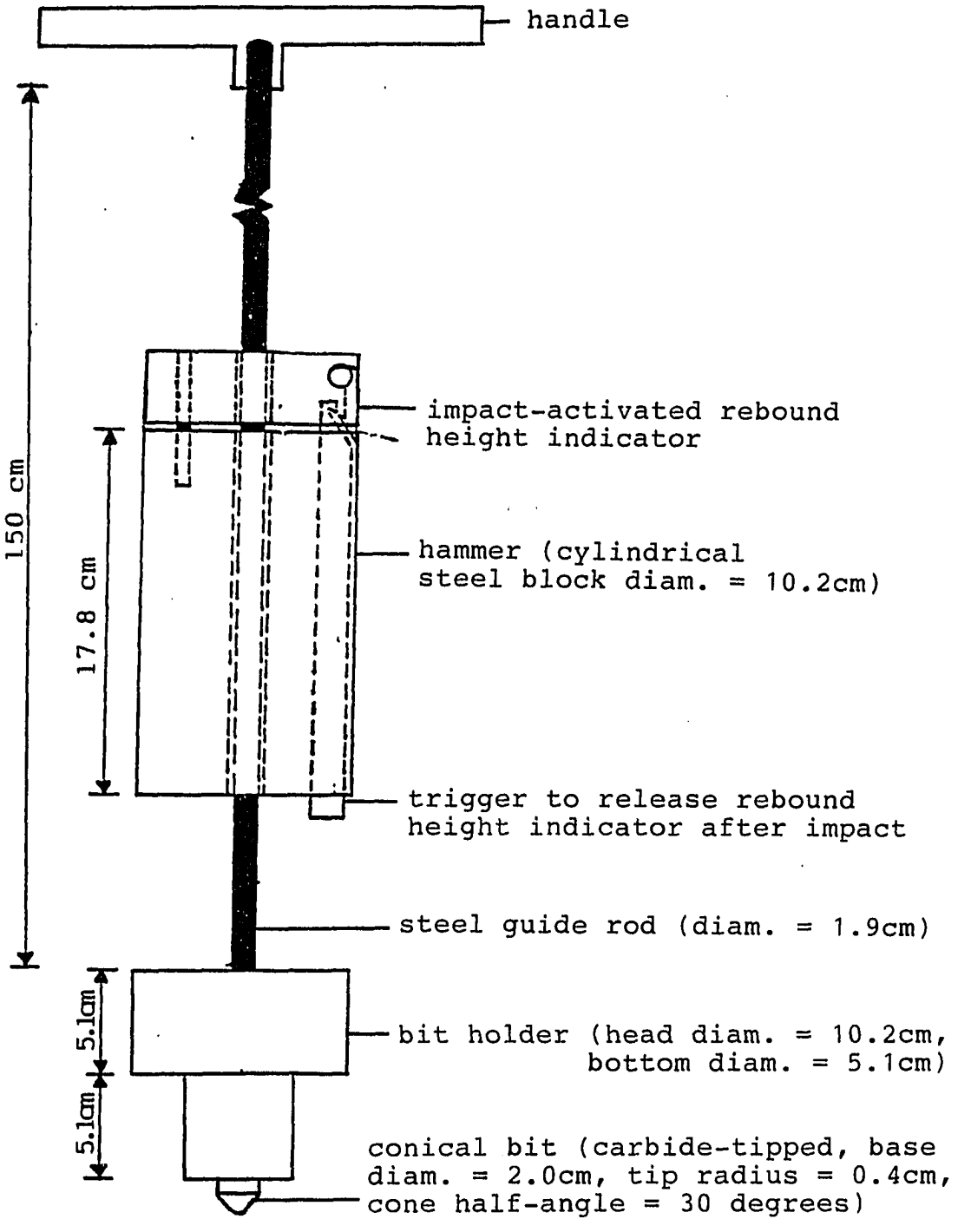

Figure 5. The Rock Fracture Hammer (RFH) developed for this research

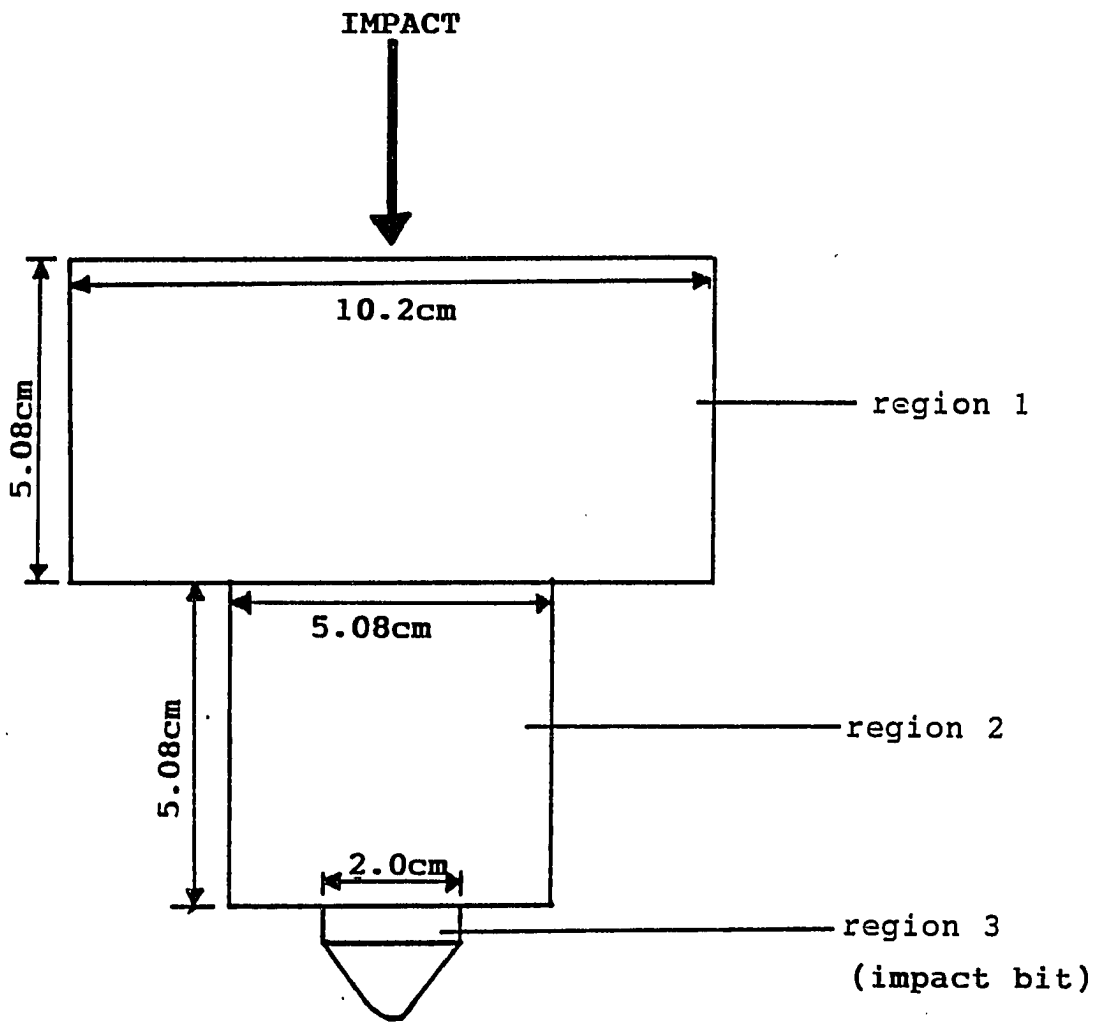

Figure 6. Impact bit holder for the Rock Fracture Hammer (RFH)

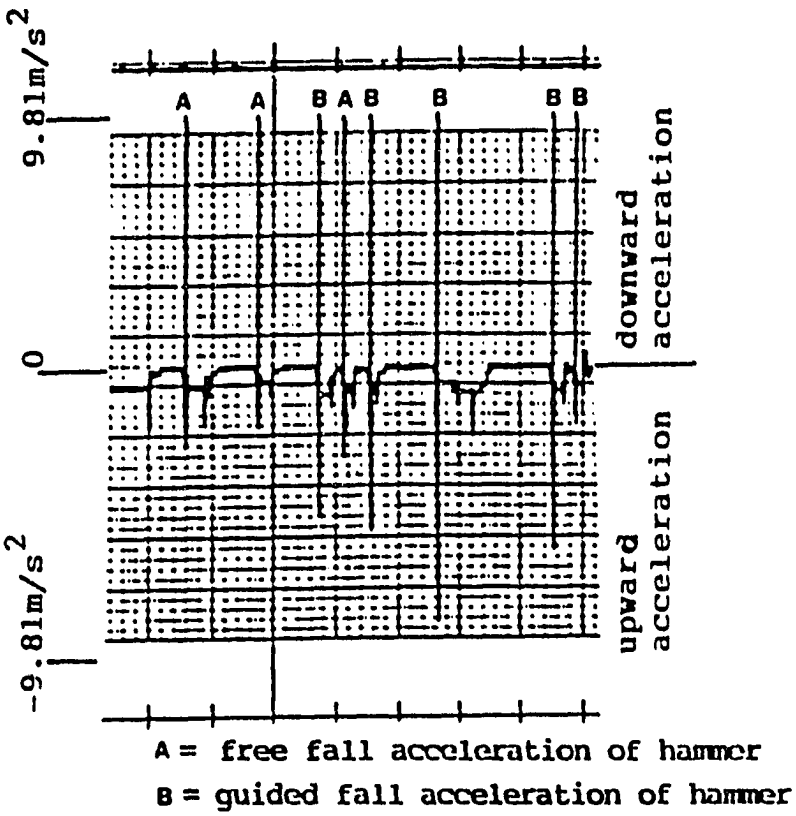

Figure 7. Comparison of free fall and guided acceleration of impact hammer for estimating impact stress and impact energy on rocks

below critical level. If the drop height, h, is such that sufficient impact energy and stress are generated, the rock is fractured and rebound is negligible.

Expressions for the impact energy, E_o, and the resulting stress, σ_m, were derived using principles of dynamics and the widely accepted research findings on wave transmission through rods discussed earlier. More detailed analyses are relegated to the Appendix. Briefly, the relationships among impact energy, impact stress, and hammer drop height are as follows:

$$E_o = 55.62h \tag{21}$$

$$\sigma_m = 503.4h^{0.5} \tag{22}$$

$$E_o = \sigma_m^2/4556.25 \tag{23}$$

where E_o = impact energy (joules)

σ_m = impact stress (MPa)

h = hammer drop height (m)

Impact energy varies linearly with drop height while impact stress varies exponentially with the drop height. Computations of impact energy and impact stress for various hammer drop heights are shown in Table 2. To avoid

interpolations, Figure 8 can also be used to determine the impact stress and impact energy corresponding to various drop heights.

C. Estimation of Critical Impact Energy

Direct use of the RFH in determining the critical impact energy, E_{oc}, is preferable. However, where the RFH is unavailable, the critical impact energy can be estimated as presented below. From equation (6),

$$\sigma_{mc} = \sigma_o = 1/n(1-2V)$$

where σ_{mc} = critical impact stress

σ_o = compressive strength of rock (static)

n = ratio of compressive to tensile strength of rock

v = Poisson's ratio of rock

$$\sigma_{mc} = \sigma_o/n(1-2v) \tag{24}$$

$$n = 1/R_o \tag{25}$$

where R_o = ratio of tensile strength to compressive strength of rock

Table 2. Values of impact stress and impact energy for various hammer drop heights

Hammer drop height h (m)	Impact stress σ_m (MPa)	Impact energy E_o (Joules)
0.10	159.19	5.562
0.20	225.13	11.124
0.30	275.72	16.686
0.40	318.38	22.248
0.50	355.96	27.810
0.60	389.93	33.372
0.70	421.17	38.934
0.80	450.25	44.496
0.90	477.57	50.058
1.00	503.40	55.620
1.10	527.97	61.182
1.20	551.45	66.744
1.30	574.00	72.306

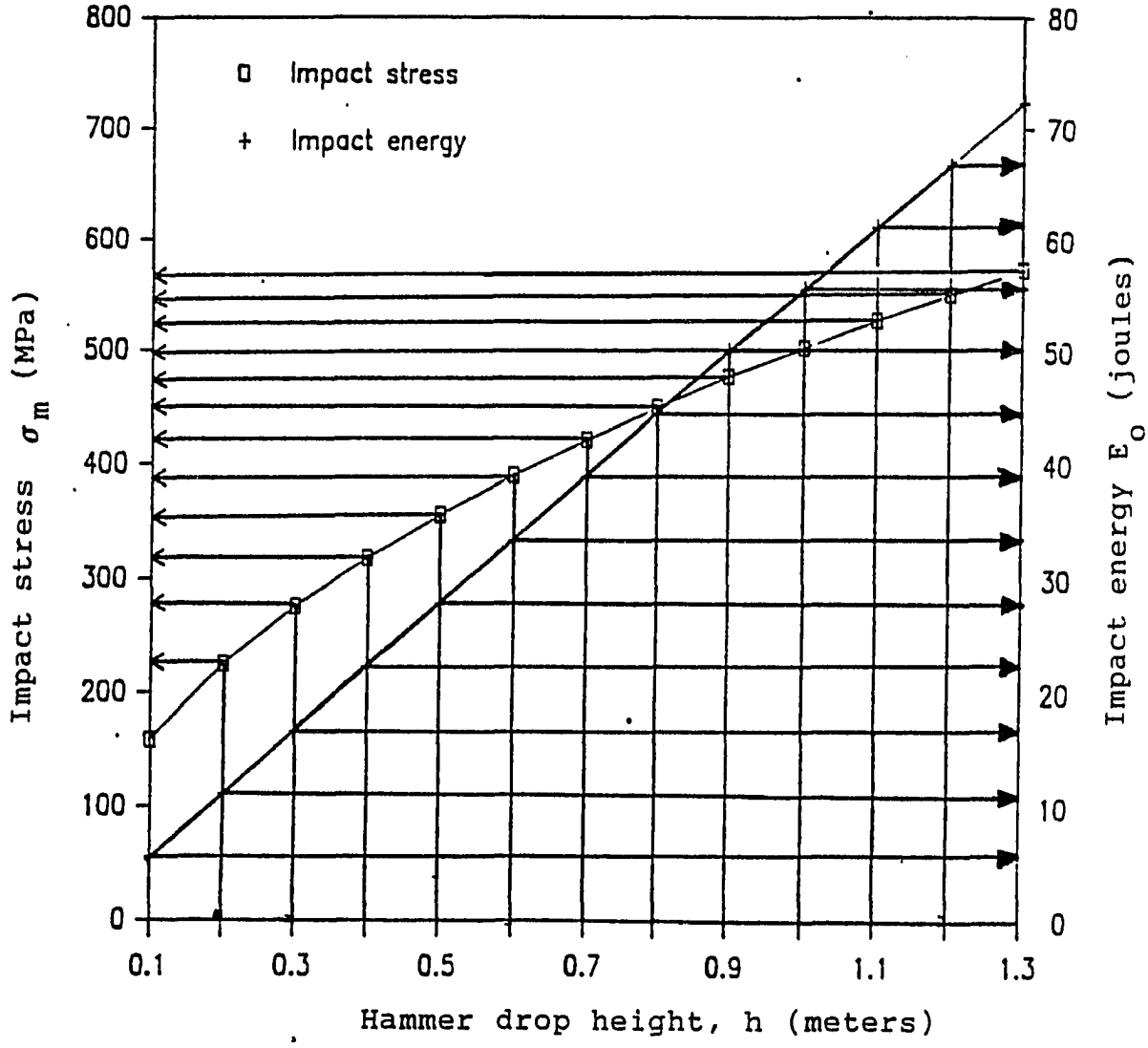

Figure 8. Chart for estimating impact energy and impact stress for the Rock Fracture Hammer (RFH)

Substituting equation (25) into equation (24), the following relationship results,

$$\sigma_{mc} = R_o\sigma_o/(1-2v) \tag{26}$$

Considering that the rock is loaded by impact, an impulse loading factor has to be applied as discussed Chapter II, Section C. From equation (7) in that chapter,

$$X = \sigma_c'/\sigma_o \tag{27}$$

where X = impulse loading factor

σ_c' = dynamic compressive strength

σ_o = static compressive strength of rock

It can be assumed that the influences of impulse loading on tensile and compressive strengths of a rock are not significantly different. Hence, the ratio, n, for the same rock is assumed to stay relatively constant numerically regardless of loading mode.

Considering equation (26), σ_o can be substituted for, resulting in

$$\sigma_{mc} = XR_o\sigma_o/(1-2v) \tag{28}$$

Equation (28) gives an estimate of the magnitude of impact stress required to fracture rock significantly. To accomplish this,

$$\sigma_m \geq \sigma_{mc} \tag{29}$$

The critical impact stress, σ_{mc}, corresponds to the critical impact energy, E_{oc}, for each rock strength class. At this threshold, the energy transfer coefficient equals unity ($K_1 = 1$)

$$E_u \cong E_o \cong E_{oc} \tag{30}$$

As established in equation (A-18) in the Appendix, the relationship between impact stress, σ_m, and impact energy, E_o, is as follows:

$$E_o = \sigma_m^2 m / 4T_1^2 T_2^2 (E/c)^2$$

A general relationship for estimating the critical impact energy, E_{oc}, required for rock fracture can be arrived at by replacing σ_m with σ_{mc} in the above equation. Hence,

$$E_{oc} = (XR_o\sigma_o/(1-2v))^2 m/4T_1^2T_2^2(E/c)^2 \quad (31)$$

where E_{oc} = critical impact energy

X = impulse loading factor

R_o = ratio of tensile strength to compressive strength of rock

σ_o = compressive strength of rock under static loading conditions

v = Poisson's ratio of rock

m = mass of impact hammer

T_1, T_2 = stress transmission factors

E = elastic modulus of impact hammer

c = sonic wave velocity through impact hammer

The Poisson's ratio of most rocks is approximately Ø.3. Equation (32) results

$$E_{oc} = 6.25(XR_o\sigma_o)^2 m/4T_1^2T_2^2(E/c)^2 \quad (32)$$

For the RFH developed for this investigation, the hammer/bit holder configuration has the following properties,

c = 5100 m/s

E = 2.07 x 1011 N/m

T_1 = 1.60 (see Appendix)

T_2 = 1.75 (see Appendix)

m = 11.34 kg

Substituting these values into equation (32), the resulting equation (33) can be used to estimate the critical impact energy, E_{oc}, for a rock when the RFH is used. However, the compressive strength of rock and the computed critical impact energy must have units of Pascals (N/m) and Joules (kgf-m) respectively.

$$E_{oc} = \frac{(6.25)(XR_o\sigma_o)^2(11.34)}{(4)(1.6)^2(1.75)^2(2.07 \times 10^{11}/5100)^2}$$

$$E_{oc} = 1.3719 \times 10^{-15} (XR_o\sigma_o)^2 \qquad (33)$$

D. Experiment Design and Test Procedures

1. Test objectives

In order to achieve the following objectives, a variety of tests were conducted on six rock types. Test objectives were as follows:

(a) Observation of the extent to which the deformation of each selected hard rock under impact loads conforms to the critical impact energy concept,

(b) Measurement of the critical impact energy level at which fractures develop significantly in different strength classes of rocks and comparison of these experimental values with theoretical estimates. The aim was to select the optimal impact energy for each strength class or a range of strength classes of rocks to minimize energy wastage.

(c) Assessment of the feasibility of repeating impacts at sub-critical energy levels.

(d) Measurement of the spacing at which cracks resulting from adjacent impacts interact. Measurement of the average radius of the fractured zone leads to an optimization of impact bit spacing for the percussion trencher. The latter is proposed in Chapter V.

(e) Measurement of the sharp decrease in rock strength (strength degradation) which should result from impact at critical energy. This is an important measure of the effectiveness of the impact loading mode.

2. Engineering properties of rocks used in the present investigation

Six rock types were used in this investigation, namely: Centerville Grey Limestone, Academy Black Granite, Lac Du Bonnet Granite, Rockville Granite, Sunset Red Granite and Anamosa Yellow Limestone. The sources of these rocks with their respective engineering properties are presented in Table 3.

Adequate variety in grain size, tensile strength and compressive strength were considered in their selection. Grain size varies from very fine-grained (< 1mm) for Centerville Grey Limestone and Anamosa Yellow Limestone to very coarse-grained (> 5mm) for Rockville Granite. The inverse proportionality between grain size and the recorded strength values should be noted. However, this relationship is violated only by Anamosa Yellow Limestone, a soft friable rock which tended to disintegrate during wet cutting.

The igneous rocks were supplied by Twin City Testing Corporation of St. Paul, Minnesota. The sedimentary rocks were supplied by Weber Stone Company of Stone City, Iowa. For each rock type, the recorded strength values are averages of about ten tests. Academy Black Granite, Rockville Granite, Lac Du Bonnet Granite and Sunset Red Granite have compressive strengths that fall within the range often reported to present problems as regards drag bit cutting. Due to the importance of the product of the brittleness index, R_o, and the compressive strength, σ_o, the product, $R_o\sigma_o$, is indicated for each rock in Table 3.

Table 3. Engineering properties of the rocks used in this investigation

ROCK	Genetic class/ Grain size group	Tensile strength t_o (MPa)	Compressive strength σ_o (MPa)	Brittleness index $R_o = t_o / \sigma_o$	$R_o \sigma_o$ (MPa)
Centerville Grey Limestone, Iowa	sedimentary, very fine-grained	23.45 (3400psi)	96.55 (14,000psi)	0.243	23.460
Academy Black Granite, Minnesota	igneous, medium-grained	16.69 (2420psi	203.44 (29,500psi)	0.082	16.682
Lac Du Bonnet Granite, Manitoba, Canada	igneous, medium-grained	13.45 (1950psi)	183.45 (26.000psi)	0.073	13.391
Rockville Granite, Minnesota	igneous, very coarse-grained	10.96 (1590psi)	182.07 (26,400psi)	0.060	10.924
Sunset Red Granite, Texas	igneous, coarse-grained	10.14 (1470psi)	133.79 (19,400psi)	0.076	10.170
Anamosa Yellow Limestone, Iowa	sedimentary, very fine-grained, friable	6.97 (1010psi)	61.52 (8920psi)	0.113	6.952

3. Strength degradation tests

Strength degradation tests conducted fell into two categories, namely,

a. Impact tests Drop tests were conducted on blocks (22 cm x 22 cm x 20 cm) carefully cut from large-sized blocks. On each rock block, the impact point was selected such that it coincided with the geometric center of the surface of the block, as shown in Figure 9. Two types of impact tests were conducted, namely, single impact test and repeated impact tests.

1) Single impact test These tests were conducted on each of the six rock types previously described. As regards the test procedure, a rock block was selected and the criss-cross pattern of sonic wave traverse lines was marked on the block as illustrated in Figure 9. A sonic wave transmitting transducer and a receiving transducer, connected to a James V-meter ultrasonic tester, were used to measure the pre-impact wave transit times along the traverse lines shown. To ensure coupling between the rock surface and the transducers, a gel was applied to the interface. Seven levels of drop height, h (0.1 m, 0.3 m, 0.5 m, 0.7 m, 0.9 m, 1.1 m, 1.3 m), corresponding to seven impact energy levels were used on each rock type. The resulting impact

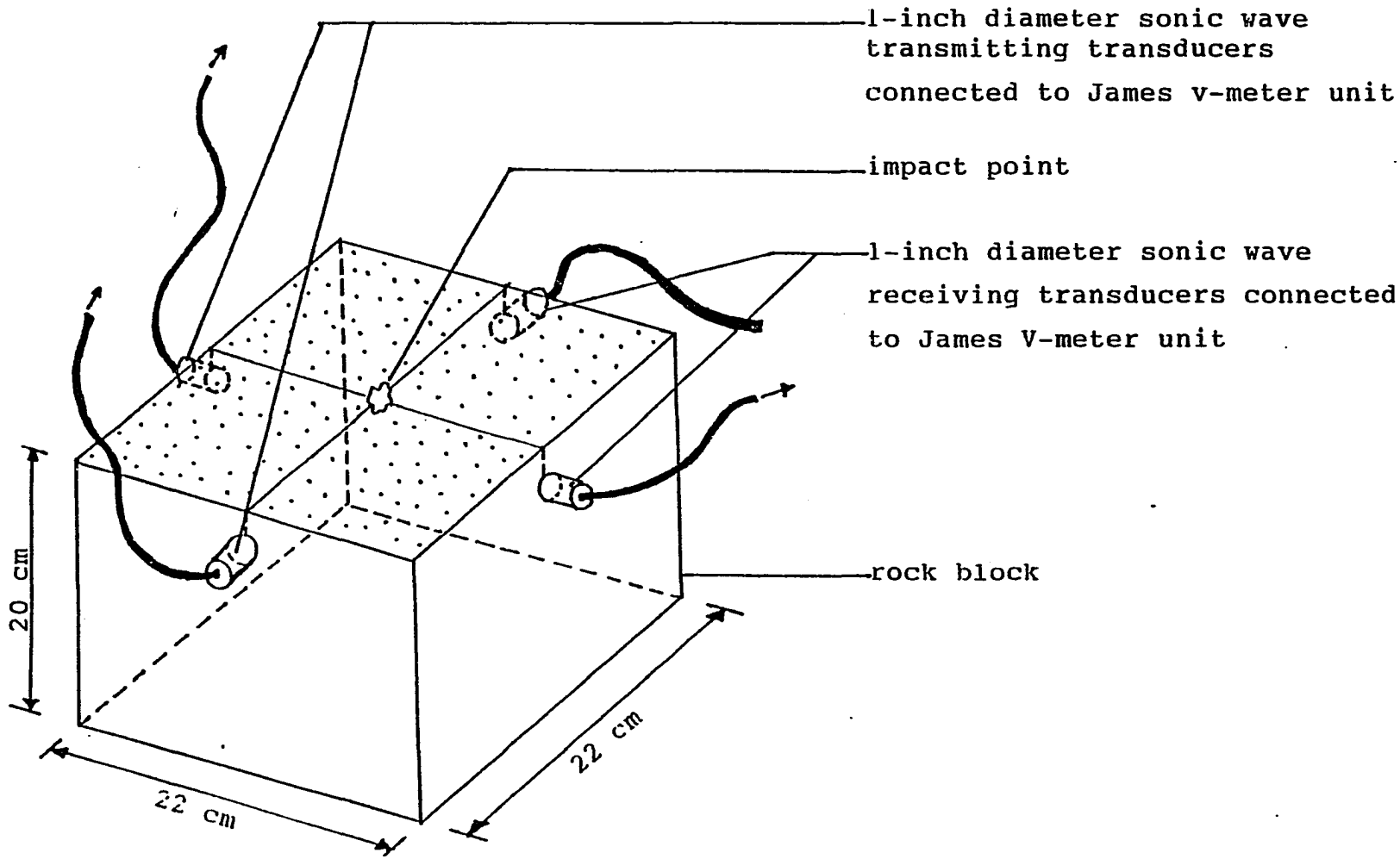

Figure 9. Arrangement of transducers on a rock block before and after impact

energy range was 5.562 Joules to 72.3Ø6 Joules. However, each rock block was impacted only once. Following the operation described earlier, the RFH axis was held normal to the rock surface and the hammer was elevated to the desirable height. With the bit resting on the impact point, the hammer was allowed to drop. Two measurements were made after impact: the hammer rebound height, h', and the sonic wave transit times along the previously marked traverse lines. From these two measurements, it was possible to compute the rebound ratio, h'/h and the percent decrease in sonic wave velocity for each drop height, on each rock type.

2) Repeated impact test Where a single impact did not result in significant decreases in both the rebound ratio, h'/h, and sonic wave velocity, it was apparent that no significant deformation occurred. To evaluate the effectiveness of repeated impacts, the hammer was raised to the same drop height, h, and allowed to drop on the same impact point as before. The rebound ratio was again measured. At each sub-critical drop height (corresponding to sub-critical impact energy), impact was repeated only once. The percentage change in either the rebound ratio, h'/h, and the energy transfer coefficient, K_1, were calculated.

b. Point load resistance test The test objective was to measure the residual strength of the region surrounding the impact point after impact at each energy level. From each impacted rock block, a 6.3 cm diameter core was made around the impact point. Each core was 2.5 cm thick. Each core was tested for residual point load resistance axially, using the Tetrametrics T-500 Point Load Tester, illustrated in Figure 10. Cores of similar dimensions were also made from regions of the same rock block which were unaffected by impact. The latter set of cores were tested as controls. Testing of cores from the same block as control minimizes the influences of rock strength variability. From the data obtained, the percentage decrease in point load resistance for each impact energy level on each rock type was computed.

4. Impact spacing tests

These tests were designed to measure average radius of the fractured zone caused by critical energy impact. Blocks of Academy Black Granite and Lac Du Bonnet Granite were used. Sonic wave transit times along traverse lines about the point, before and after impact were measured. Transducers were evenly coupled on the rock surfaces with gel. The transducers were connected to a James V-meter

Ultrasonic Tester which is illustrated in Figure 11. The experimental set-ups were as shown in Figures 12 and 13.

Using increases in sonic wave transit times as the bases, the fractured zone of radius, q, was delineated.

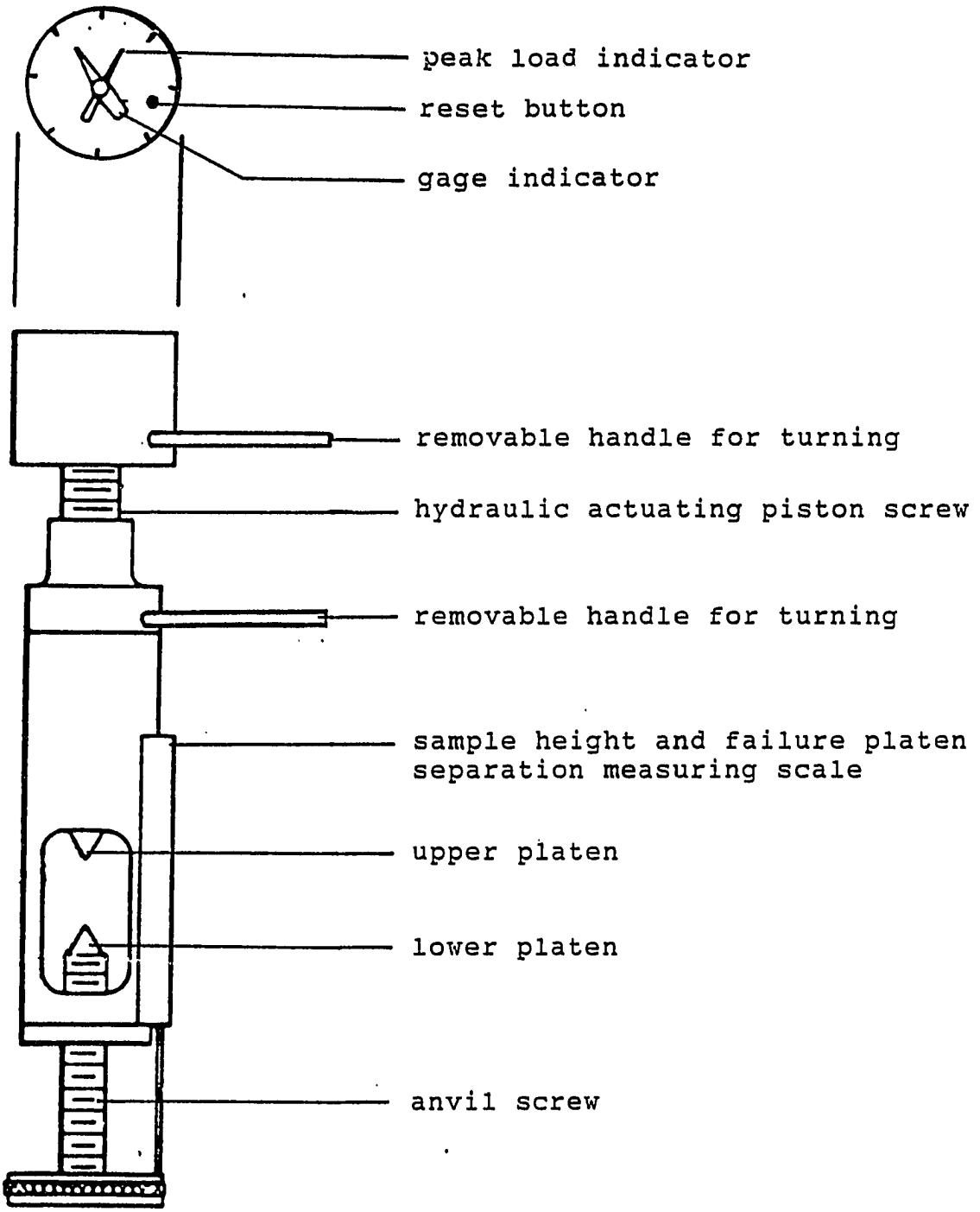

Figure 10. Schematic of the Terrametrics T-500 Point Load Tester used in this investigation

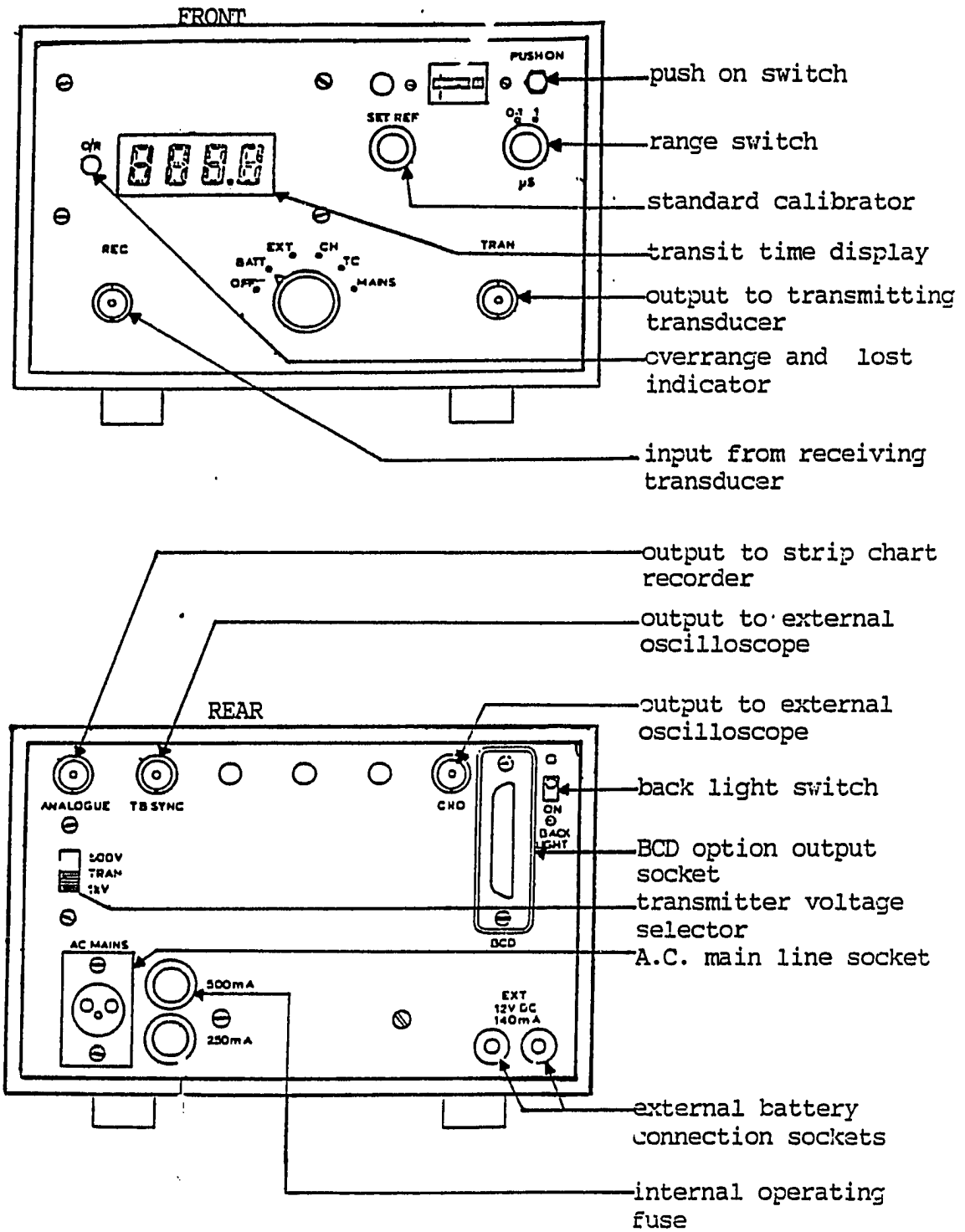

Figure 11. Controls for James V-Meter Ultrasonic Tester (James Electronics Inc., 1980)

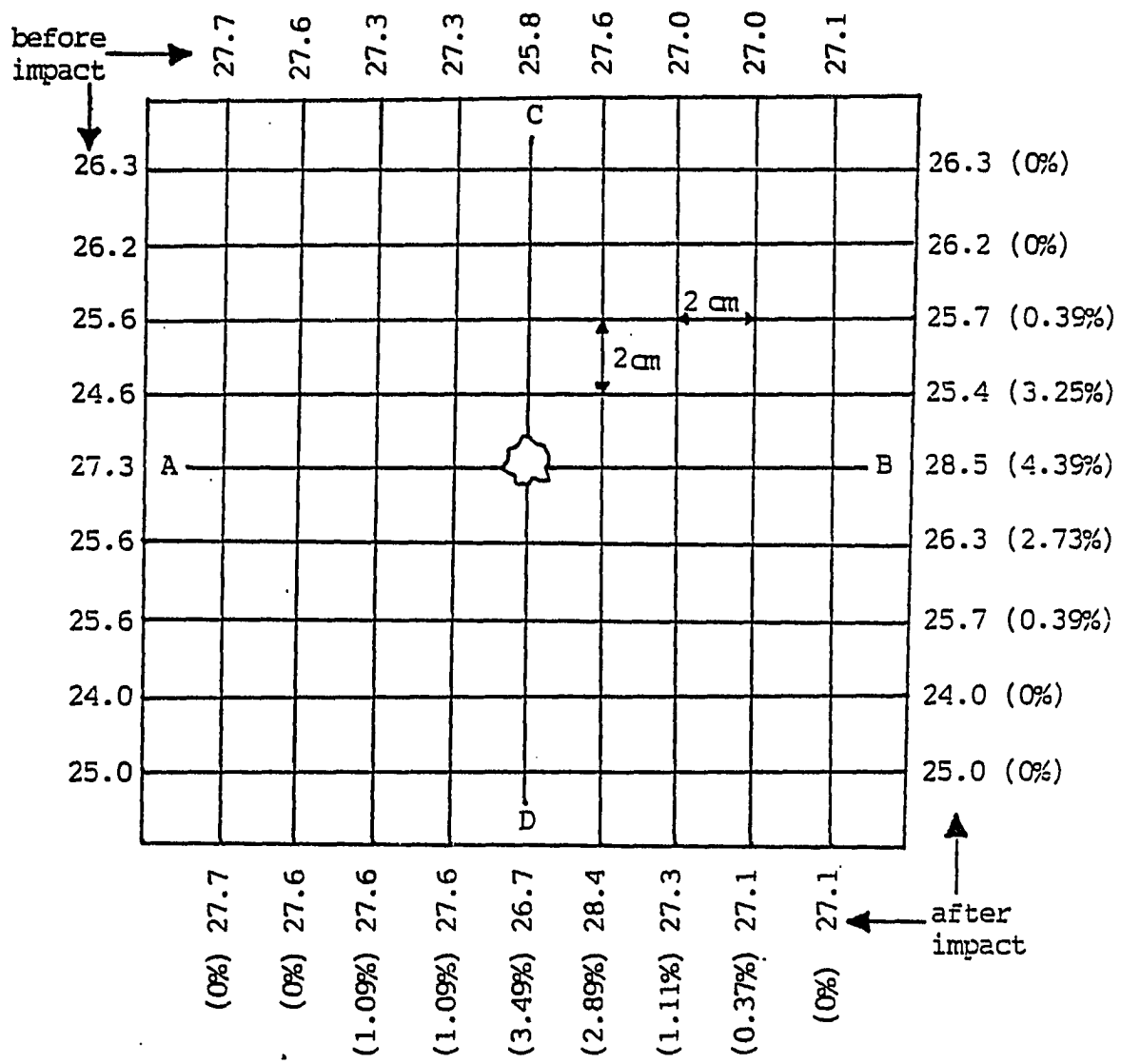

Figure 12. Plan view of selected sonic wave traverse lines for Academy Black Granite. Transit times are shown in microseconds before and after impact (% increases shown in brackets)

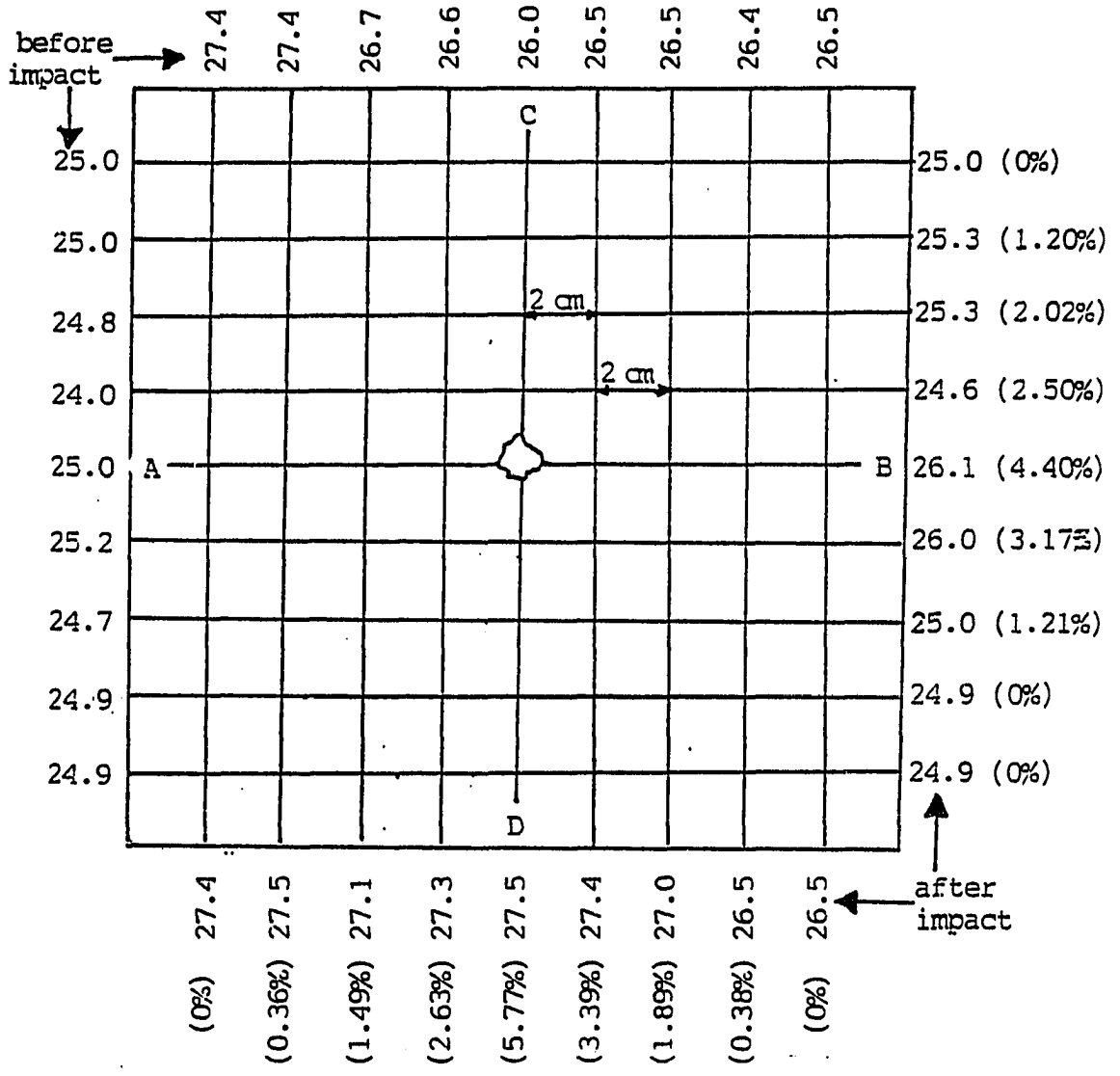

Figure 13. Plan view of selected sonic wave traverse lines for Lac Du Bonnet Granite. Transit times are shown in microseconds before and after impact (% increases shown in brackets)

IV. ANALYSES OF RESULTS

A. Observations on Deformation under Single Impacts

Experimental results for each of the six rock types investigated are presented in Tables 4 through 9. These results are further illustrated graphically in Figures 14 through 25. For each rock, there is a sharp decrease in rebound ratio, h'/h, and hence a sharp increase in energy transfer coefficient, K_1, at some threshold impact energy level. Single impacts at energy levels below the critical value result in higher rebound ratios and hence, lower energy transfer coefficients. K_1 values generally exceed Ø.95 in the super-critical impact energy regime for the various rocks.

Plots of impact energy, E_o, versus K_1 (Figures 14, 16, I5, 2Ø, 22 and 24) show positive slopes in the sub-critical impact energy range. This situation indicates that for each rock, even before the critical impact energy, E_{oc}, is attained, the impact is progressively plastic. A plausible explanation would be the existence of flaws, anisotropy and inhomogeneity in rocks which prevent a completely elastic response upon impact. Stress singularity or infinity at the tip of the impact bit caused local crushing even in the sub critical impact encrgy range. Generally, the crater size

increased with impact energy. The direct proportionality between the impact energy, E_o , and the crater size is responsible for the observed progressive increase in K_1 before the attainment of E_{oc}.

In the super-critical energy range, decrease in slopes are observed on the same plots. These decreases mean a transition to predominantly plastic impact. Energy transfer coefficients, K_1 ranging from Ø.7 to Ø.8 are often assumed in percussive drilling of rock. Hakalehto (1972) and McCarthy (1982), assume transfer coefficients of Ø.7 and Ø.8 respectively. In this investigation, K_1 values are all in excess of Ø.95. Whereas in their investigations, the authors refer to the energy actually used in rock crushing, K_1 values referred to in the present investigation include crushing energy and energy expended on such phenomena as heat generation, wave transmission through the rock and fragment ejection from the impact crater. Tests designed to determine the proportion of impact energy expended on various rock deformation phenomena indicate that for wave transmission and fragment ejection, the total fraction of impact energy dissipated is about Ø.18 (Kabo, Goldsmith and Sackman, 1977). Since no significant amount of energy is expended on heat in this low velocity impact regime, the heat energy can be ignored. By subtracting Ø.18 from the

range of super-critical energy values, an estimate can be made of the range of transfer coefficients for energy actually expended on rock deformation. This range comes out to be approximately Ø.79-Ø.81.

Permanent rock deformation can occur in response to crushing, cracking, or both, so it is desirable to note which mode dominates at each impact energy level on any given rock. Figures 15, 17, 19, 21, 23 and 25 illustrate the deformation modes for the rocks tested. Sonic wave transmission through rocks is sensitive to the presence of discontinuities (flaws or cracks). Wave transit times increase and hence, velocities decrease along the same traverse lines if cracks resulted from an impact. If the deformation mode is predominantly crushing, significant decreases in sonic wave velocities would not be observed. Results show that single impacts in the sub-critical impact energy range result largely in minor crushing with minor cracking. For all rocks tested except Anamosa Yellow Limestone, sonic wave velocity decreases sharply at an impact energy level corresponding to that determined using the rebound method. This indicates crack development.

Table 4. Results of single impact tests on Centerville Grey Limestone

Impact energy E_{oc} (joules)	% Decreases in sonic velocity	Rebound ratio h'/h	Energy transfer $K_1 = 1-(h'/h)$	% Decrease in point load resistance
5.56	0.19	0.160	0.840	1.3
16.69	0.42	0.117	0.883	2.6
27.81	0.86	0.090	0.910	1.8
38.93	0.87	0.086	0.914	5.0
50.06	1.33	0.078	0.922	7.5
61.18=E_{oc}	2.53	0.027	0.973	75.0
72.31	2.99	0.029	0.971	76.3

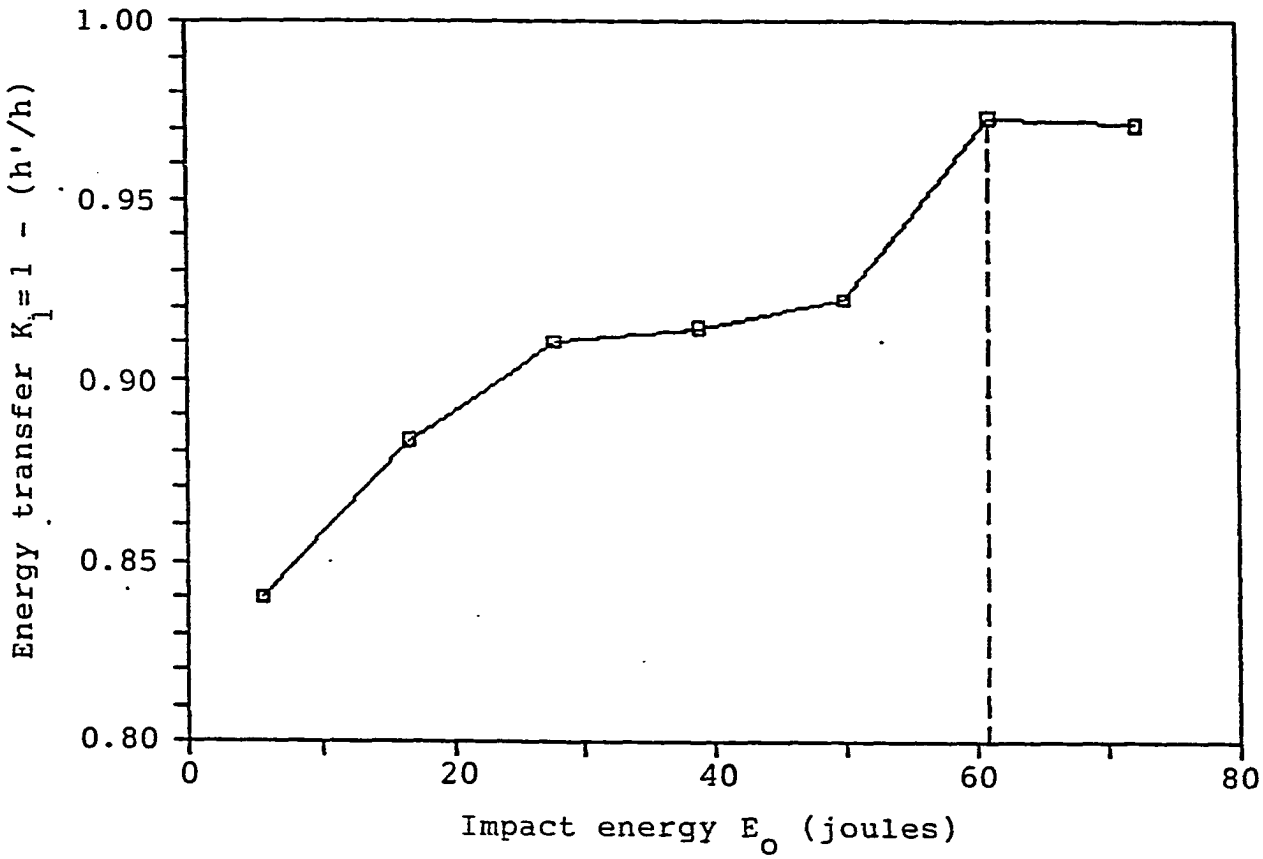

Figure 14. Energy transfer at various single impact energies, Centerville Grey Limestone (critical impact energy = 61.18 J)

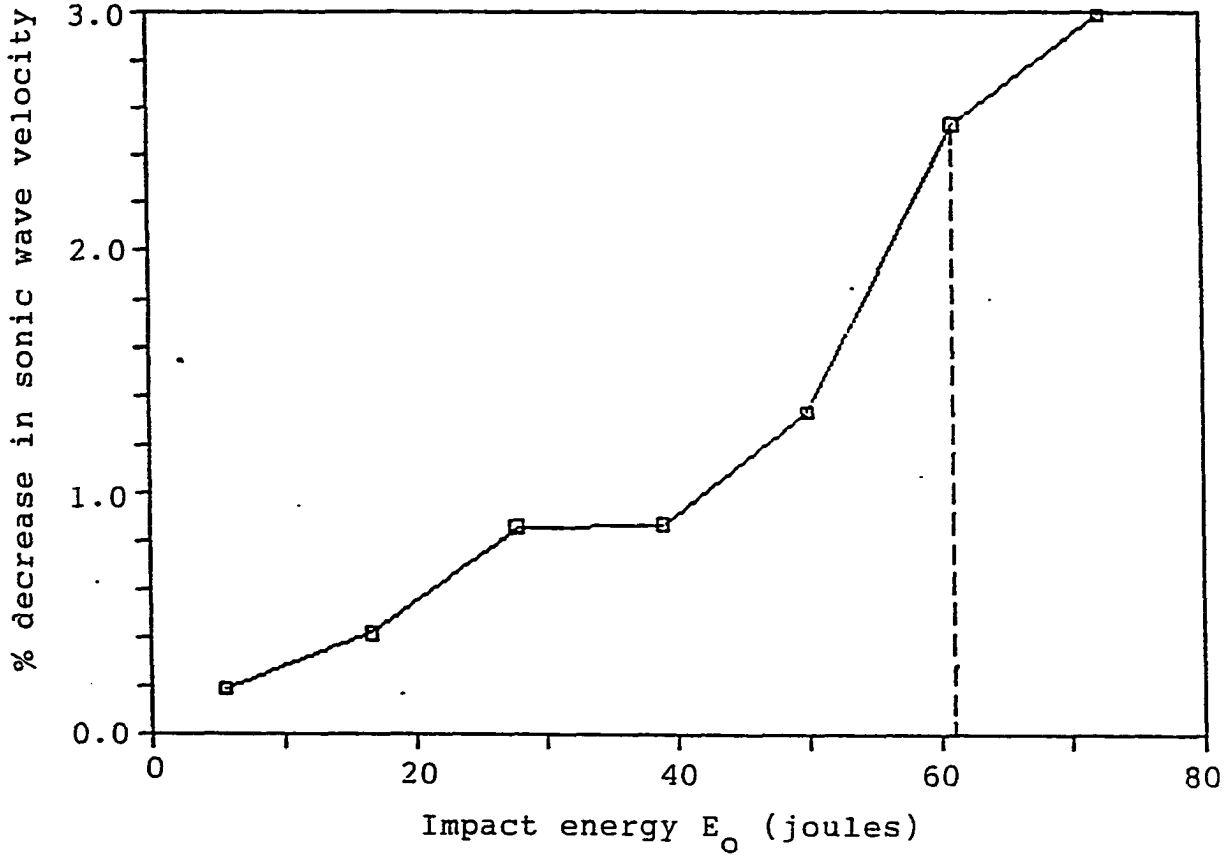

Figure 15. Percentage decrease in sonic wave velocity caused by single impacts at various energy levels, Centerville Grey Limestone (critical impact energy = 61.18 J)

Table 5. Results of single impact tests on Academy Black Granite

Impact energy E_{oc} (joules)	% Decreases in sonic velocity	Rebound ratio h'/h	Energy transfer $K_1 = 1-(h'/h)$	% Decrease in point load resistance
5.56	0.40	0.150	0.850	2.1
16.69	0.57	0.116	0.884	4.9
27.81	1.04	0.090	0.910	4.9
38.93	1.22	0.064	0.036	7.7
$50.06=E_{oc}$	4.65	0.022	0.978	44.1
61.18	5.39	0.009	0.991	46.9
72.31	5.88	0.007	0.993	49.7

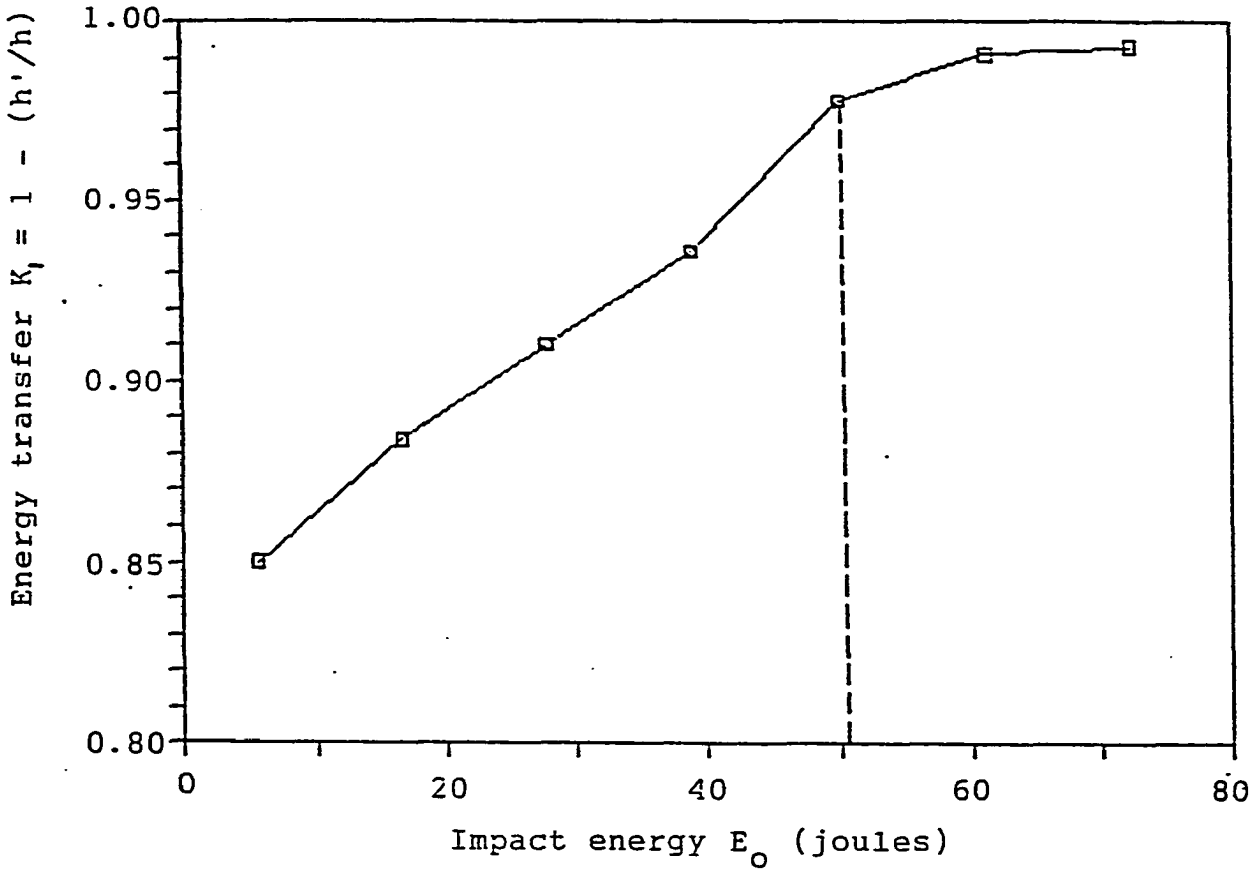

Figure 16. Energy transfer at various single impact energies, Academy Black Granite (critical impact energy = 5Ø.Ø6 J)

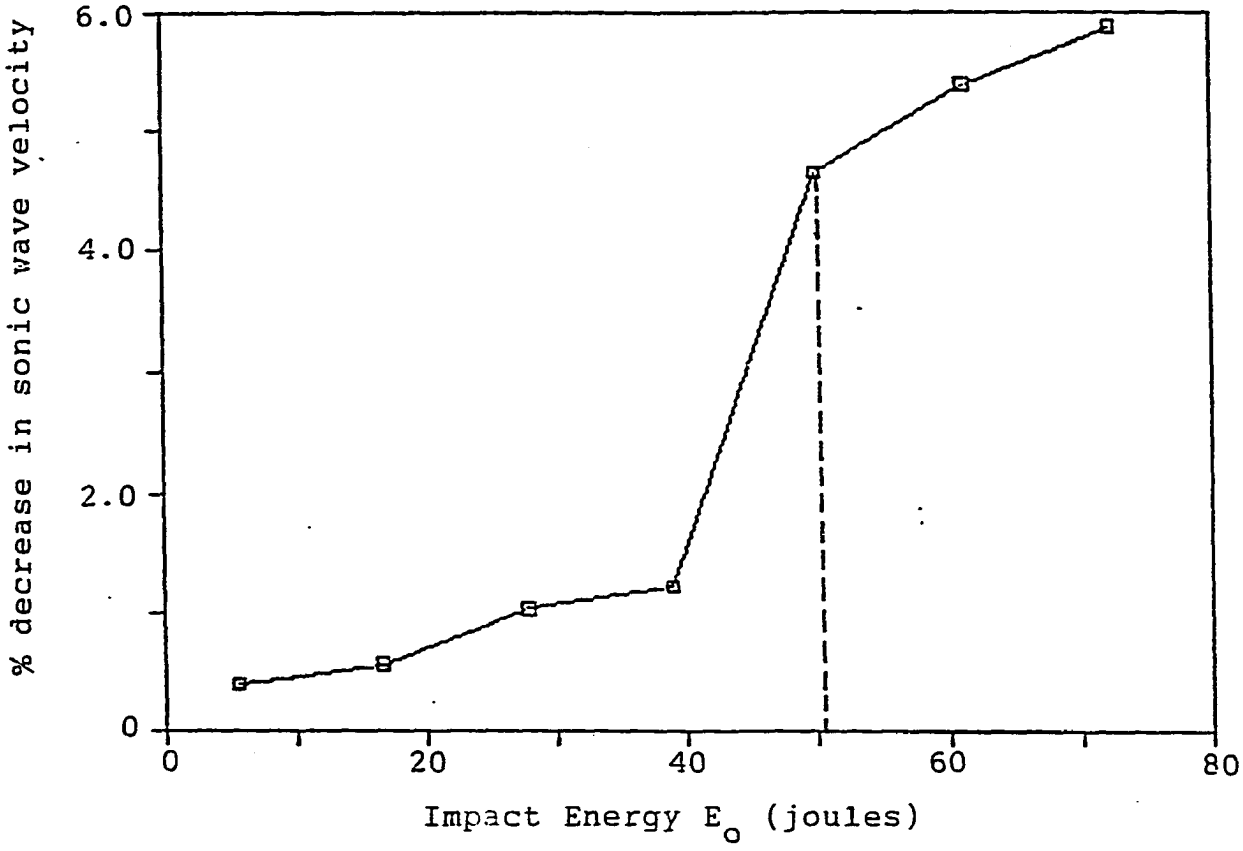

Figure 17. Percentage decrease in sonic wave velocity caused by single impacts at various energy levels, Academy Black Granite (critical impact energy = 50.06 J)

Table 6. Results of single impact tests on Lac Du Bonnet Granite

Impact energy E_{oc} (joules)	% Decreases in sonic velocity	Rebound ratio h'/h	Energy transfer $K_1 = 1-(h'/h)$	% Decrease in point load resistance
5.56	0.79	0.150	0.850	0
16.69	1.01	0.100	0.900	6.7
27.81	1.67	0.100	0.900	8.3
$38.93=E_{oc}$	5.86	0.021	0.979	40.0
50.06	5.97	0.016	0.983	45.8
61.81	6.07	0.014	0.986	51.6
72.31	7.24	0.008	0.992	66.6

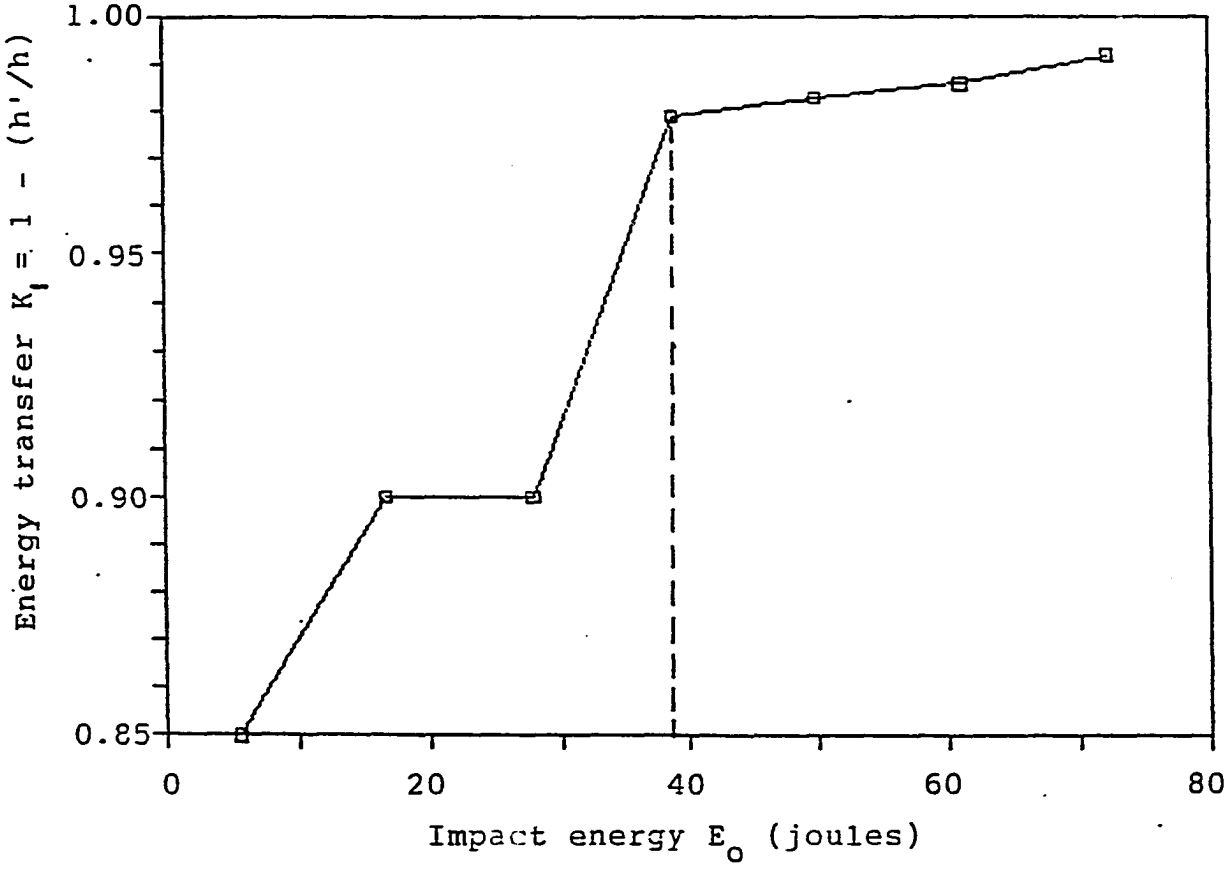

Figure 18. Energy transfer at various single impact energies, Lac Du Bonnet Granite (critical impact energy = 38.93 J)

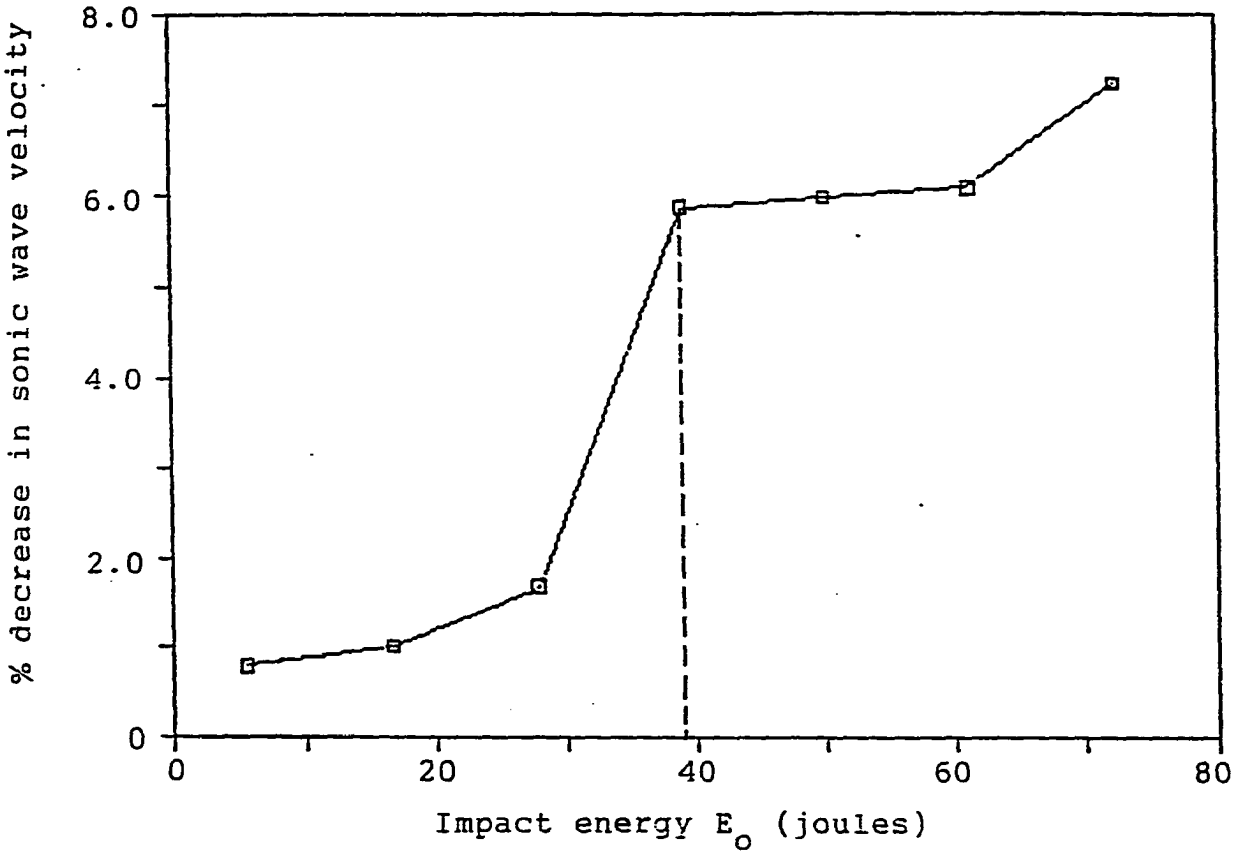

Figure 19. Percentage decrease in sonic wave velocity caused by single impacts at various energy levels, Lac Du Bonnet Granite (critical impact energy = 38.93 J)

Table 7. Results of single impact tests on Rockville Granite

Impact energy E_{oc} (joules)	% Decreases in sonic velocity	Rebound ratio h'/h	Energy transfer $K_1 = 1-(h'/h)$	% Decrease in point load resistance
5.56	0.89	0.100	0.900	1.7
16.69	1.19	0.100	0.900	3.4
27.81	3.59	0.080	0.920	6.9
38.93=E_{oc}	6.30	0.028	0.972	39.6
50.06	6.89	0.011	0.989	47.4
61.18	7.57	0.027	0.973	50.9
72.31	8.60	0.038	0.962	56.9

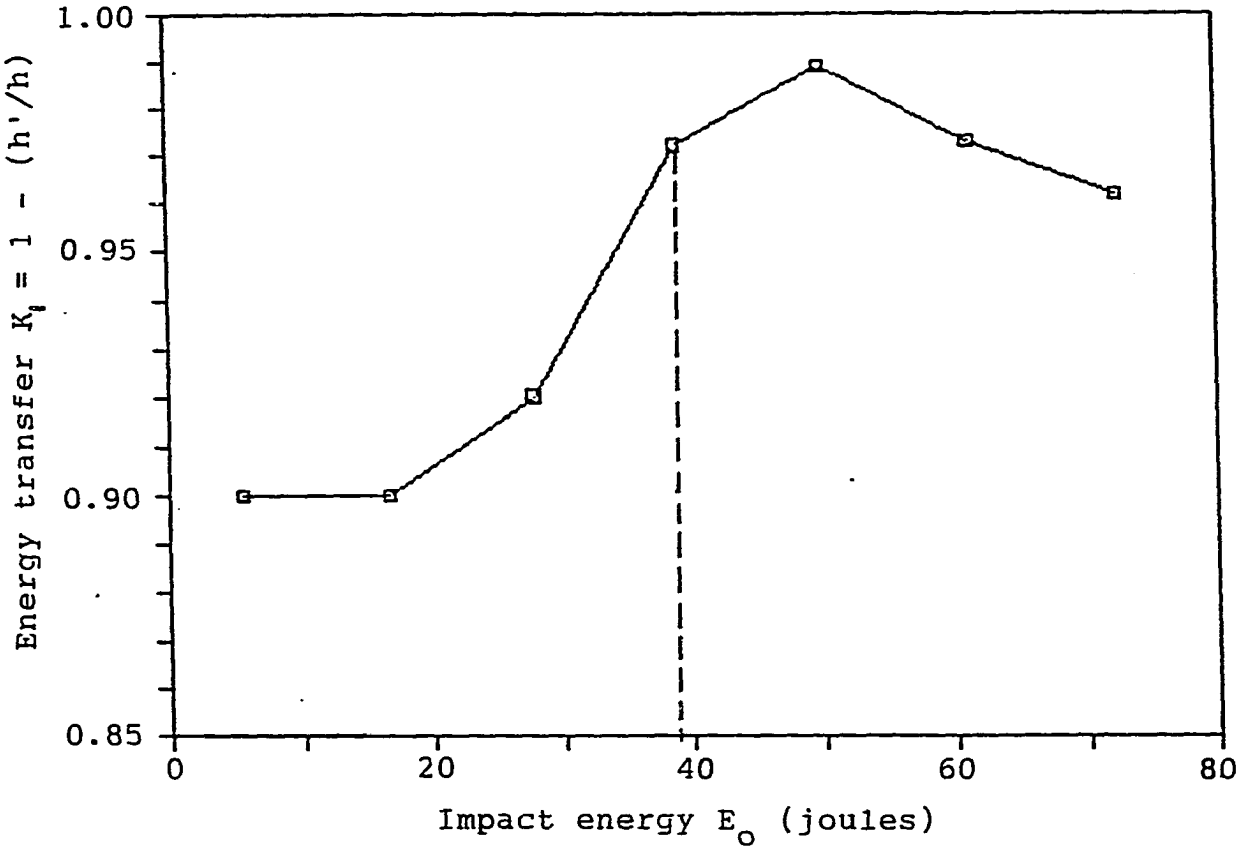

Figure 20. Energy transfer at various single impact energies, Rockville Granite (critical impact energy = 38.93 J)

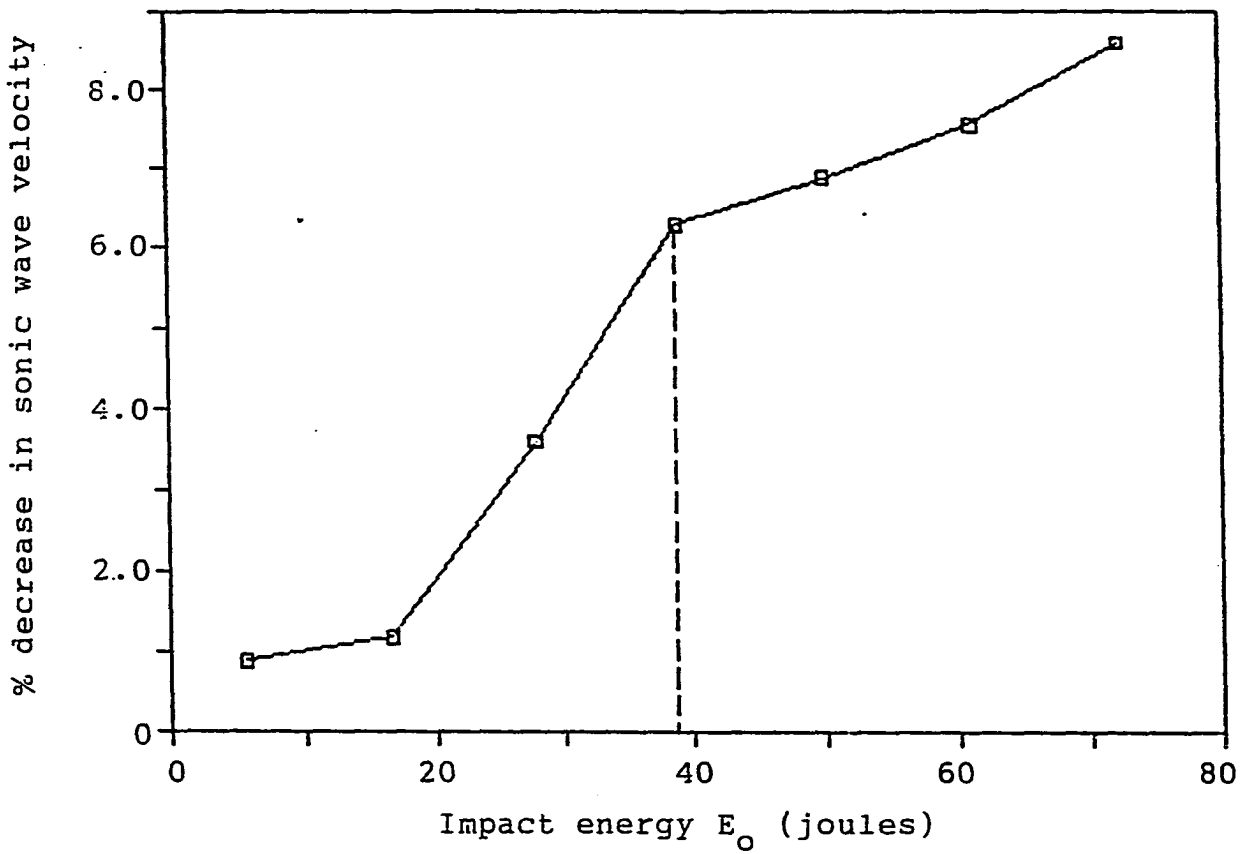

Figure 21. Percentage decrease in sonic wave velocity caused by single impacts at various energy levels, Rockville Granite (critical impact energy = 38.93 J)

Table 8. Results of single impact tests on Sunset Red Granite

Impact energy E_{oc} (joules)	% Decreases in sonic velocity	Rebound ratio h'/h	Energy transfer $K_1 = 1-(h'/h)$	% Decrease in point load resistance
5.56	0.67	0.110	0.890	8.4
16.69	1.07	0.100	0.900	13.7
27.81	1.61	0.080	0.920	15.8
38.93=E_{oc}	4.98	0.014	0.985	32.6
50.06	5.20	0.022	0.978	38.9
61.18	5.54	0.018	0.981	45.3
72.31	5.93	0.008	0.992	51.6

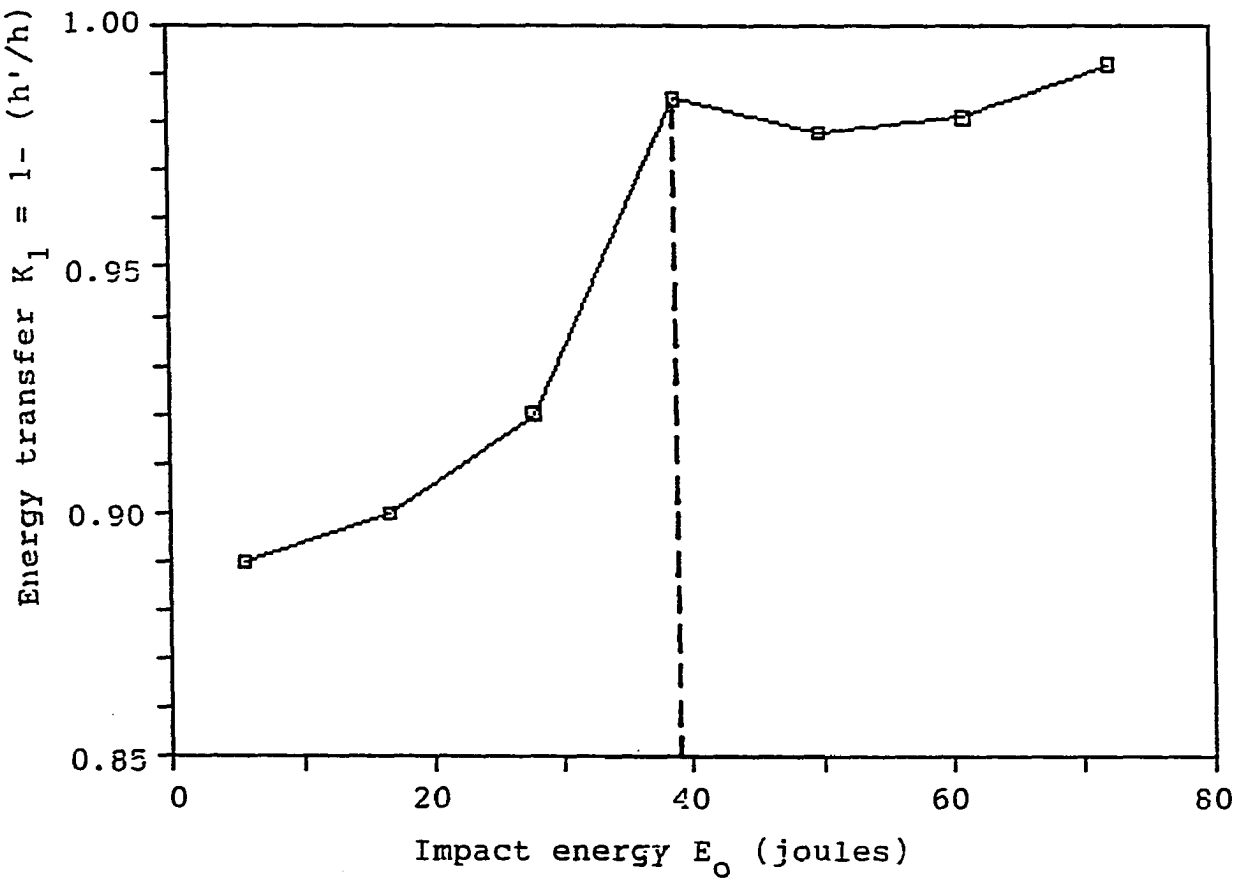

Figure 22. Energy transfer at various single impact energies, Sunset Red Granite (critical impact energy = 38.93 J)

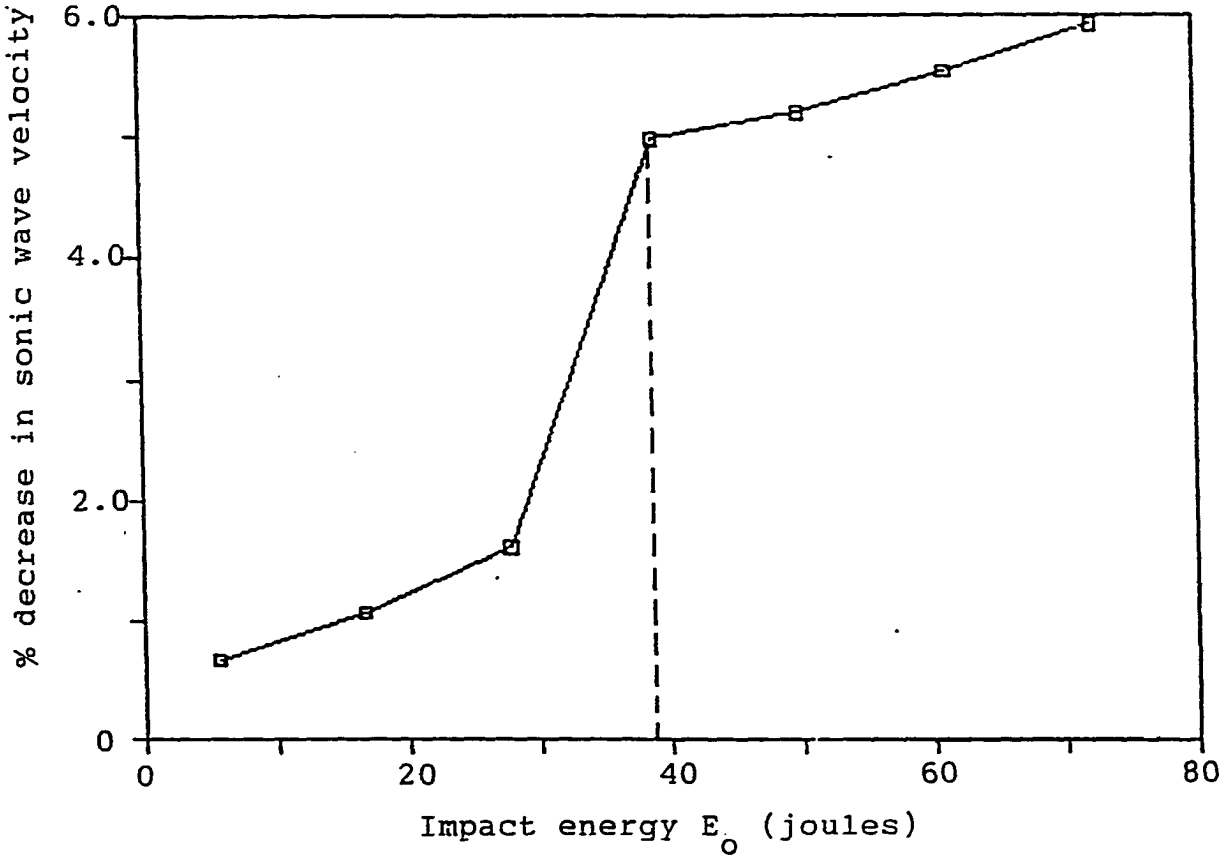

Figure 23. Percentage decrease in sonic wave velocity caused by single impacts at various energy levels, Sunset Red Granite (critical impact energy = 38.93 J)

Table 9. Results of single impact tests on Anamosa Yellow Limestone

Impact energy E_{oc} (joules)	% Decreases in sonic velocity	Rebound ratio h'/h	Energy transfer $K_1 = 1-(h'/h)$	% Decrease in point load resistance
5.56	0.36	0.080	0.920	10.0
16.69	0.46	0.067	0.933	25.0
27.81=E_{oc}	0.96	0.020	0.980	40.0
38.93	1.04	0.014	0.986	50.0
50.06	1.76	0.011	0.989	70.0
61.18	4.96	0.004	0.996	70.0
72.31	5.04	0.003	0.997	88.0

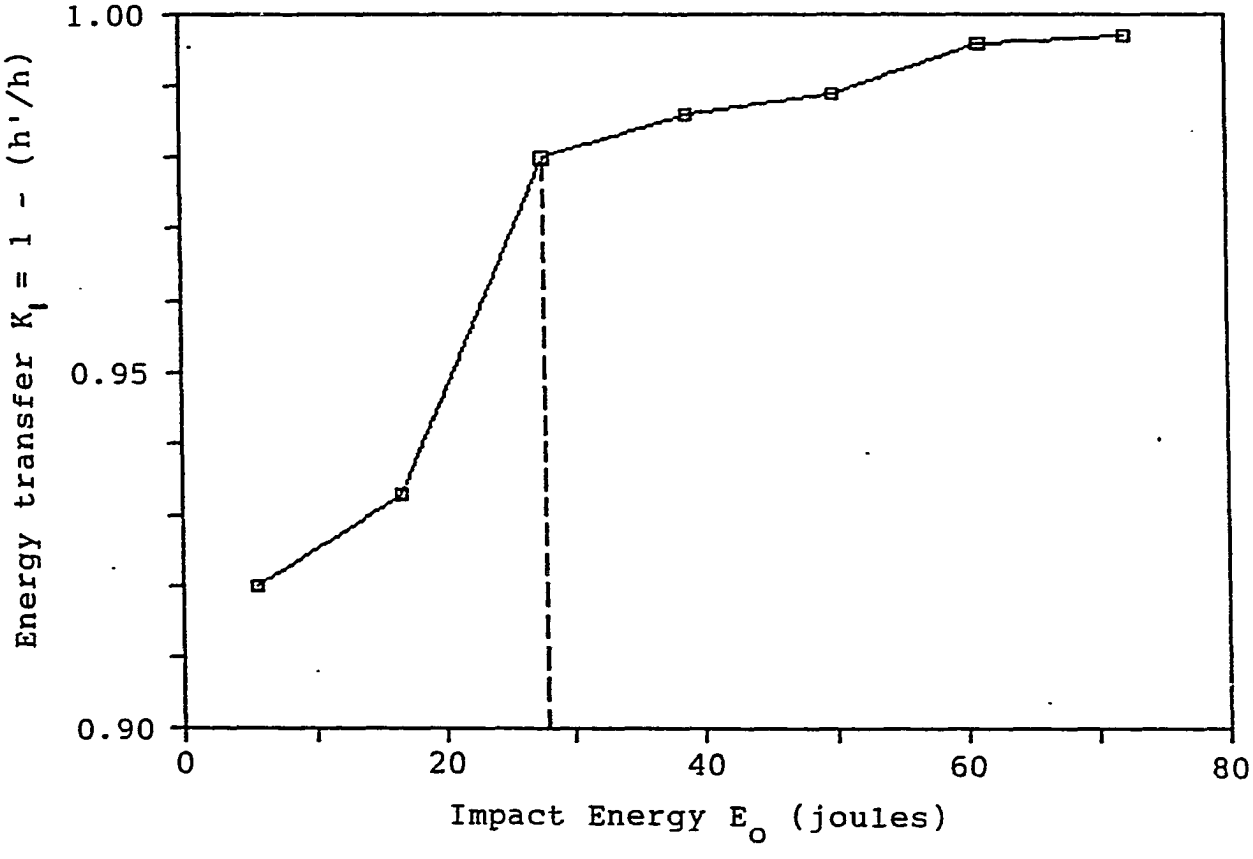

Figure 24. Energy transfer at various single impact energies, Anamosa Yellow Limestone (critical impact energy = 27.81 J)

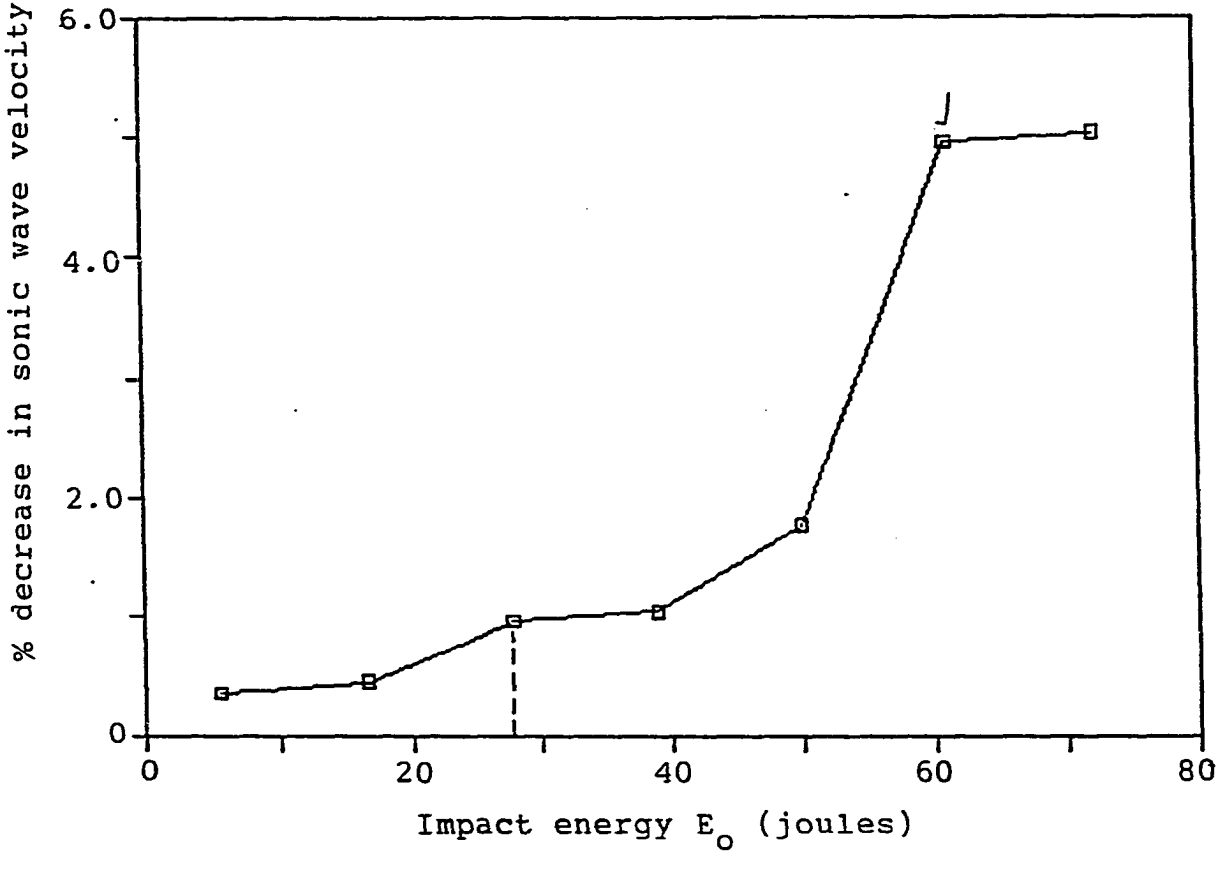

Figure 25. Percentage decrease in sonic wave velocity caused by single impacts at various energy levels, Anamosa Yellow Limestone (critical impact energy = 27.81 J)

Above this critical impact energy, sonic wave velocities do not decrease significantly with increase in the energy of single impact. Crushing becomes an important deformation mode in this region. This implies that in addition to the development of cracks, separated rock material is crushed extensively.

The existence of a critical impact energy for each rock is confirmed by the match between sharp decreases in both the rebound ratio, h'/h, and sonic wave velocity at the same impact energy level, for all the rocks except Anamosa Yellow Limestone. Tables 4 through 8 show these matches. Table 9 indicates development of delayed cracking in the same rock. This rock is very porous and friable, with a tendency to soften and disintegrate when cut with a water-cooled electric saw. Such a behavior may have inhibited crack growth but promoted extensive crushing almost to the scale of punching failure.

B. Strength Degradation Test Results

Further confirming the initial concept, decreases in point load resistance of impacted rock samples show similar trends to the rebound ratio and sonic wave velocity data. Comparisons are made in Table 10. A complete set of results for all the rocks tested is presented in Table 11. Within

the sub-critical impact energy range, only minimal percentage (up to 10%) decreases in point load resistance result. An exception is Anamosa Yellow Limestone for reasons earlier given. For each rock, at and above the critical impact energy, the decrease in point load resistance is high (about 40% to 75%).

Figures 26 through 31 illustrate the significance of rebound ratios with respect to percentage decreases in point load resistance values for the six rocks tested. The scatter in the plots can be explained by the fact that both parameters plotted were dependent variables in the experiments. Nevertheless, it can be observed that strength reduction for rebound ratios in the sub-critical impact energy range is more predictable. This is the range for a predominantly elastic impact. Above the critical energy, greater degrees of scatter are observed for most of the rocks. The complex combination of cracking and extensive crushing of composite materials like rocks introduces unpredictability in the latter case.

If the rebound method is used to measure rock strength parameters such as dynamic hardness and dynamic modulus of elasticity, tests should be conducted below the critical impact energy. To measure strength variation among a

Table 10. Comparisons of impact energy at intense cracking (sonic wave velocity tests), critical impact energy (rebound tests), and impact energy at sharpest % decrease in point load resistance

Rock	R_o σ_o (MPa)	Lowest impact energy at intense cracking obtained from sonic wave measurements (joules)	Rebound critical energy E_{oc} (joules)	Lowest impact energy at sharpest % decrease in point load resistance (joules)
Centerville Grey Limestone, Iowa	23.460	61.18	61.18	61.18
Academy Black Granite, Minnesota	16.682	50.06	50.06	50.06
Lac Du Bonnet Granite, Canada	13.391	38.93	38.93	38.93
Rockville Granite, Minnesota	10.924	38.93	38.93	38.93
Sunset Red Granite Texas	10.170	38.93	38.93	38.93
Anamosa Yellow Limestone, Iowa	6.952	61.18	27.81	27.81

Table 11. Point load resistance values for each rock before impact and after various levels of single impact

Rock	Point load resistance (newtons).							
	Impact energy E_o (joules)							
	0	5.56	16.69	27.81	38.93	50.06	61.18	72.31
Centerville Grey Limestone	17,792	17,570	17,347	17,481	16,902	16,458	4,448	4,226
Academy Black Granite	15,902	15,568	15,123	15,123	14,678	8,889	8,006	8,006
La Du Bonnet Granite	13,344	13,344	12,454	12,232	8,006	7,228	6,447	5,782
Rockville Granite	12,899	12,677	12,454	11,787	7,784	6,783	6,338	5,560
Sunset Red Granite	10,564	9,674	9,118	8,896	7,117	6,450	5,782	5,115
Anamosa Yellow Limestone	2,224	2,002	1,668	1,334	1,112	667	667	267

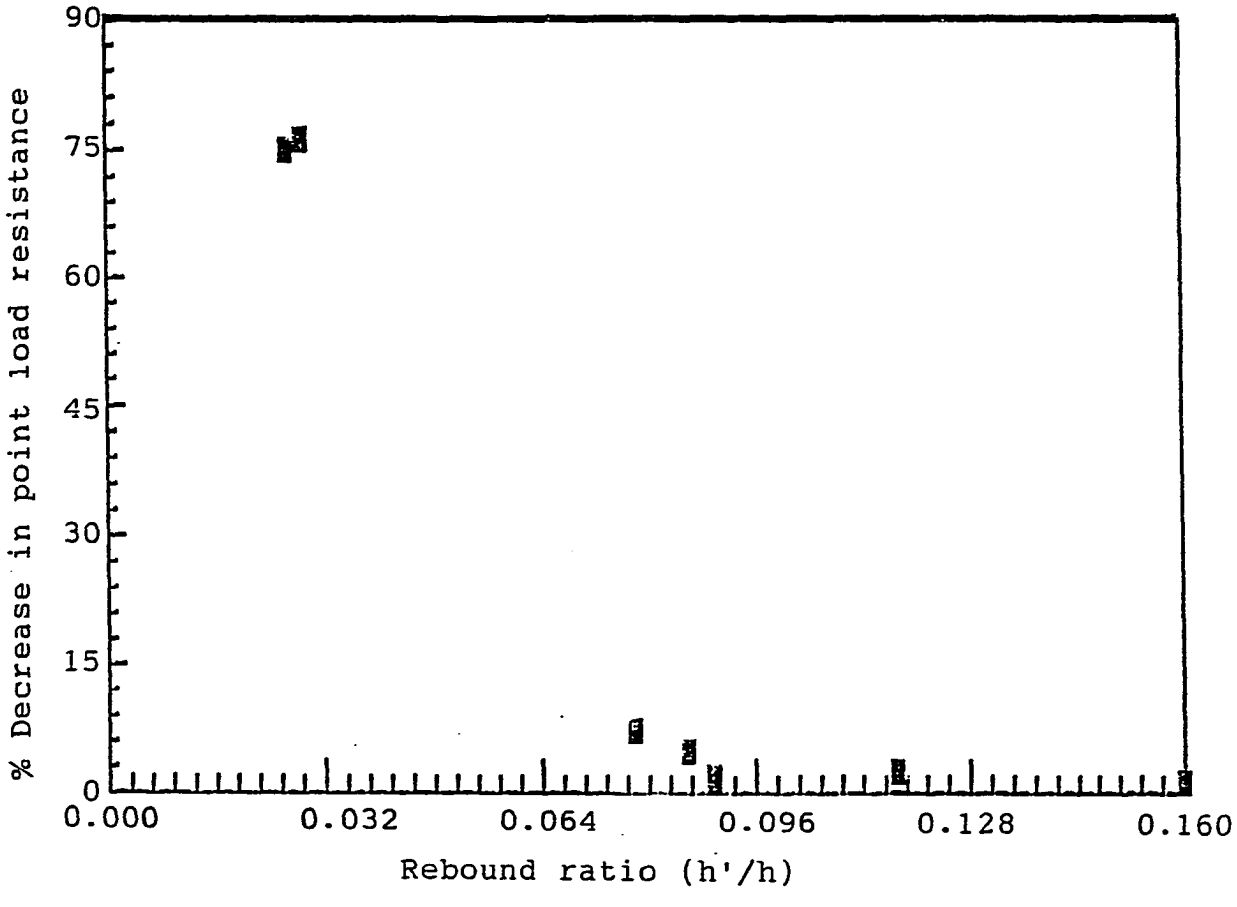

Figure 26. Relationship between hammer rebound ratio and residual rock strength, single impacts, Centerville Grey Limestone

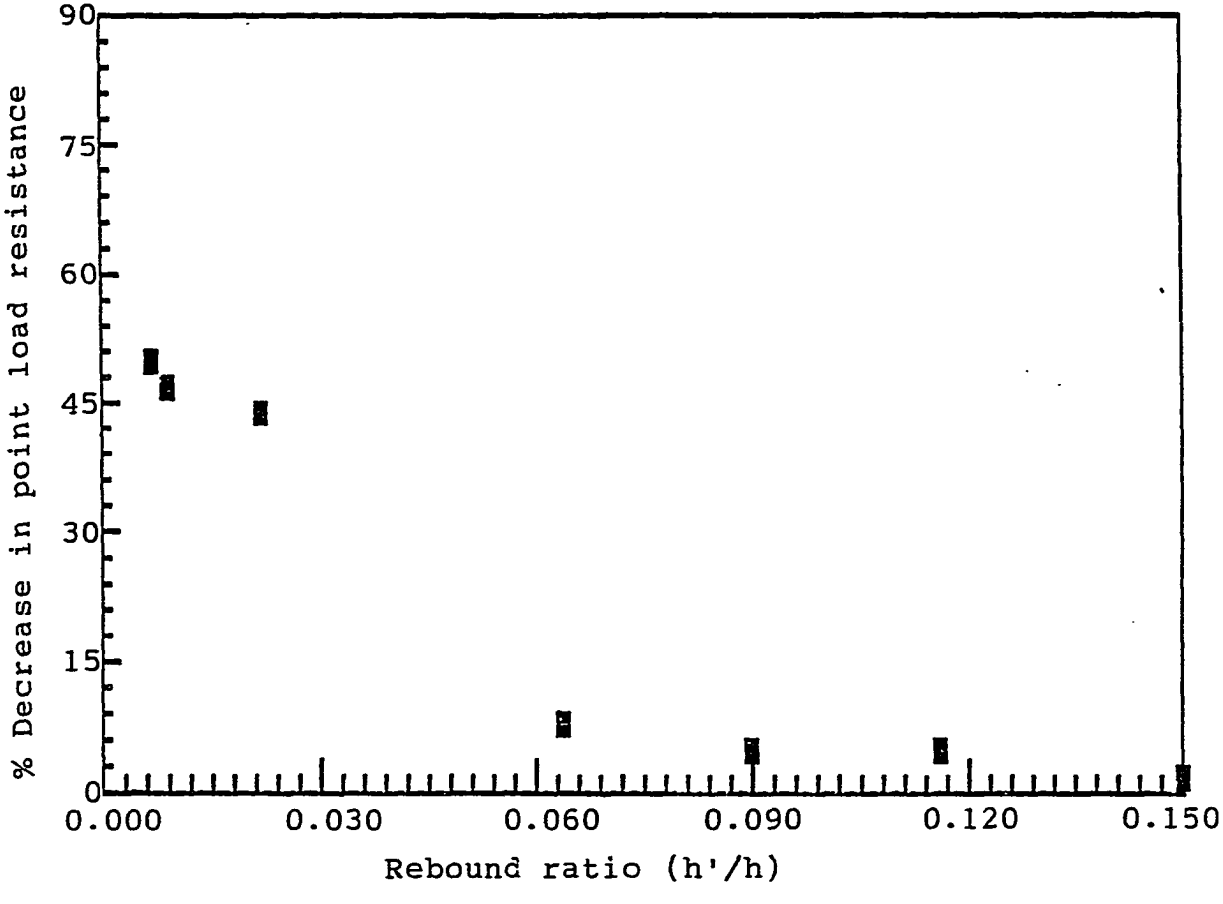

Figure 27. Relationship between hammer rebound ratio and residual rock strength, single impacts, Academy Black Granite

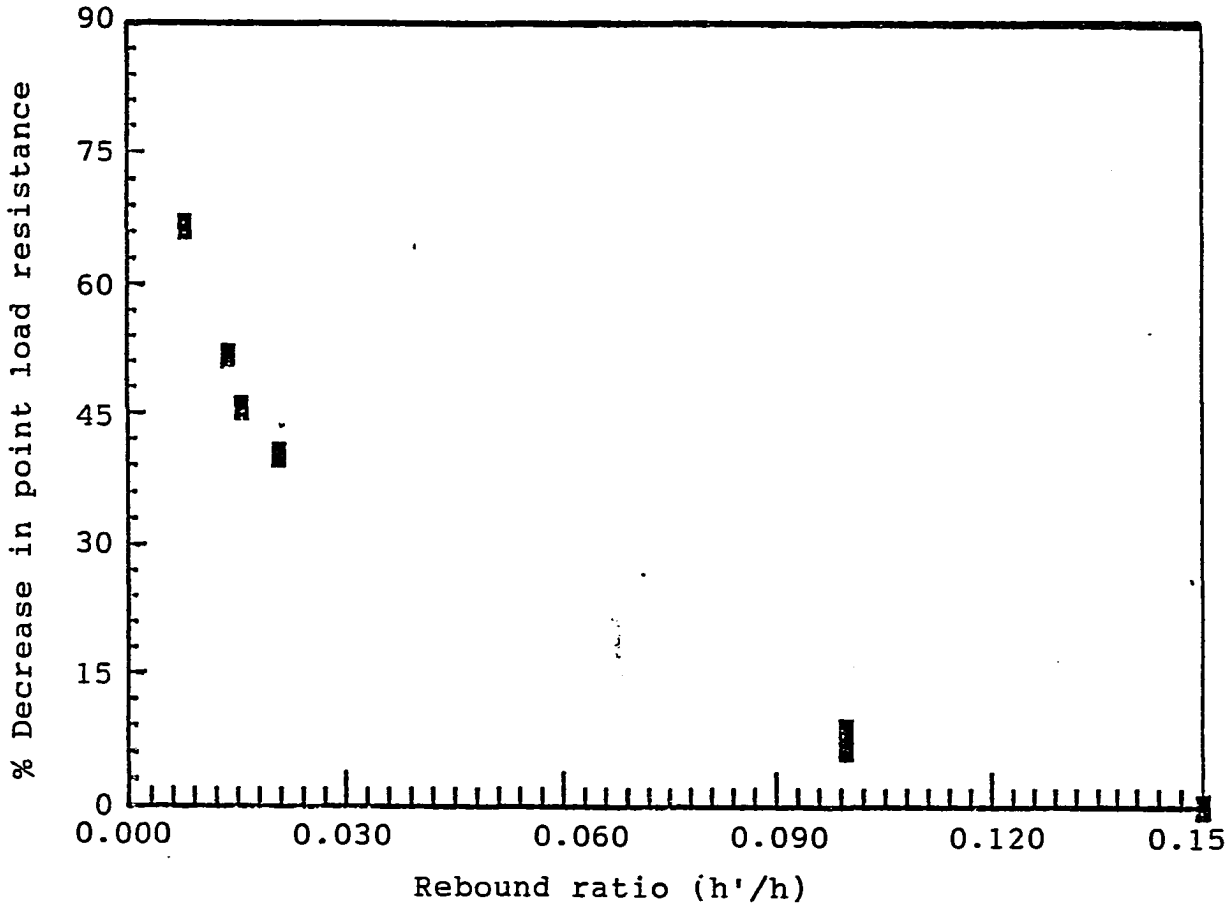

Figure 28. Relationship between hammer rebound ratio and residual rock strength, single impacts, Lac Du Bonnet Granite

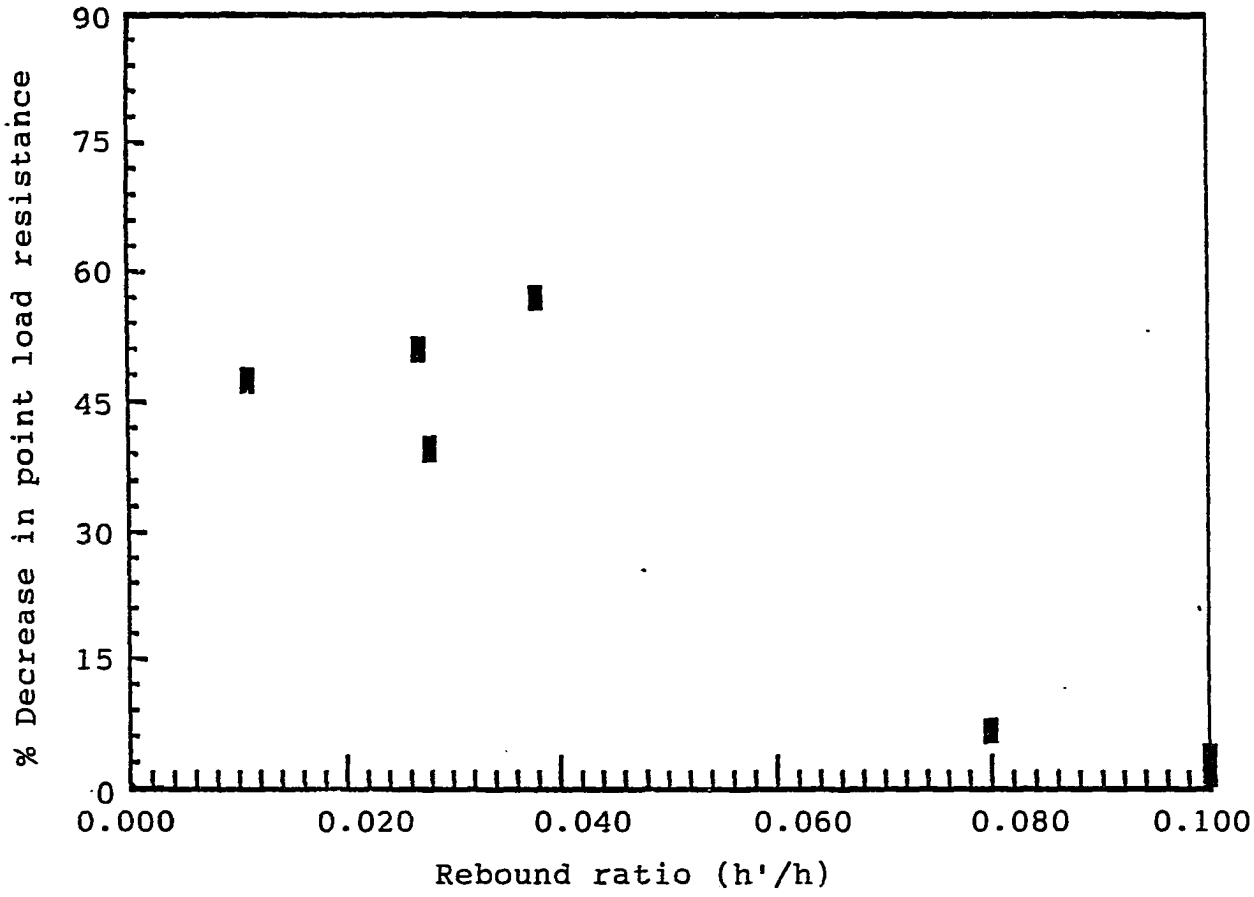

Figure 29. Relationship between hammer rebound ratio and residual rock strength, single impacts, Rockville Granite

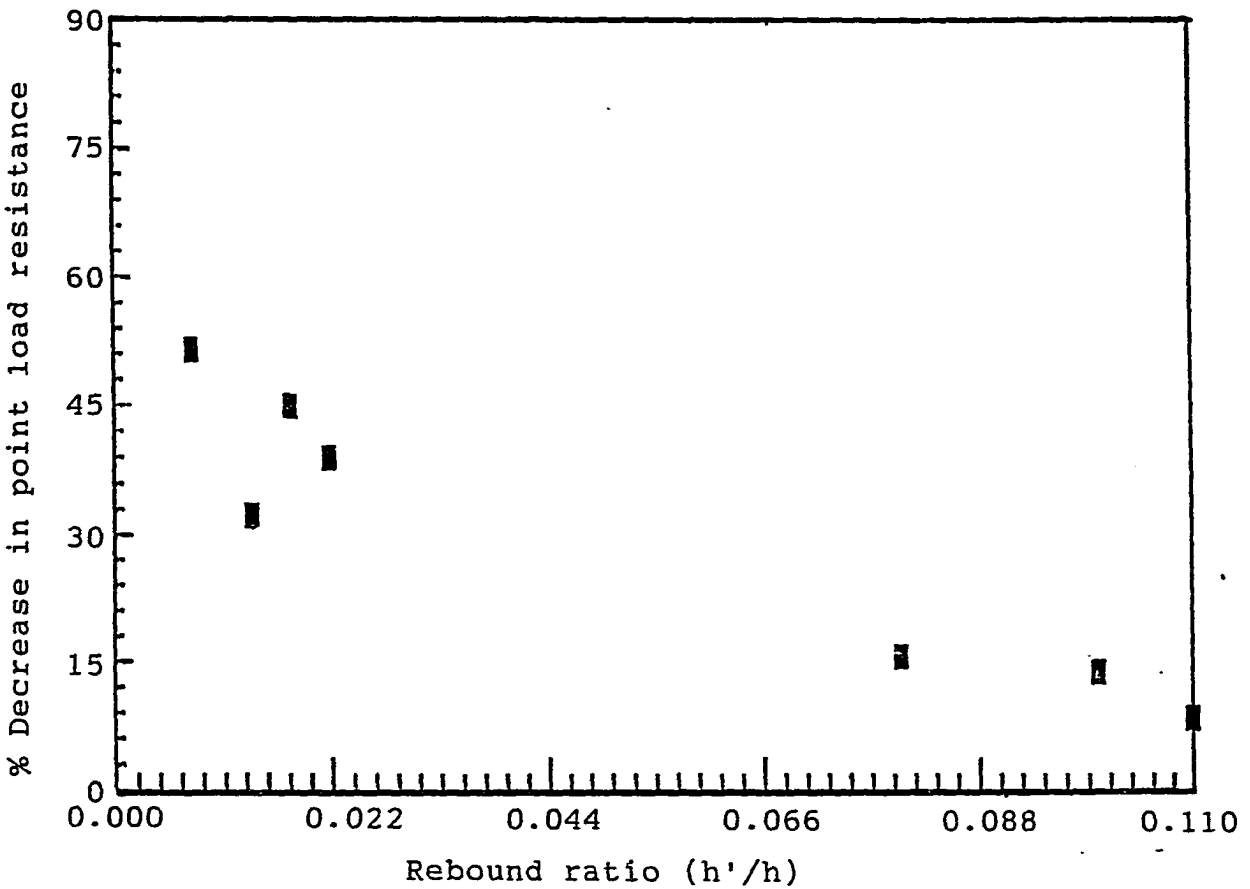

Figure 30. Relationship between hammer rebound ratio and residual rock strength, single impacts, Sunset Red Granite

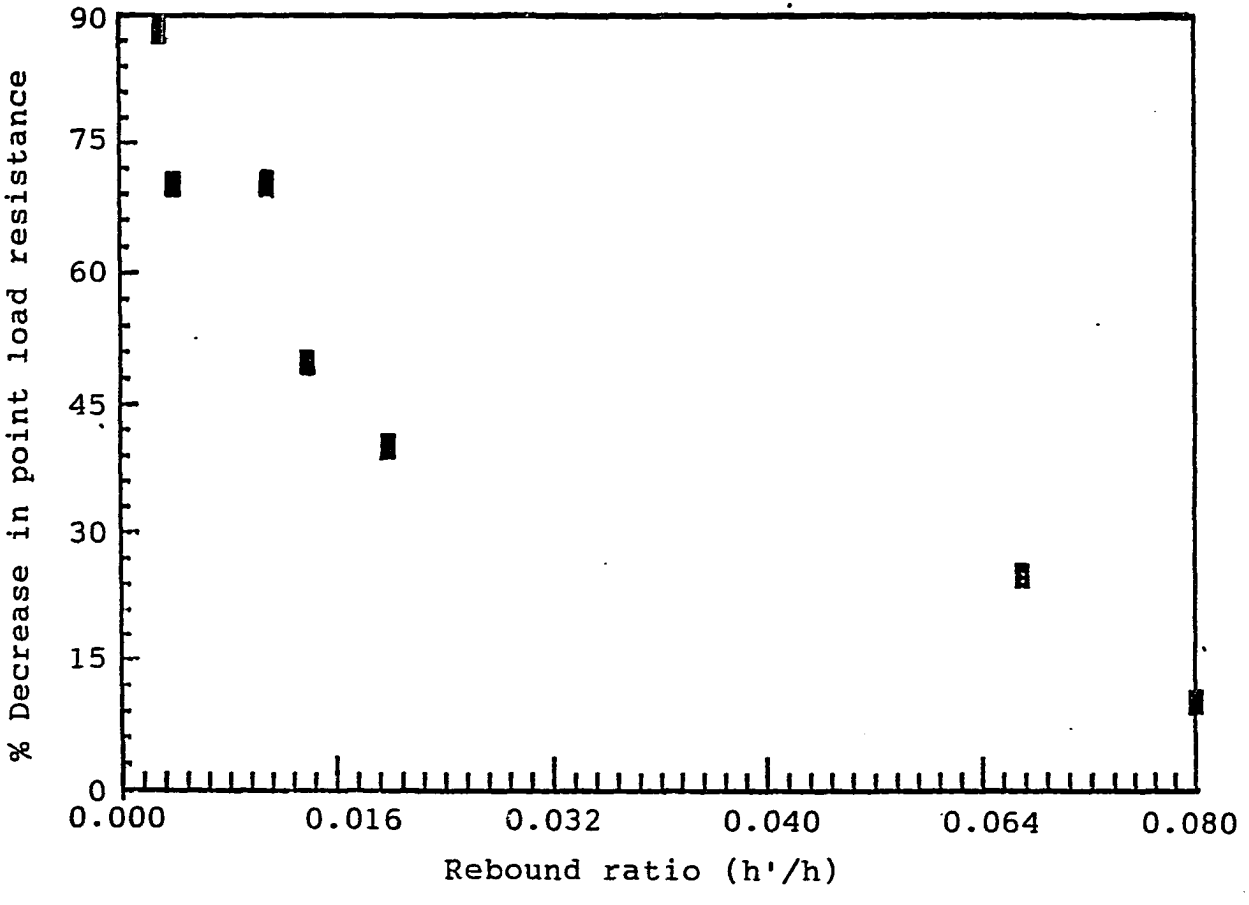

Figure 31. Relationship between hammer rebound ratio and residual rock strength, single impacts, Anamosa Yellow Limestone

variety of rocks, impact energy (E_o) and drop height (h) must be kept constant, as usually done with the Schmidt Rebound Hammer (ASTM C805). The rebound heights, h', would then be a measure of various rock strength parameters including dynamic hardness and dynamic modulus of elasticity.

C. Effectiveness of Repeated Blows at Sub-critical Impact Energy

Results of repeated single impact tests on all rocks at energy levels below critical are shown in Tables 12 through 17. These results indicate that less than 6% increase in energy transfer is produced. Generally, the increases in energy transfer are larger for impact repetitions at higher sub-critical energy levels.

These test results confirm that the energy required to extend flaws in a rock must be supplied in a single high energy blow rather than by repetition of several low energy blows. For the same loading device, the flaw size distribution within each rock defines its strength.

Table 12. Results of tests to evaluate the effectiveness of repeated single impacts at sub-critical energy on Centerville Grey Limestone (critical energy = 61.18 J)

Impact energy E_o (joules)	Rebound ratio, h'/h		Energy transfer $K_1 = 1-(h'/h)$		% change in K_1
	single impact	double impact	single impact	double impact	
5.56	0.160	0.160	0.840	0.840	0
16.69	0.117	0.117	0.883	0.883	0
27.81	0.090	0.080	0.910	0.020	+1.1
38.93	0.086	0.071	0.914	0.929	+1.6
50.06	0.078	0.056	0.922	0.944	+2.4

Table 13. Results of tests to evaluate the effectiveness of repeated single impacts at sub-critical energy on Academy Black Granite (critical energy = 50.06 J)

Impact energy E_o (joules)	Rebound ratio, h'/h		Energy transfer $K_1 = 1-(h'/h)$		% change in K_1
	single impact	double impact	single impact	double impact	
5.56	0.150	0.150	0.850	0.850	0
16.69	0.116	0.100	0.884	0.900	+1.8
27.81	0.090	0.060	0.910	0.940	+3.3
38.93	0.064	0.050	0.936	0.950	+1.50
50.06	-----	-----	-----	-----	-----

Table 14. Results of tests to evaluate the effectiveness of repeated single impacts at sub-critical energy on Lac Du Bonnet Granite (critical energy = 38.93 J)

Impact energy E_o (joules)	Rebound ratio, h'/h		Energy transfer $K_1 = 1-(h'/h)$		% change in K_1
	single impact	double impact	single impact	double impact	
5.56	0.150	0.150	0.850	0.850	0
16.69	0.100	0.083	0.900	0.917	+1.9
27.81	0.100	0.090	0.900	0.910	+1.1
38.93	-----	-----	-----	-----	-----
50.06	-----	-----	-----	-----	-----

Table 15. Results of tests to evaluate the effectiveness of repeated single impacts at sub-critical energy on Rockville Granite (critical energy = 38.93 J)

Impact energy E_o (joules)	Rebound ratio, h'/h		Energy transfer $K_1 = 1-(h'/h)$		% change in K_1
	single impact	double impact	single impact	double impact	
5.56	0.100	0.100	0.900	0.900	0
16.69	0.100	0.067	0.900	0.933	+3.67
27.81	0.080	0.060	0.920	0.940	+2.17
38.93	-----	-----	-----	-----	-----
50.06	-----	-----	-----	-----	-----

Table 16. Results of tests to evaluate the effectiveness of repeated single impacts at sub-critical energy on Sunset Red Granite (critical energy = 38.93 J)

Impact energy E_o (joules)	Rebound ratio, h'/h		Energy transfer $K_1 = 1-(h'/h)$		% change in K_1
	single impact	double impact	single impact	double impact	
5.56	0.110	0.110	0.890	0.890	0
16.69	0.100	0.083	0.900	0.917	+1.9
27.81	0.080	0.050	0.920	0.950	+3.3
38.93	-----	-----	-----	-----	-----
50.06	-----	-----	-----	-----	-----

Table 17. Results of tests to evaluate the effectiveness of repeated single impacts at sub-critical energy on Anamosa Yellow Limestone (critical energy = 27.81 J)

Impact energy E_o (joules)	Rebound ratio, h'/h		Energy transfer $K_1 = 1-(h'/h)$		% change in K_1
	single impact	double impact	single impact	double impact	
5.56	0.080	0.040	0.920	0.960	+4.34
16.69	0.007	0.013	0.933	0.987	+5.78
27.81	-----	-----	-----	-----	-----
38.93	-----	-----	-----	-----	-----
50.06	-----	-----	-----	-----	-----

D. Comparison of Calculated and Experimental Critical Energy Values

Equation (32) is the general relationship for the estimation of the critical impact energy, E_{oc}, for rocks. When numerical values of various Rock Fracture Hammer (RFH) properties are plugged in, equation 33 results. Use of equation (33) requires choice of a suitable value for X, the impulse loading factor, discussed earlier.

For the rocks investigated, the best fit value for X is 12.Ø63. This value falls within the range of 6.5 to 13.Ø reported for a variety of rocks by Rinehart (1966). Using an X value of 12.Ø63 for all the rocks, calculated E_{oc} values are compared with experimental E_{oc} values in Table 18. Considering rock inhomogeneity and the complexities of stress wave transmission and reflections through steel rods, there is some agreement between estimated and experimental E_{oc} values. The resulting correlation coefficient, r^2, is Ø.92. Plots for all six rock types are shown in Figure 32. The only sedimentary rocks tested were Centerville Grey Limestone and Anamosa Yellow Limestone. Figure 32 shows that estimated and experimental values of E_{oc} for these two rocks vary significantly.

Table 18. Comparison of experimental and calculated critical impact energy values at a dynamic loading factor (X value) of 12.Ø63 (correlation coefficient = Ø.92)

Rock	$R_o \sigma_o$ (N/m^2)	Experimental E_{oc} (Joules)	Calculated E_{oc} at X = 12.063 (Joules)
Centerville Grey Limestone	2.346×10^7	61.18	109.87
Academy Black Granite	1.668×10^7	50.06	55.54
Lac Du Bonnet Granite	1.340×10^7	38.93	35.85
Rockville Granite	1.100×10^7	38.93	24.16
Sunset Red Granite	1.020×10^7	38.93	20.77
Anamosa Yellow Limestone	6.952×10^6	27.81	9.65

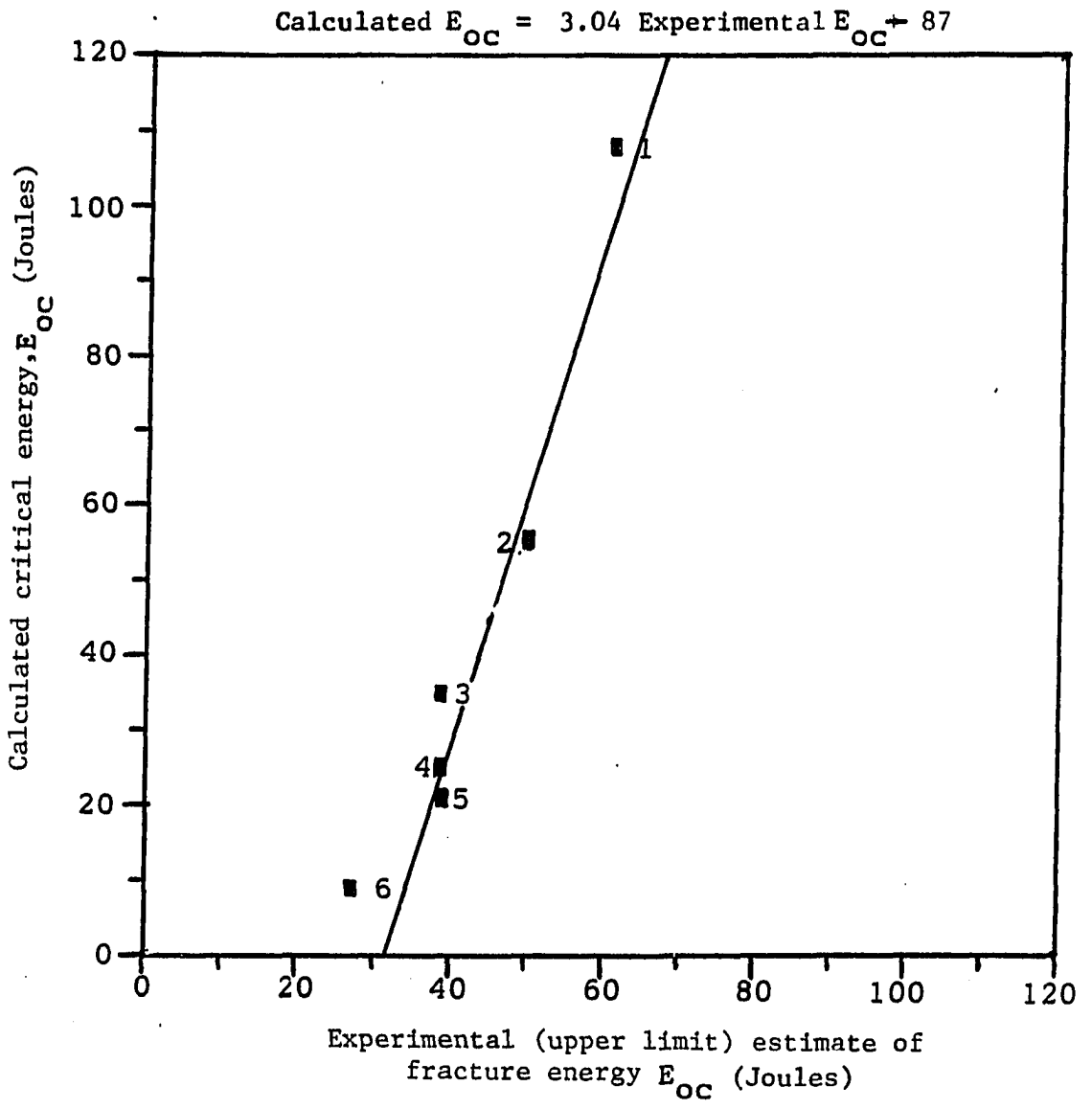

1. Centerville Grey Limestone
2. Academy Black Granite
3. Lac Du Bonnet Granite
4. Rockville Granite
5. Sunset Red Granite
6. Anamosa Yellow Granite

Figure 32. Plots of experimental versus calculated critical impact energies for the rocks investigated in this study

For Centerville Grey Limestone, an experimental value of 61.18 Joules was obtained; the calculated value for this rock is 109.87 Joules. The difference observed may be due to the influences of bedding planes in the rock, which ranged in spacing from 2 to 4 cm and were clearly visible. Because of these weakness planes, Centerville Grey Limestone, cracked at a lower impact energy than would have been estimated from its calculated material strength. Anamosa Yellow Limestone is porous and friable and tends to compact rather than fracture. This explains the observed disparity between the calculated and measured critical impact energies.

To determine impulse loading factor for each rock, computations were made using the following relationship;

$$X = (E_{oc}/(1.3719 \times 10^{-15})(R_o\sigma_o)^{0.5}$$

where X = impulse loading factor of rock

E_{oc} = experimental critical impact energy of rock (Joules)

R_o = brittleness ratio; i.e., the ratio of tensile to compressive strength

σ_o = compressive strength under static loading conditions

Results are as shown in Table 19. Computed values of X range from 9.002 for Centerville Grey Limestone to 20.480

Table 19. Experimental impulse loading factors for rocks investigated in this study

ROCK	$R_o \sigma_o$ (N/m^2)	Experimental impulse loading factor X
Centerville Grey Limestone	2.348×10^7	9.002
Academy Black Granite	1.668×10^7	11.452
Lac Du Bonnet Granite	1.340×10^7	12.571
Rockville Granite	1.100×10^7	15.314
Sunset Red Granite	1.020×10^7	16.515
Anamosa Yellow Limestone	6.952×10^6	20.480

for Anamosa Yellow Limestone, implying that the dynamic strength of rock can be as much as twenty times greater than the quoted static strength values.

E. Radius of the Fractured Zone

Results of impact spacing tests on Academy Black Granite and Lac Du Bonnet Granite are shown in Figures 33 and 34, respectively. Actual sonic wave transit times before and after impact at critical energy are shown along with percentage increases in Figures 12 and 13. These results indicate that the radius of the fractured zone for brittle rocks can range from 4 to 7 cm. Direction AB is more fractured than direction CD in Academy Black Granite. The reverse is true for Lac Du Bonnet Granite. Furthermore, the lateral extent of the fractures vary with direction. These two observations are attributable to rock anisotropy. Preferred orientation of minerals within the rocks could make some directions more prone to fracture than others.

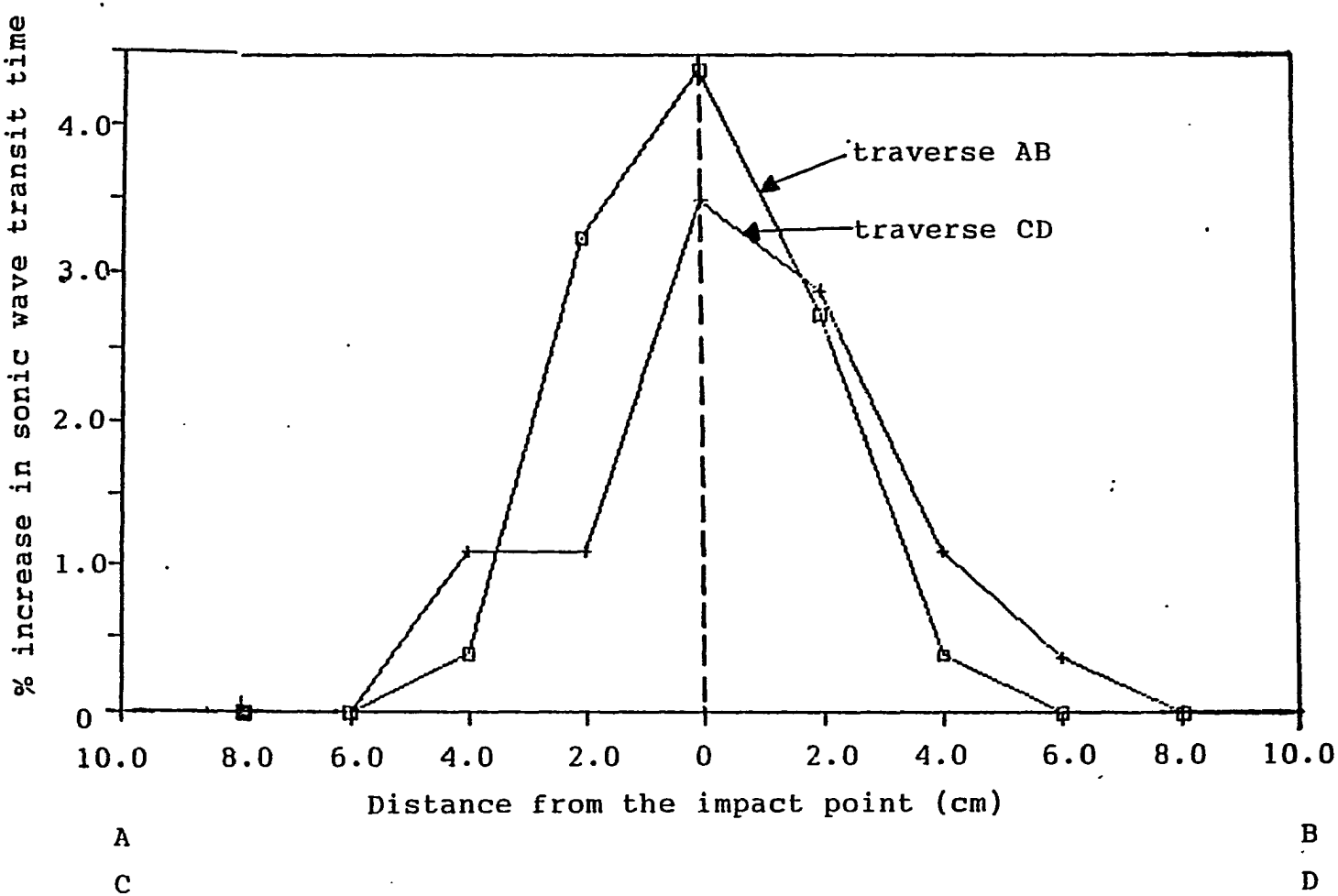

Figure 33. Radius of fractured zone around point of impact, single critical energy impact, Academy Black Granite (critical impact energy = 50.06 J)

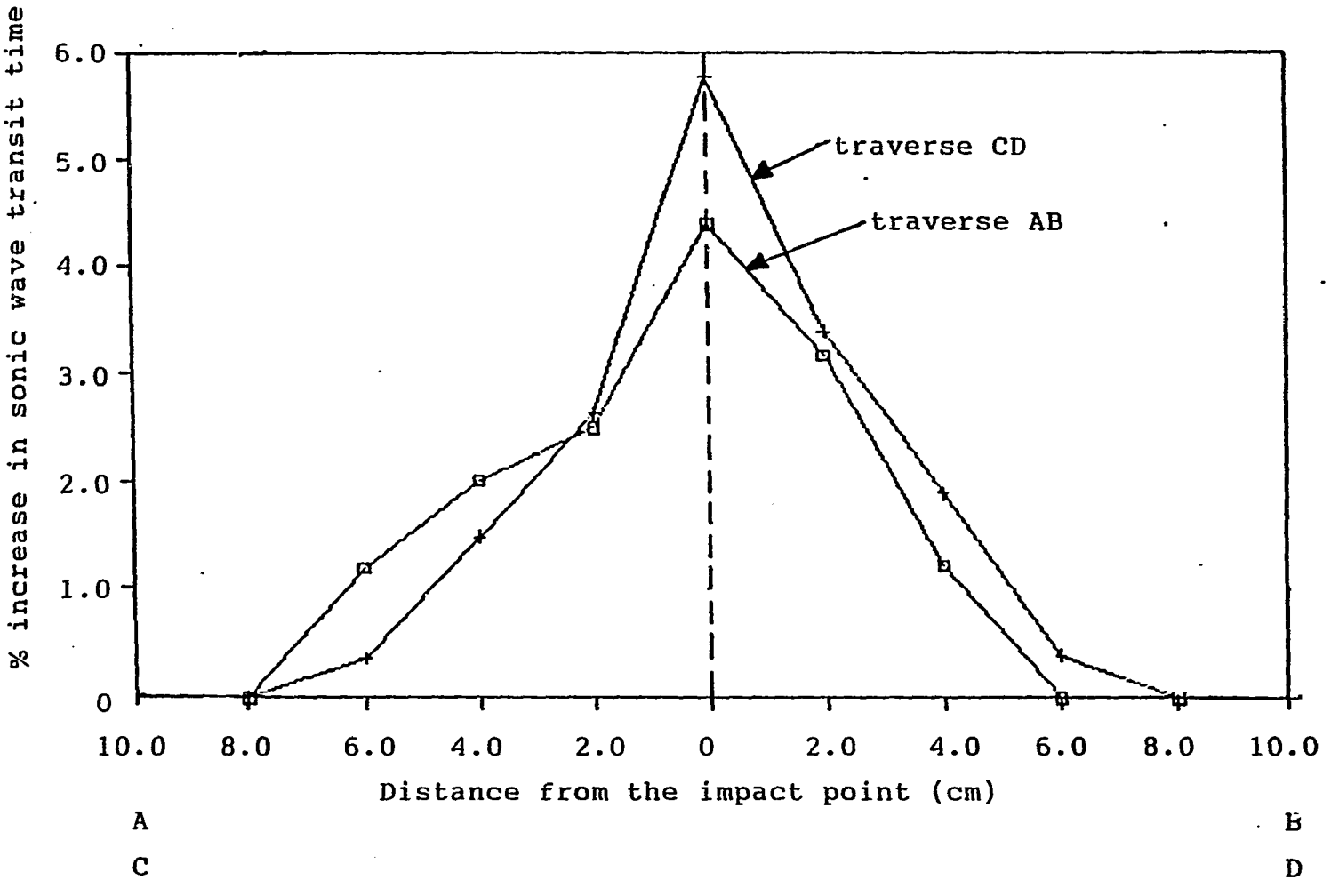

Figure 34. Radius of fractured zone around point of impact, single critical energy impact, Lac Du Bonnet Granite (critical impact energy = 38.93 J)

V. APPLICATION TO TRENCHING

A. The Rotary Trencher

A typical boom type rotary trencher is shown in Figure 35. The cutting unit consists of a boom which terminates in a wheel; a chain with drag bits spaced along its length is wound around the boom. The boom is hinged at the tractor end and can be lowered into a trench for continuous cutting.

To excavate a trench, the boom is forced against the rock surface such that the drag bits come in contact with the surface. The thrust or vertical force on the bits is primarily due to the pulling force exerted by the tractor traveling in the direction of trench advance. The rotary action of the wheel generates drag (horizontal force). The bits then rip into the rock surface and gouge off fragments.

Hard, intact rocks require large penetration and drag forces. These force requirements appear to exceed the force exertion capacities of existing rotary trenchers. Thus, rotary trenchers are only suitable for low to medium strength rocks.

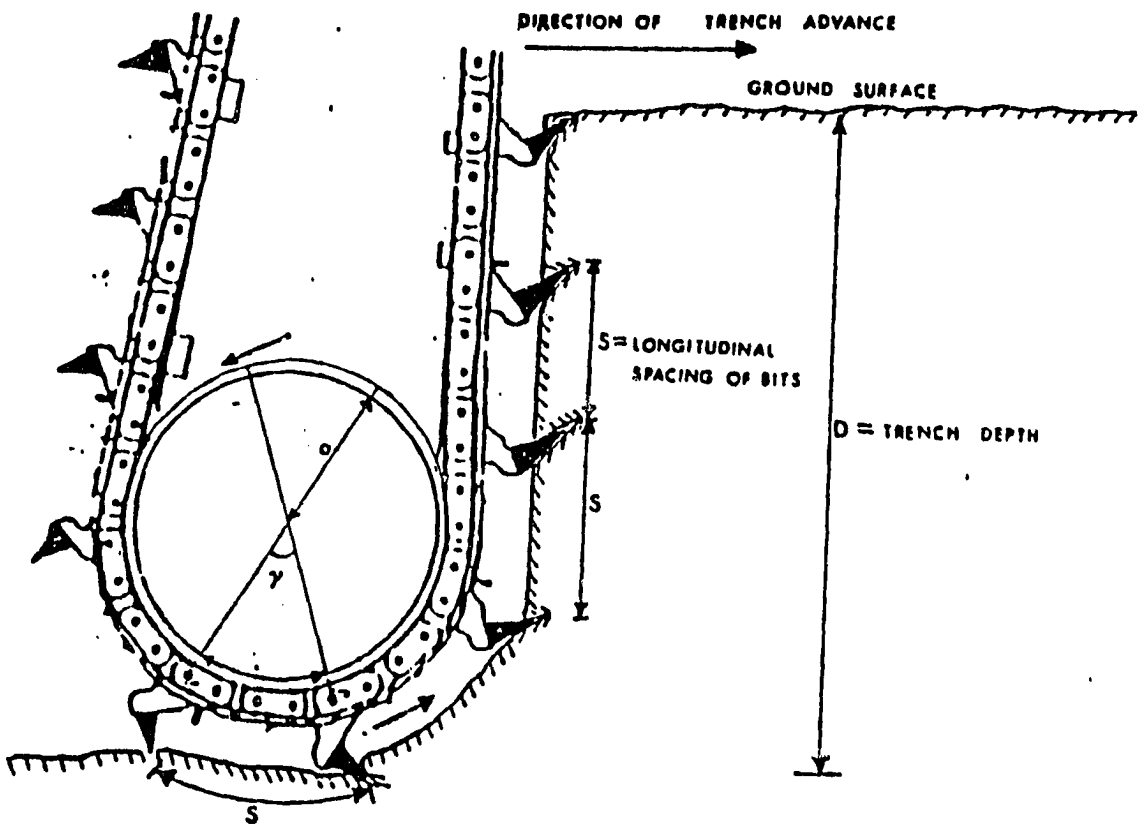

Figure 35. Boom of the available rotary trencher

B. Proposed Percussion Trencher

The proposed percussion trencher would excavate rock using both rotary action and percussive impacts. Basically, the rock surface would be weakened by percussion; this should reduce its resistance to subsequent drag bit action.

The booms of the proposed percussion trencher and the existing rotary trencher are compared in Figure 36. The rational design of the proposed percussion trencher boom is illustrated in Figure 37. Impact bits (A) are attached at hinges (B) in the revolving chain. These bits can deflect downwards and penetrate the rock when hit by pneumatically-actuated hammers (C). Each hammer is contained in a chamber (D) and its action is controlled with a spool valve (E). In turn, the spool valves are actuated by triggers (F) which ride along, on the back side of the chain.

When a trigger aligns beneath a spool valve, the spool spring (G) is compressed. This causes the valve to release pressurized air into the top section of the chamber, forcing the hammer downwards as at y. The hammer then hits the link bearing the impact bit. This makes the bit penetrate the rock surface, and should cause the rock to fracture (if the impact energy is above the minimum required value, E_{oc}).

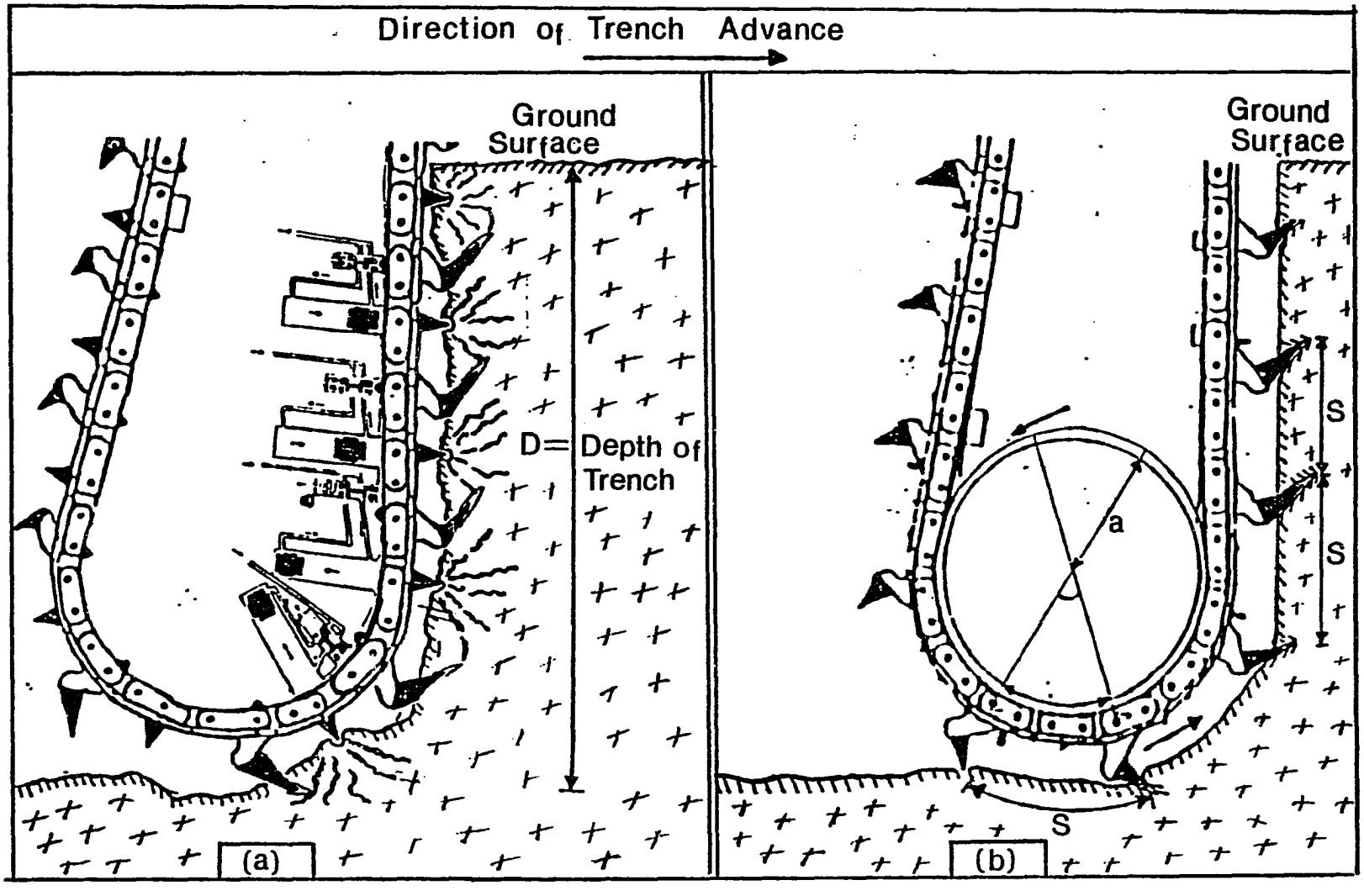

Figure 36. Proposed percussion trencher boom (a) compared with available rotary trencher boom (b)

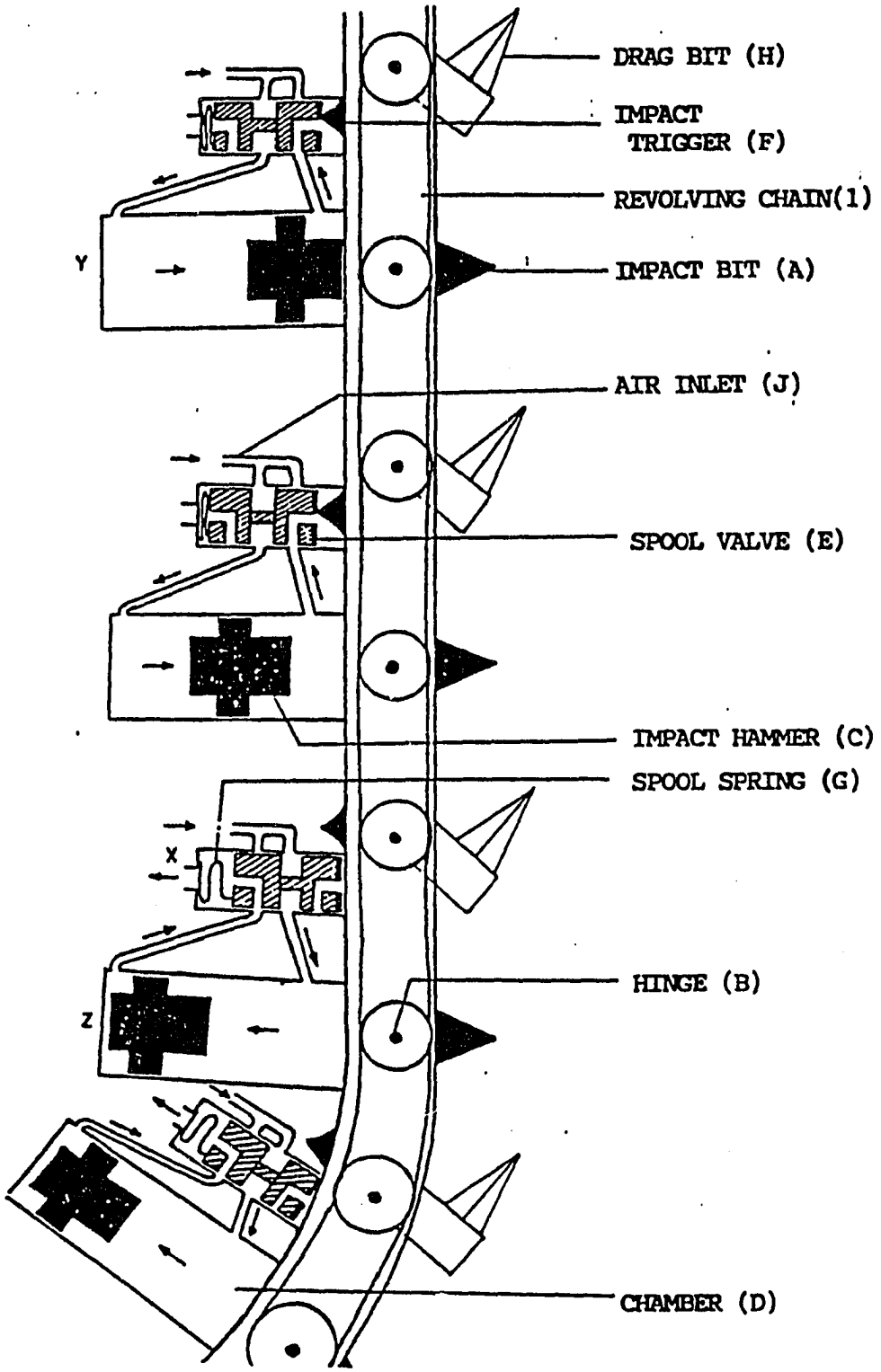

Figure 37. Impact mechanism for the proposed percussion trencher

Impact bits are attached such that when the trigger appears beneath a spool valve, an impact bit will appear beneath the associated hammer chamber (as at y). When the trigger is not beneath a spool valve (as at x), the spool spring relaxes and air movement reverses, moving the hammer moves up to the top of the chamber (as at z). This action repositions the bit for subsequent impact. These actions are synchronized over the entire boom.

The interaction between drag bits and the fractures resulting from percussive impact is shown in Figure 38.

C. Relevance of Test Results to Percussion Trencher Design and Operation

Point load test results indicate that a decrease in rock strength (as much as 75%) can result from the application of percussive impacts. Point loads approximate loading by conical or pencil-shaped drag bits. Close to the ground surface and in the presence of impact-induced flaws, bridges of intact material are largely unconfined, as illustrated in Figure 38. This situation lends some credence to the use of point load resistance as an additional test in the evaluation of impact energy effectiveness.

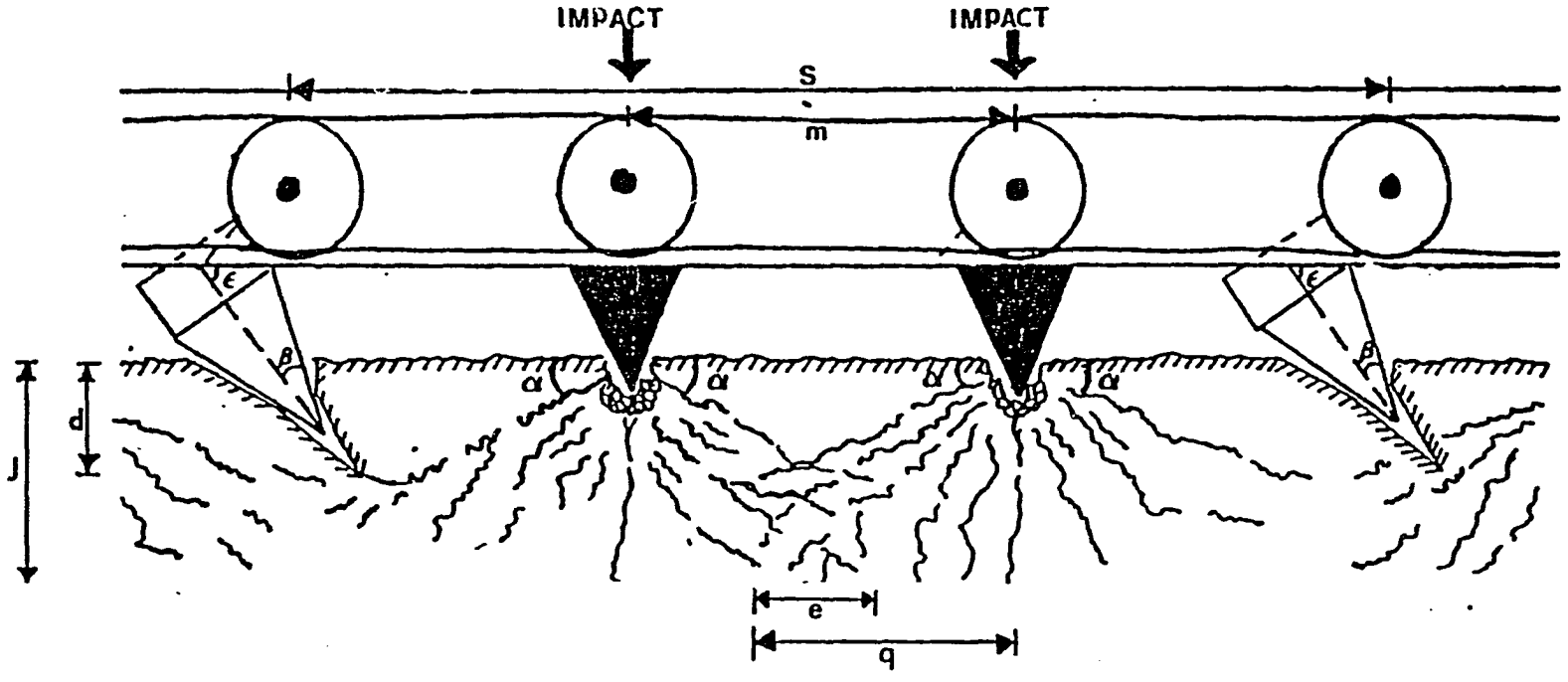

S = longitudinal spacing of drag bits

m = spacing of impact bits

j = depth of impact fracture penetration

d = depth of cut

ϵ = drag bit angle of attack

β = cone half-angle of drag bit

α = fracture angle

q = radius of zone of impact fracture

e = region of intersection of adjacent impact fracture zones

Figure 38. Interaction between impact fractures and drag bits

The design impact energy selected for the proposed percussion trencher should be high enough for breakage of rocks of a wide strength range. However, the impact energy should not be excessive; otherwise, crushing may result. The rocks investigated ranged in compressive strength, σ_o, from 61.52 MPa (8920 psi) to 203.44 MPa (29,500 psi). The brittleness ratio, R_o, ranged from 0.06 to 0.243. For these ranges of rock strength parameters, a design impact energy level of about 65 Joules would suffice, when reasonably sharp bits are used. For rocks with strength parameters that do not fall within these numerical ranges, equation (33) can be used to estimate the required impact energy. Alternatively, field tests can be conducted with the Rock Fracture Hammer (RFH) to determine the optimal impact energy level, following the recommendations given in the next subsection. The second alternative is especially important if various percussion trenchers are built, each with a rated impact energy capability. Percussion trencher selection would then be possible without rock coring and subsequent laboratory tests for strength.

An appreciation of cutting force requirements in drag bit operation is an important prerequisite for a proposal on an improvement scheme. For this reason, a conception of the

rock deformation processes under an isolated drag bit is presented. Figure 39 represents an attempt at completely relating these phenomena to the variation in bit force as the bit progresses along the cutting profile. It is common knowledge that force displacement curves for drag bits operating in brittle rocks are jagged. An example is the result of work by Morrell and Wilson (1983).

Drag bit action on rocks is a discontinuous process. It involves force build-up, indentation, fracturing, bit acceleration, and crushing. In this conception, four main zones of bit action are recognized, as shown in Figure 39. In zone 1, the bit penetrates the rock. Owing to the brittleness of most hard rocks, the depth of bit penetration is less than the depth of cut. Zone 1 should place the highest force demand on the drag bit, and hence, the machine. Secondly, it directly relates to the size of fragments removed. During normal laboratory drag bit cutting experiments, zone 1 is absent since the depth of cut is already fixed. There is no need for the penetration of the drag bit to the depth of cut in fixed depth cutting. The force peak in zone 1 is the threshold force for the development of a major fracture which could decrease in the presence of fractures caused by percussive impacts. This

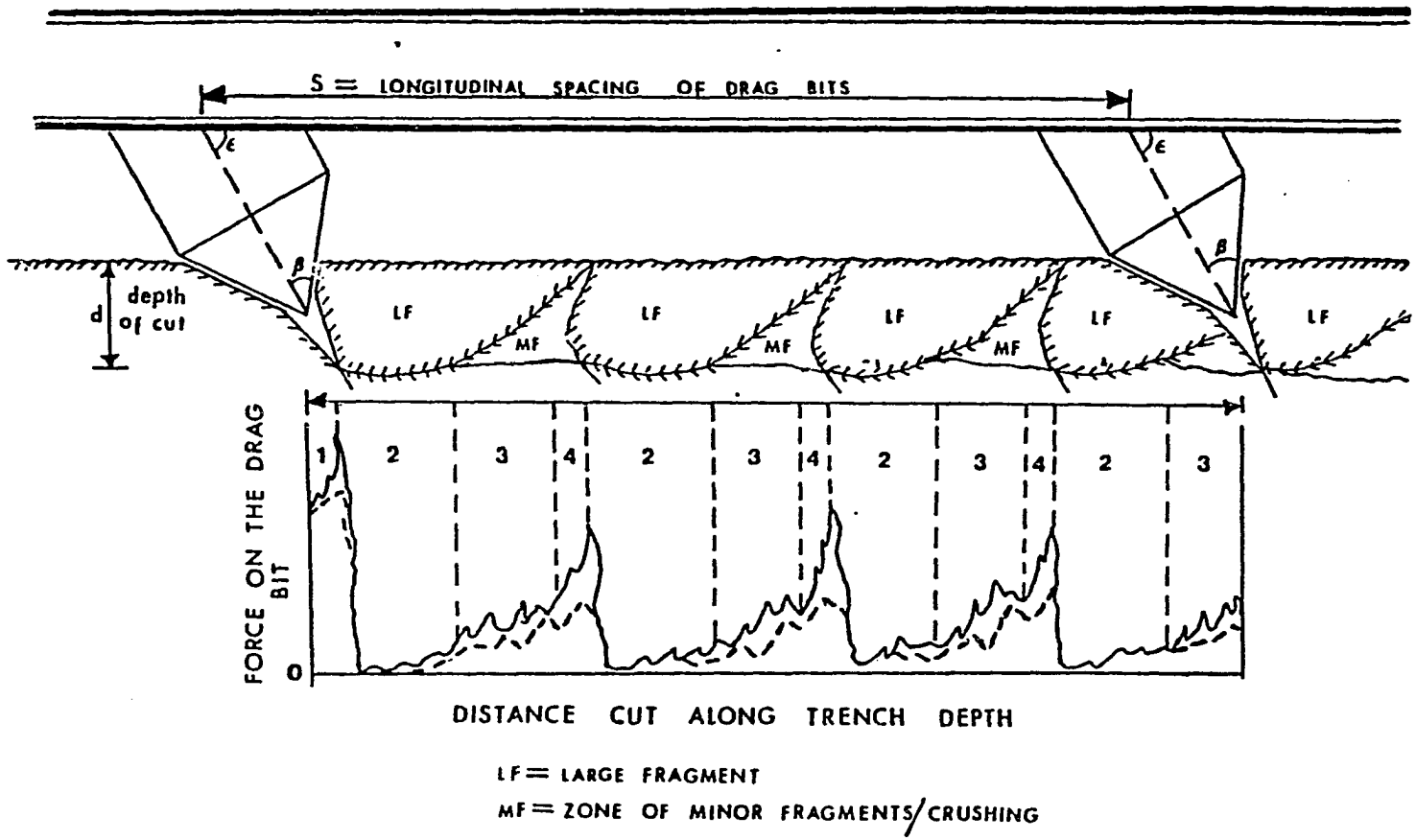

Figure 39. Comparison of the relationship between resisting forces on drag bits of the proposed percussion trencher (broken lines) and the available rotary trencher (solid lines) during rock cutting

investigation has shown that the resistance to point loads can decrease by as much as 70%. For the percussion trencher, the broken lines represent the force threshold, which is lower than that of the existing rotary trencher (solid lines) in Figure 39.

In zone 2, a major fracture develops and runs in an upward trajectory to intersect the previous cutting profile at a low angle. A large fragment, LF, results from this fracture. Simultaneously, the force on the drag bit falls rapidly to zero as the bit loses contact with the rock. The bit accelerates, thus effecting a dynamic situation until contact with the rock is re-established. Towards the end of zone 2, this contact is already sufficient for the development of friction, therefore, a build-up of resisting force occurs.

In zone 3, enough contact between the bit and the rock has been established for fracturing and local crushing to reach significant levels. In the presence of impact induced fractures, crushing, which consumes a lot of bit energy could be minimized since fragments could be dislodged before significant force build-up. Due to the geometry of the major fracture developed earlier in zone 2, the height of material to be crushed or fractured increases approximately linearly with cutting distance. The force also reflects this situation by increasing gradually.

In zones 2 and 3, the vertical force should be high enough to keep the bit in contact with the rock. The magnitude of required vertical force should be lower for the proposed percussion trencher than for the existing rotary trencher. In zone 4, minor fragmentation and crushing have reached a stage in which a ledge of rock presents itself at nearly full height. In brittle rocks, this zone may be insignificant as a major fracture would immediately develop with little or no indentation. In less brittle rocks, an indentation occurs leading to a rapid increase in the bit force. Subsequently, a major fracture develops again. Zones 2, 3 and 4 repeat for a single drag bit as many times as the longitudinal bit spacing, S, allows.

Small sized fractures may also develop below the cutting profile, parallel to the orientation of the drag bits. Next to bit penetration, indentation to the depth of cut should account for the highest force peaks during drag bit cutting. Since the penetration force is absent in laboratory fixed-depth cutting, indentation forces may represent the force peaks observed during bit advance. The resultant force discussed above can also be resolved into horizontal and vertical components.

Results of the impact spacing tests can be applied to design of the percussion trencher. As illustrated in Figure 40, three impact spacing situations can occur. Non-overlapping spacing may require high drag bit forces to dislodge fragments. Overlapping spacing may result in the removal of tiny fragments. Critical or near-critical spacing seems desirable. Results of this investigation show that q, the radius of the fractured zone at critical impact energy, ranges from 4 to 7 cm. Consequently, the optimum spacing range for impact bits is 8 to 14 cm. The impact bits could interact with drag bits as illustrated earlier in Figure 38.

Figure 41 shows three possible arrangements of drag bits for placement of impact points on the boom of the percussion trencher. These are identified as colinear, intermediate, and staggered.

In a colinear arrangement, drag bits are arranged colinearly with the impact points and cut the rock directly through these points.

In the intermediate arrangement, the drag bits cut through fractured regions between columns of impact points. Test results indicate the intensity of fracturing decreases with distance from the impact point (Figures 33 and 34), so

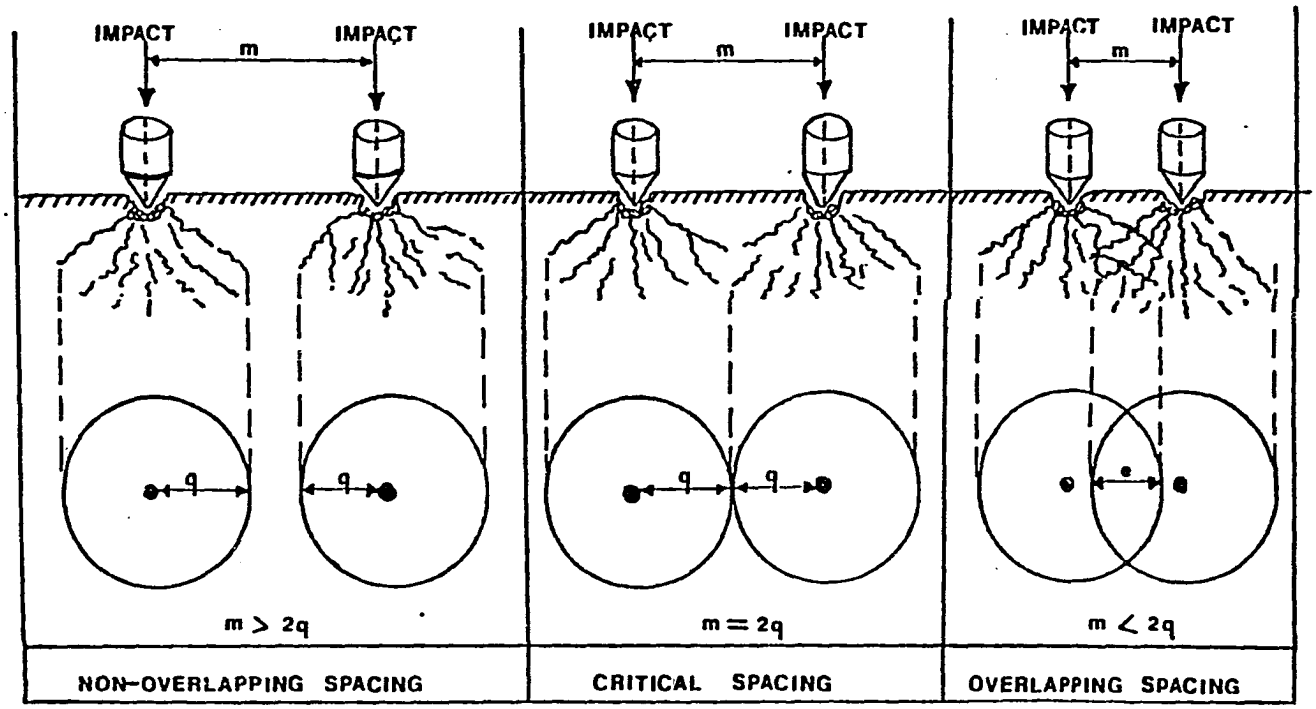

Figure 40. Effect of impact spacing on interaction of subsurface cracks in brittle rock

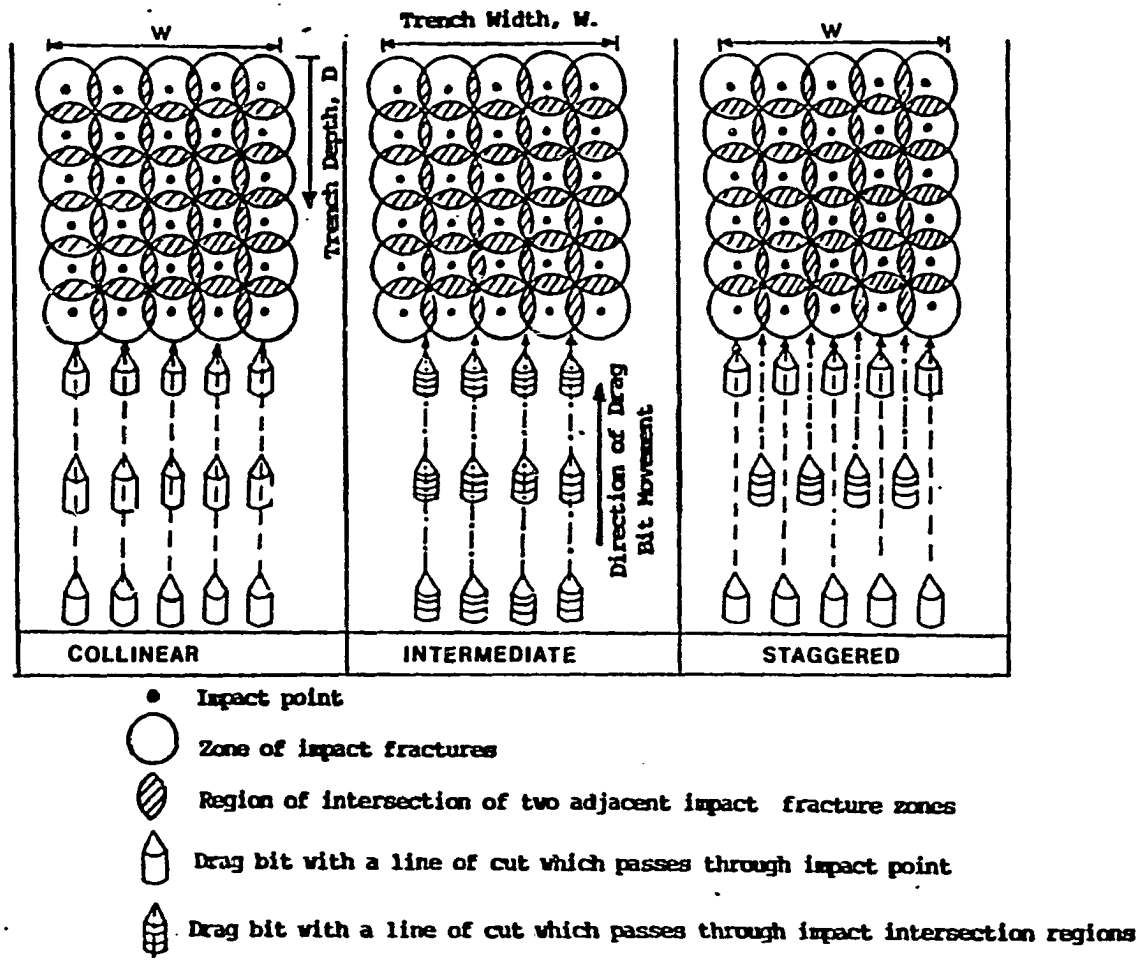

Figure 41. Alternative arrangements of drag bits on the proposed trencher boom

the bits may be predicted to encounter greater resisting forces (i.e., unbroken rock) when the intermediate arrangement is used. It is also possible that the bit would dislodge fragments between columns of impact points.

In a staggered arrangement, some bits would cut through impact points while others would cut between them. Staggering the impact points rather than the drag bit locations would be a variation of this arrangement.

In each of these configurations, rows or columns of impact points should be spaced from 8 to 14 cm apart. This spacing is proposed to ensure that the bit always cuts through regions where impact-induced fractures exist.

D. Use of the Rock Fracture Hammer (RFH) in the Field

The Rock Fracture Hammer (RFH) developed and used in this research is compact and portable but sturdy. These properties make it ideal for field measurement of impact strength of rocks, a fact which limits the need for coring and laboratory strength testing.

The philosophy underlying the use of the RFH should be differentiated from that of the Schmidt Rebound Hammer (ASTM C805), as the latter has and uses a single energy level on all rocks. Since the Schmidt Rebound Hammer only measures surface hardness and does not impose failure loads, the associated deformation is largely elastic (as required for rebound of the hammer). The rebound height, h', has been related to a number of rock strength parameters including uniaxial compressive strength and modulus of elasticity. Examples are reports by Poole and Farmer (1980), Deere and Miller (1966), Dhir and Sangha (1972), and Hucka (1965). As a result of loading in the elastic deformation range, the Schmidt Rebound Hammer is recognized as a non-destructive tester.

In contrast, the RFH is a destructive tester for rocks at various energy levels. It can impose fracture level loads on rocks. It is less sensitive to the hardness of surficial minerals in the rock. It is recommended that to evaluate rock impact resistance for percussion trencher selection, drop tests be conducted at various drop heights, h, between 0.1 m and 1.3 m. For each drop height, the rebound height, h', would be recorded. From a plot of rebound ratio, h'/h, against hammer drop height, h, similar

to that illustrated in Figure 42, the drop height corresponding to the critical impact energy, E_{OC}, can be determined as shown. Examples of this plot using data for all the rocks tested are presented in Figures 43 through 48. The percussion trencher rated somewhat above this impact energy level would then be selected for trenching in this rock.

It must, however, be emphasized that the RFH can be used only to determine the required magnitude of impact energy. It measures, largely, the rock material strength rather than the rock mass strength. In the prediction of trenching rate, rock mass strength factors such as size, orientation, and spacing of discontinuities play an important role.

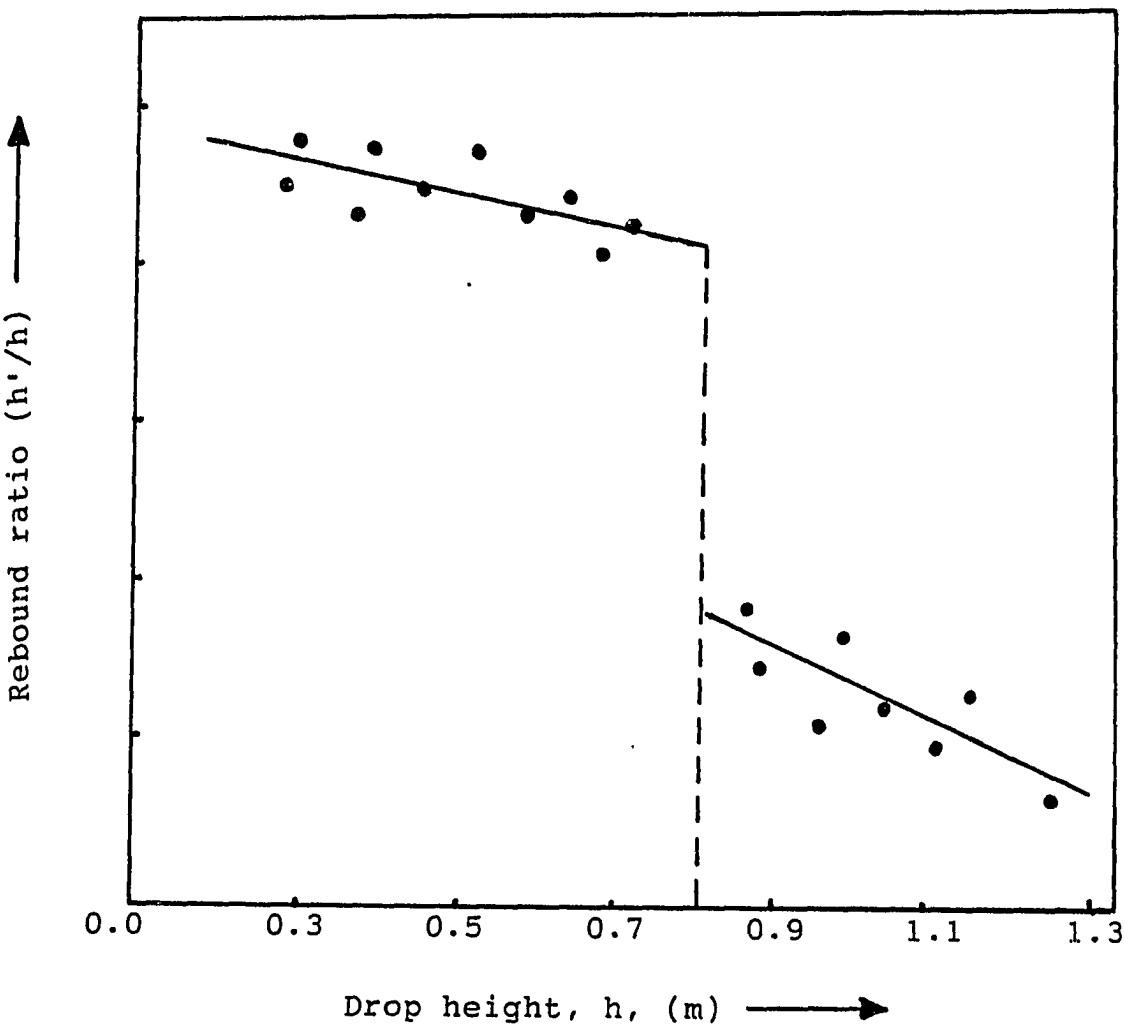

Figure 42. Suggested plot for estimating critical impact energy and stress for any rock, using the Rock Fracture Hammer (RFH)

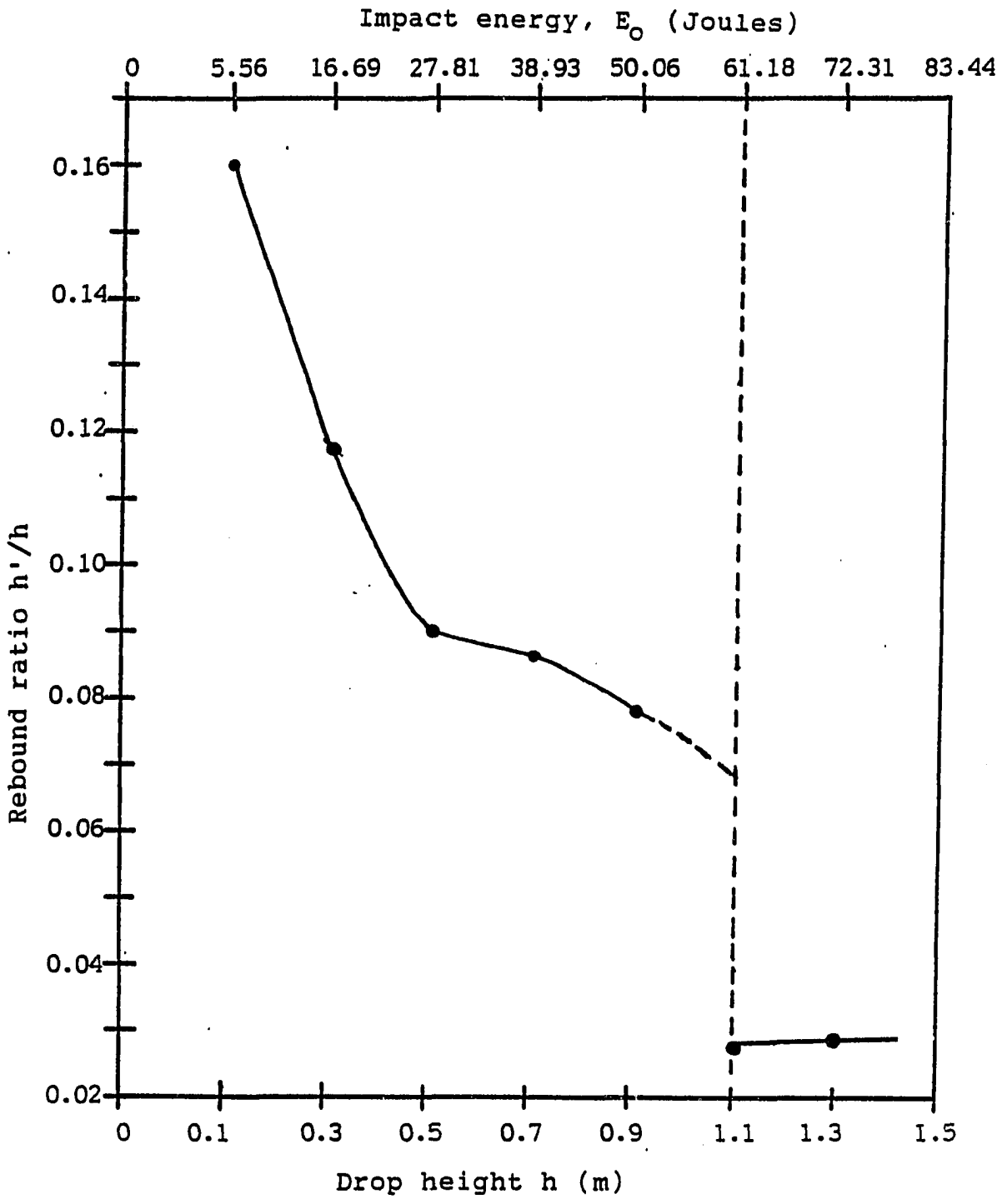

Figure 43. Recommended plot for estimating critical impact energy, Centerville Grey Limestone

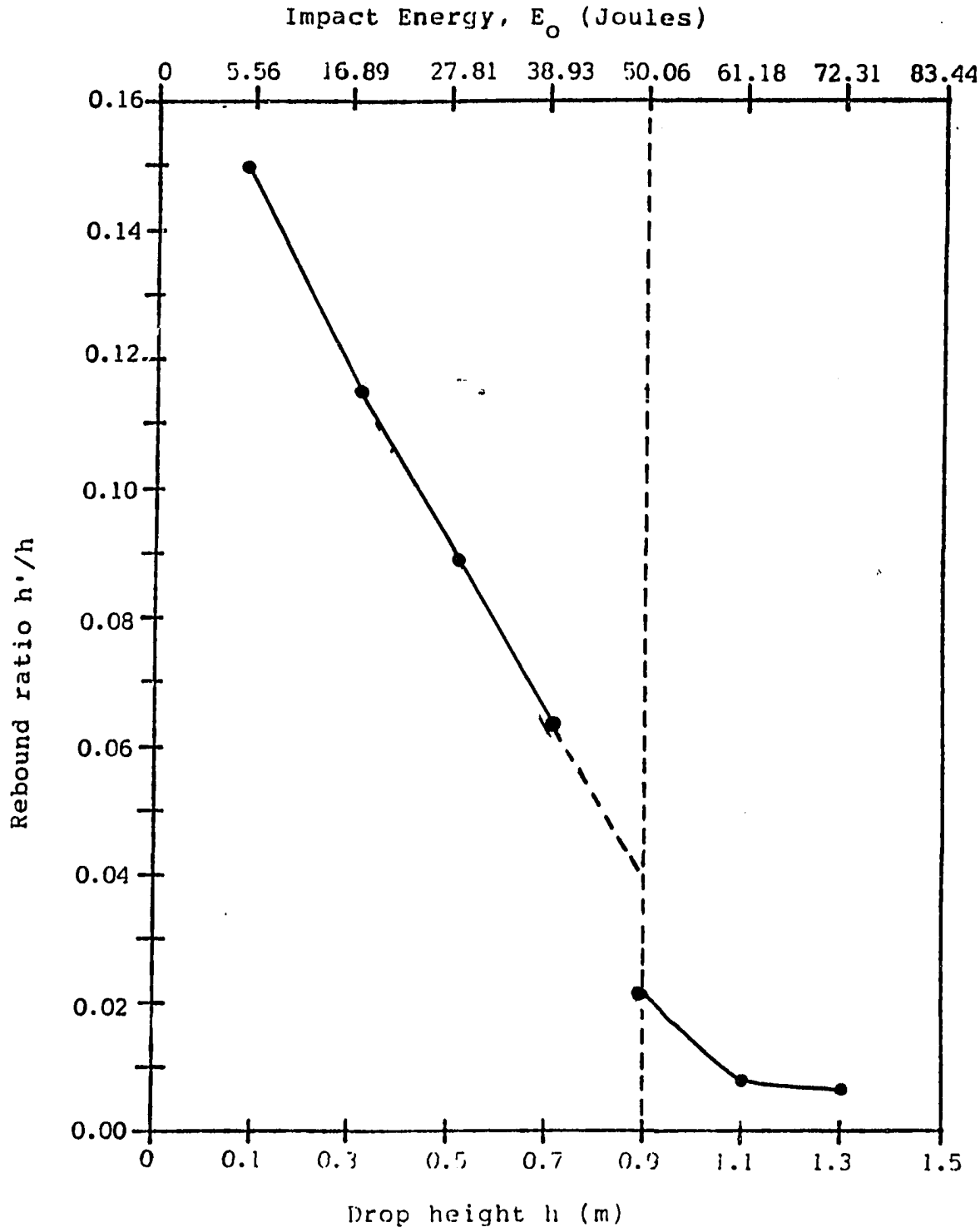

Figure 44. Recommended plot for estimating critical impact energy, Academy Black Granite

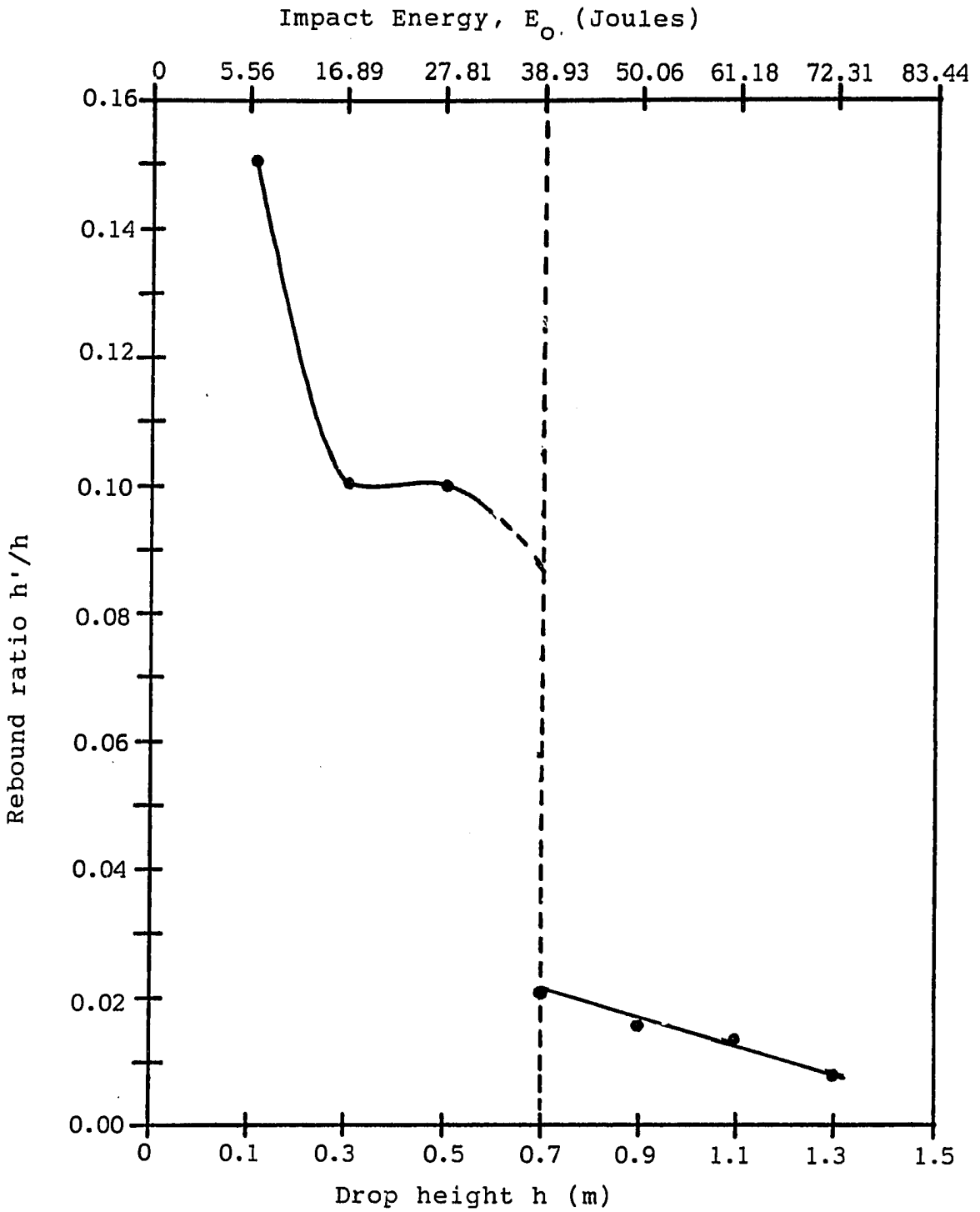

Figure 45. Recommended plot for estimating critical impact energy, Lac Du Bonnet Granite

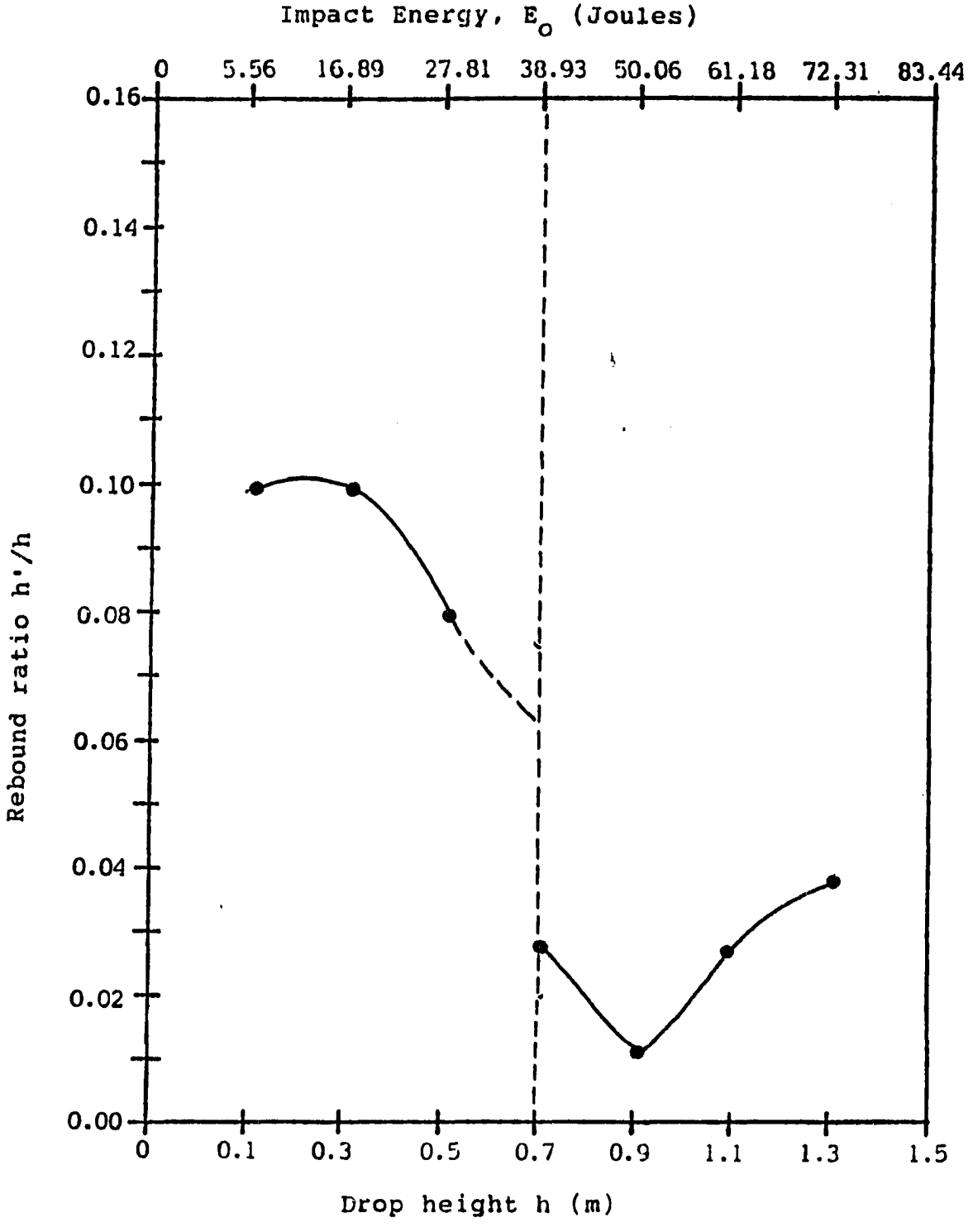

Figure 46. Recommended plot for estimating critical impact energy, Rockville Granite

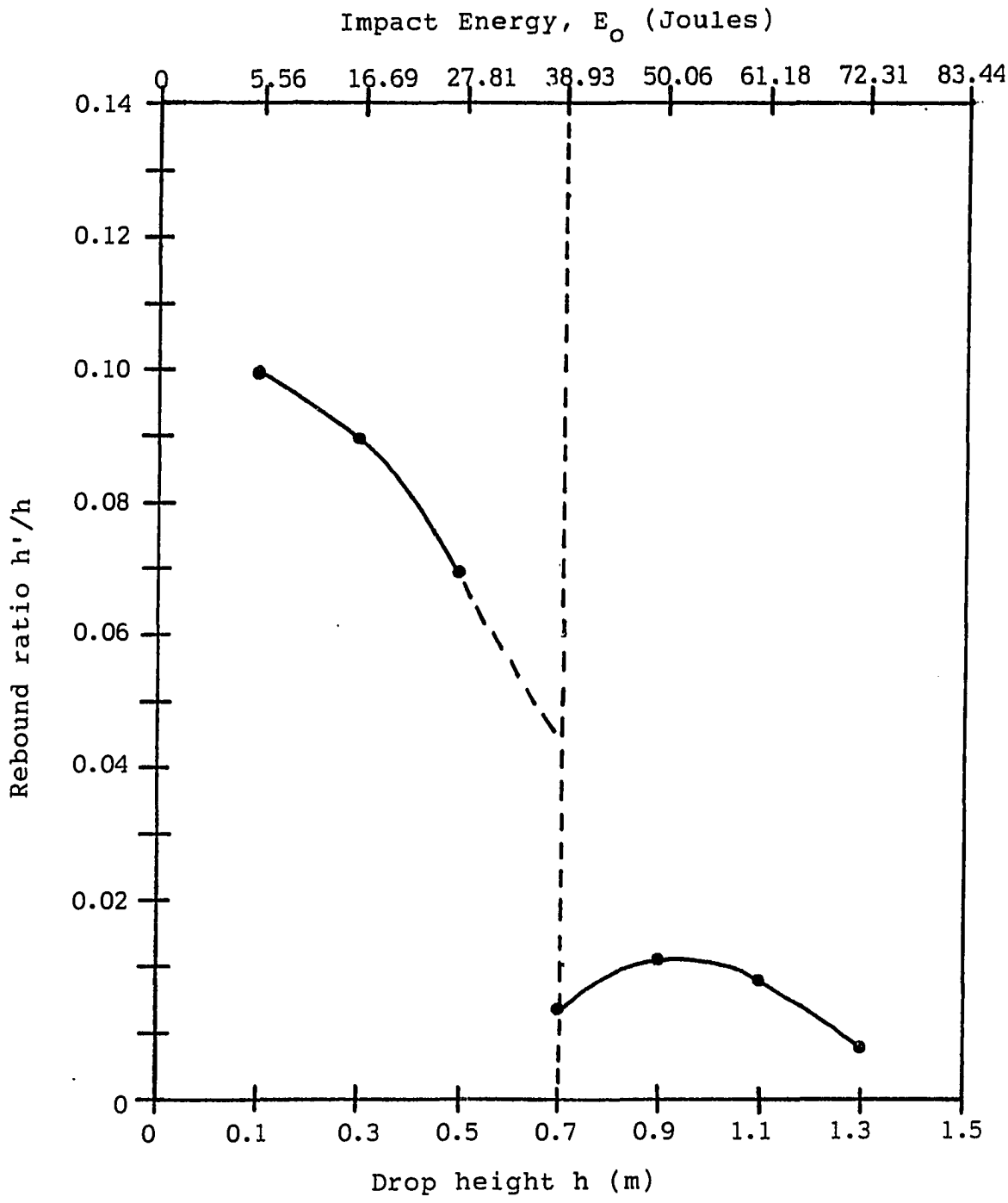

Figure 47. Recommended plot for estimating critical impact energy, Sunset Red Granite

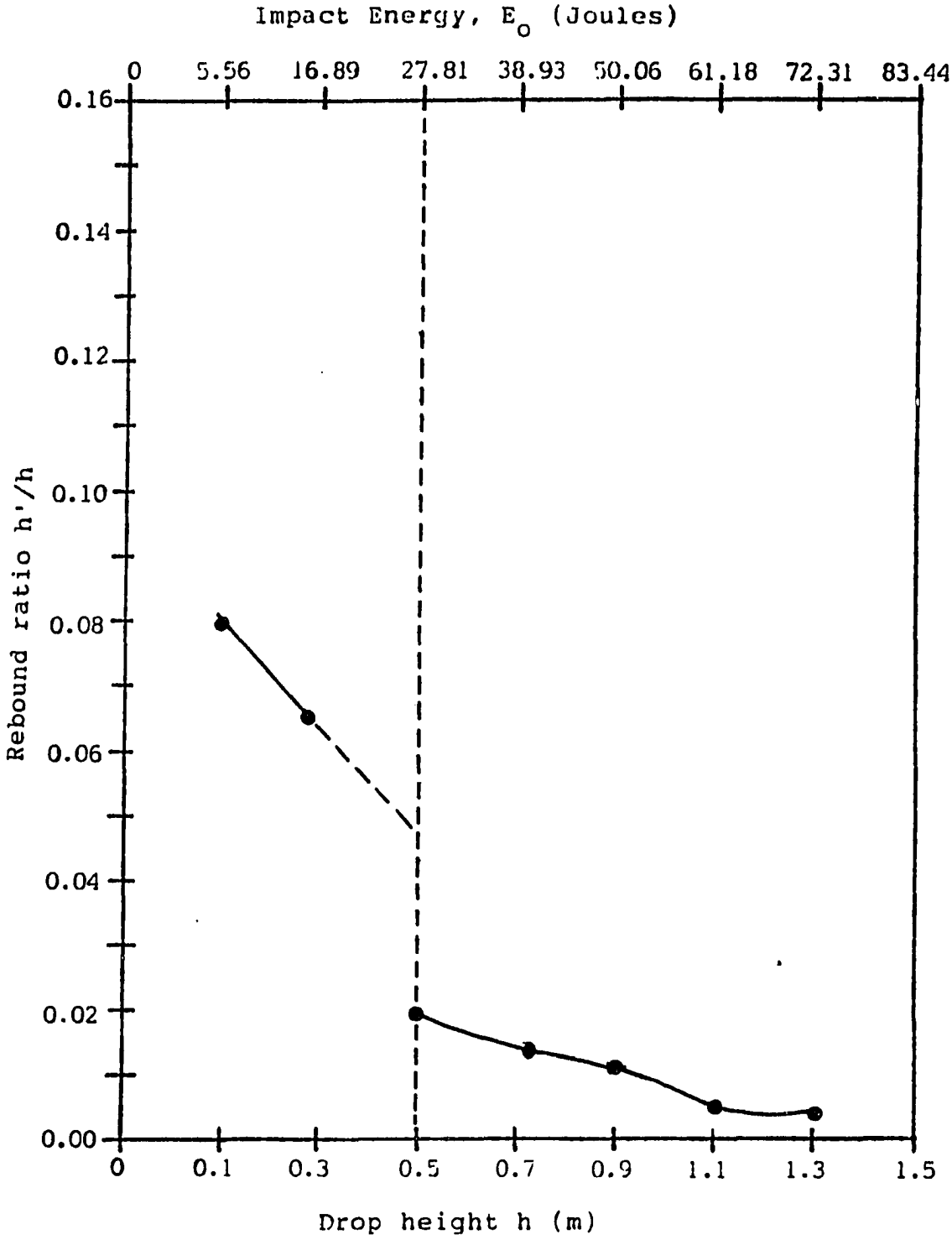

Figure 48. Recommended plot for estimating critical impact energy, Anamosa Yellow Limestone

VI. CONCLUSIONS

(a) There exists a critical impact energy corresponding to the critical impact stress for each rock, at which it fractures extensively.

(b) Single impacts at sub-critical energy levels cause predominantly elastic deformation with local crushing; deformation in the super-critical energy range is in both the fracturing and crushing modes.

(c) Estimates of the impact energy required for rock breakage differ significantly from actual measurements. Sometimes the difference is as much as 90 percent. For this reason, it is necessary to measure the impact resistance of the rock to be broken, whether in a laboratory sample or in situ. One cannot completely rely on estimates calculated from theory.

(d) When the same impact device is used, the critical impact energy for each rock is directly proportional to the square of the product of its compressive strength and brittleness ratio.

(e) The ratio of impact strength to static strength (the impulse loading factor) can be as high as 20.

(f) Test results indicate that a trencher that combines percussive loading modes with drag bit action could reduce cutting force requirements for hard rocks by as much as 70%, due to pre-fracture.

(g) The Rock Fracture Hammer (RFH) can be used in the field to measure the critical impact energy for rocks; although the percussion trencher is not yet available, this measurement would aid in selecting a suitable percussion trencher (i.e., one rated at, or slightly above, the energy level required to break a particular rock) when the trencher is built.

(h) The RFH has an advantage of over other portable rock strength measuring instruments because it can impose failure loads on rocks in situ.

(i) A bit spacing of 8 to 14 cm. can lead to interaction among sub-surface cracks caused by super-critical energy impacts on rocks.

VII. RECOMMENDATIONS FOR FURTHER STUDY

This investigation opens up a number of other possible inquiries, including rock mass classification for trenching, comparative studies of the effects of impact bit/point arrangement on drag bit cutting forces, prediction of trenching rates for trenchers, and development of a crushing index. Recommendations for further study in these areas are discussed in more detail below.

A. Rock Mass Classification for Trenching

Laboratory tests on rocks are often conducted on small core samples of intact material. Rocks decrease in strength as they increase in size, primarily because it is more probable that large strength-controlling discontinuities will be present in large-sized samples. Examples of discontinuities found in rocks are cracks, bedding planes, weak grain boundaries or faults. These discontinuities are a plausible explanation for the often observed disparity between laboratory and field specific energies in rock excavation.

A weakness of laboratory methods is the inability to evaluate synergistic effects of discontinuity properties and moisture conditions found in the field. Since laboratory strength values do not give a complete picture of rock strength, it follows that they should not be

regarded as the sole index of rock mass strength. Thus, there exists a challenge to characterize the rock mass with a single numerical index that accounts for significant rock mass properties. In such an index, these properties must be weighted to incorporate their relative importance to overall rock mass strength.

At present, there exists no suitable system of classifying rock masses for trenching purposes. Analysis of the three main rock mass classification systems (Table 20) shows that they rate parameters that are irrelevant to trenching and/or ignore relevant parameters. Therefore, the need exists to develop a classification system suitable for trenching. Such a scheme would gain widespread acceptance after field validation. When combined with the test results presented herein and the proposition on `intact' rock strength, it would be possible to select candidate rocks for either rotary or percussive trenching.

B. Comparative Studies of the Effects of Impact Bit/Point Arrangement on Drag Bit Cutting Forces

As explained in Chapter V, Section C, and illustrated in Figure 41, three possibilities exist with respect to the arrangement of impact bits relative to drag bit locations on the boom of the proposed percussion trencher. These options are colinear, intermediate, and staggered arrangements. The

Table 20. Deficiencies of the three major rock classification systems as regards their applicability to mechanical rock trenching

	PARAMETER	RSR System (Wickham et al 1972)	GEOMECH. System (RMR) (Bieniawski1973)	Q-System (Barton et al 1974)	RELEVANCE OF PARAMETER TO MECHANICAL TRENCHING OF ROCKS
	Purpose	Tunneling	Tunneling, Mining, Slopes, Foundations	Tunneling, Chambers	
1	Shape/dimension of cross section of excavated space	yes	no	no	yes
2	Stand-up time	no	no	no	no
3	Unsurpported span	no	no	no	no
4	Permanence of support	no	yes	yes	no
5	Type of support	no	yes	yes	no
6	Groundwater inflow/pressure	yes	yes	yes	yes
7	Swelling stresses	no	no	yes	no
8	Effects of change in stress	no	no	yes	no
9	Rock Quality Designation (RQD)	yes	yes	yes	yes
10	Rock brittleness	no	no	no	yes
11	Uniaxial strength	no	yes	yes	yes
12	Joint density/spacing/frequency	yes	yes	no	yes
13	Joint orientation	yes	yes	no	yes
14	Number of discontinuity sets	no	no	yes	yes
15	Degree of linkage of discontinuities	no	no	no	yes

criteria for the selection of any of the three options should be minimum cutting forces and minimum specific energy. Laboratory drag bit experiments conducted on large-sized blocks could indicate the best arrangement.

C. Prediction of Trenching Rates for Trenchers

One of the advantages of mechanical excavation over blasting is the continuity of operations. Trenching rates have a direct bearing on labor cost and hence, the cost of the entire operation. Predictive mathematical models that relate trencher characteristics, trench dimensions, and rock strength parameters to trenching rate are presently unavailable. The trial and error approach becomes the only open option. This involves taking a particular trencher to the site with the attendant probability that it may not have the capacity to trench at an economic rate. Many contractors are justifiably unwilling to adopt the trial and error approach in trencher selection. Economically, this situation implies less sales of mechanical trenchers as contractors opt for blasting.

The development of analytical relationships between trenching rate, machine power, bit characteristics, and a composite rock mass strength index would be an attempt at solving this problem. It would be simple to factor in the

effect of percussive impacts on such a rock strength index and arrive at a trenching rate for any trencher, percussive or rotary.

D. Development of a Crushing Index

Slopes of energy versus deformation curves are another area of further investigation. The recommended approach for this problem is similar to investigating the deformation pattern of rocks at various loading rates. This would give some indication about the crushing index of the rock. Growth of the crushed zone around the impact point with increasing impact energy is responsible for the slopes. Unfortunately, the slopes exhibited some variability which could not be related to the available rock strength data for the rocks used in this investigation.

VIII. REFERENCES

Appl, G. C., Rao, B. N. and Walker, B. H. "Effects of ALCL3 Additive While Cutting Granite with a Single Diamond." Industrial Diamond Reviews 41 (June, 1981): 312-318.

Barton, N., Lien, R. and Lunde, J. "Engineering Classification of Rock Masses for the Design of Tunnel Support." Rock Mech. 6, No. 4 (1974): 189-236.

Bieniawski, Z. T. "Engineering Classification of Jointed Rock Masses." Trans. South African Institution of Civil Engineers 15, No. 12 (1973): 335-344.

Birkimer, D. L. "A Possible Fracture Criterion for the Dynamic Tensile Strength of Rock." Proc. of the Twelfth U.S. Symp. on Rock Mech., University of Missouri, Rolla, Nov., 1970.

Cherepanov, G. P. and Sokolinsky, V. B. "On Fracturing of Brittle Bodies by Impact." Engineering Fracture Mechanics 4 (1972): 205-214.

Deere, D. U. and Miller, R. P. "Engineering Classification and Index Properties for Intact Rock." Technical Report No. AFWL-TR-65-116. Air Force Weapons Laboratory, New Mexico, 1966.

Dhir, R. K. and Sangha, C. M. "Rock Strength." Colliery Guardian 1 (May 1972): 252-256.

Dubugnon, O. "An Experimental Study of Water Assisted Drag Bit Cutting of Rocks." First U.S. Water Jet Symp., Lakewood, Colorado, April, 1981.

Dutta, P. K. "A Theory of Percussive Drill Bit Penetration." Int. J. Rock Mech. Min. Sci. 9 (1972): 543-567.

Dutta, P. K. "The Determination of Stress Waveforms Produced by Percussive Drill Pistons of various Geometrical Designs." Int. Rock Mech. Min. Sci. 5 (1968): 501-518.

Engelmann, W. H. , Watson, P. J., Tuzinski, P. A. and Pahlam, J. E. "Zeta Potential Control for Simultaneous Enhancement of Penetration Rates and Bit Life in Rock Drilling." U.S. Bureau of Mines R.I. 1903 (1987): 1-18.

Fairhurst, C. "Wave Mechanics of Percussive Drilling." Mine and Quarry Engineering 3 (April, 1961): 169-178.

Fischer, M. D. "Stress Pulses in Percussive Drilling." Proc. Int. Symp. on Mining Res., University of Missouri, Rolla, Missouri, Feb., 1961.

Fowell, R. J., Johnson, S. T., and Ip, C. K. "Further Studies in Water Jet Assisted Drag Tool Applications in Rock Materials." Third U.S. Water Jet Symp., Pittsburgh, Pennsylvania, May, 1985.

Furby, J. "Strain Waves in an Impact." Fluid Power Equipment in Mining, Quarrying and Tunnelling. Proc. Joint Conf. of the Inst. of Mech. Engineers, London, Feb., 1974.

Geier, J. E. and Hood, M. "Waterjet-assisted Drag Bit Cutting in Medium Strength Rock: A Fundamental Investigation." Proc. Twenty-eighth U.S. Symp. on Rock Mech., Tuscon, Arizona, June, 1987.

Gnirk, P. F. and Cheatham, J. B. "An Experimental Study of Single Bit Tooth Penetration into Rock at Confining Pressures 0-5000 psi." Trans. Am. Inst. Min. Engineers 234 (1965): 11-130.

Goldsmith, W and Wu, W. "Response of Rocks to Impact Loading by Bars with Pointed Ends." Rock Mech. 13 (1981): 157-184.

Hakalehto, K. O. "Energy Required to Break Rock by Percussive Drilling." Proc. of the Fourteenth U.S. Symp. on Rock Mech., Pennsylvania State University, University Park, Pennsylvania, 1972.

Hertz, H. "J. Reine Angew." Math. 92: 156 (full English Translation in Hertz, H., Miscellaneous Papers, MacMillan London, 1896).

Hood, M. "Cutting Strong Rock with a Drag Bit Assisted by High Pressure Water Jets." J. South Afr. Inst. of Mining and Metall. 77 (1976): 79-90.

Hucka, V. "A Rapid Method of Determining the Strength of Rocks In-Situ." Int. J. Rock Mech. Min. Sci. 2 (1965): 127-134.

Hustrulid, W. A. "Theoretical and Experimental Study of Percussive Drilling of Rock." Ph.D. Thesis. University of Minnesota, Minnesota, Dec., 1968.

Hustrulid, W. A. "Percussive Drilling of Quartzite." J. of South Afr. Inst. of Mining and Metall. 1 (1971): 245-268.

Hustrulid, W. A. and Fairhurst, C. "A Theoretical and Experimental Study of the Percussive Drilling of Rock: Part I - Theory of Percussive Drilling." Int. J. of Rock Mech. Min. Sci. 8 (1971a): 311-333.

Hustrulid, W. A. and Fairhurst, C. "A Theoretical and Experimental Study of the Percussive Drilling of Rock: Part II - Force-Penetration and Specific Energy Determinations." Int. J. of Rock Mech. Min. Sci. 8 (1971b): 335-356.

Jahn, R. "Das Drehsschiagbohren Glaucoff." Mining Journal 1 (1954): 1086-1093.

James Electronics Incorporated. Instruction Manual for Model C-4902 and Model C-4901 V-Meter. James Electronics, Inc., Chicago, Illinois, 1980.

Kabo, M., Goldsmith, W. and Sackman, J. L. "Impact and Comminution Processes in Soft and Hard Rock." Rock Mech. 9 (1977): 213-243.

Kumano, A. and Goldsmith, W. "Behavior of Diorite Under Impact by Variously-shaped Projectiles." Rock Mech. 15 (1982a): 25-40.

Kumano, A. and Goldsmith, W. "An Analytical and Experimental Investigation of the Effect of Impact on Coarse Granular Rocks." Rock Mech. 15 (1982b): 67-97.

Ladanyi, B. "Rock Failure Under Concentrated Loading." Proc. of Tenth U.S. Symp. on Rock Mech., University of Texas at Austin, Austin, Texas, May, 1968.

Larson, D. A., Morrell, R. J., and Mades, J. F. "An Investigation of Crack Propagatiion with a Wedge-Indenter to Improve Rock Fragmentation Efficiency." U.S. Bureau of Mines R.I. 9106 (1987): 1-28.

Long, V. V. "An Investigation Aimed at Improving the Efficiency of Percussive Rock Drilling." J. of South Afr. Inst. of Mining and Metall. I (Feb. 1966): 276-296.

Lundberg, B. "Efficiency of Percussive Drilling With Extension Rods." Int. J. Rock Mech. Min. Sci. and Geomech. Abstracts 24, No. 4 (1987): 213-222.

Lundquist, R. G. and Anderson, C. F. "Energetics of Percussive Drills-Longitudinal Strain Energy." U.S. Bureau of Mines R.I. 7329 (1969): 1-23.

McCarthy, D. "Percussive Drilling Economics - A Function of Productivity and Reliability." Proc. of the Fourteenth Canadian Rock Mech. Symp., Vancouver, Canada, 1982.

Miller, M. H. and Sikarskie, D. L. "On the Penetration of Rock by Three-dimensional Indentors." Int. J. Rock Mech. Min. Sci. 5 (1968): 375-398.

Morrell, R. J. and Wilson, R. J. "Toward Development of a Hard-Rock Mining Machine-Drag Cutter Experiments in Hard, Abrasive Rocks." U.S. Bureau of Mines R.I. 8784 (1983): 1-19.

Paone, J., Madson, D. and Bruse, W. E. "Drillability Studies - Laboratory Percussive Drilling." U.S. Bureau of Mines, R.I. 7300 (1969): 1-22.

Paul, B. and Sikarskie, D. L. "A Preliminary theory of Static penetration by a Rigid Wedge into a Brittle Material." AIME Trans. 232 (1965): 372-385.

Poole, R. W. and Farmer, I. W. "Consistency and Repeatability of Schmidt Hammer Rebound Data during Field Testing." Int. J. Rock [tech. Min. Sci. and Geomech. Abstracts 17 (1980): 167-171.

Rabia, H. "Specific Energy as a Criterion for Drill Performance Prediction." Int. J. Rock Mech. Min. Sci. Geomech. Abstracts 19 (1982): 39-42.

Reichmuth, D. R. "Correlation of Force - Displacement Data with Physical Properties of Rock for Percussive Drilling Systems." Proc. of the Fifth U.S. Symp. on Rock Mech., University of Minnesota, Minneapolis, May, 1963.

Rinehart, J. S. "Reaction of Rock to Impulsive Loads." Proc. of First Congress of the Int. Soc. of Rock Mech., Lisbon, Portugal, Sept., 1966.

Schmidt, R. L. "Drillability Studies - Percussive Drilling in the Field." U.S. Bureau of Mines R.I. 7684 (1972): 1-31.

Straughn, J. "High Pressure Water Jet Applications to Roadheaders." Third U.S. Water Jet Symp., Pittsburgh, Pennsylvania, May, 1985.

Street, N. and Wang, F. D. "Surface Potentials and Rock Strength." Proc. of First Int. Congress of the Int. Soc. of Rock Mech., Lisbon, Portugal, Sept. 1966.

Styler, A. M. and Thimons, E. D. "Analysis of Rock Chips Produced during Waterjet-assisted Cutting." U.S. Bureau of Mines R.I. 9073 (1987): 1-14.

Timoshenko, S. and Gooddier, A. M. Theory of Plasticity. McGraw-Hill Book Company, New York, 1954.

Tutlucglu, L., Hood, M. and Barton, C. "An Investigation of the Mechanisms of Water Jet Assistance on the Rock Cutting Process." Proc. of the Twenty-Fourth U.S. Symp. on Rock Mech., Texas A and M University, College Station, Texas, June, 1983.

Unger, H. F. and Fumanti, R. R. "Percussive Drilling with Independent Rotation." U.S. Bureau of Mines R.I. 7692 (1972) 1-21.

Westwood, A. R. C. "Environment-enhanced Disintegration of Hard Rocks." Conf. on Research in Excavation Technology, Vail, Colorado, Oct., 1975.

Wickham, G. E. , Tiedeman, H. R. and Skinner, E. H. "Ground Support Prediction Model (RSR Concept)." Proc. of the First Rapid Excavation, Tunneling Conf., AIME, New York, NY 1972.

IX. APPENDIX: IMPACT STRESS AND IMPACT ENERGY ESTIMATION EQUATIONS

A. Impact Stress

Percussive drilling investigations (Lundquist and Anderson, 1969, and Furby, 1974) have indicated that when a drop hammer hits a rock surface directly, the maximum stress developed is given by

$$\sigma_p = (E/c)V_f \qquad \text{(A-1)}$$

where

σ_p = peak stress developed

E = modulus of elasticity of the hammer

c = sonic wave velocity through hammer

V_f = hammer impact velocity

From basic principles of dynamics

$$V_f = (V_o^2 + 2ah)^{0.5} \qquad \text{(A-2)}$$

where

V_o = initial velocity of hammer

a = acceleration of hammer

h = drop height of hammer

In this investigation, the hammer starts its fall from a rest position, therefore, $V_o = 0$. Consequently,

$$V_f = (2ah)^{0.5} \qquad \text{(A-3)}$$

Substituting for V_f in equation (A-1) with equation (A-3),

$$\sigma_p = (E/c)(2ah)^{0.5} \qquad \text{(A-4)}$$

In the configuration used in this research, the hammer does not hit the rock directly. As shown in Figure 5, the hammer hits the bit holder, at the bottom of which is attached a sphero-conical carbide-tipped impact bit. Previous investigations (Fairhurst 1961, Hustrulid 1968, 1971, Hustrulid and Fairhurst 1971) have indicated that the peak stress does not develop instantaneously since the condition at the bit end varies from a free end state initially to a fixed end state subsequently. Furthermore, the stress decays exponentially with time.

In this analysis, it is assumed that there is a perfect match between the hammer and the drill bit holder. At any neck in the drill bit holder as shown in Figure 6, the initially developed stress assumes a new magnitude due to reflections and change in cross-sectional area. At the two necks in the drill bit holder, appropriate stress transmission factors, T_1 and T_2, are applied to initial stresses to estimate the new stress levels. Therefore, following results of theoretical and experimental work by Dutta (1968) and with reference to Figure 6,

$$T_1 = 2D_1^2/(D_1^2 + D_3^2) \qquad \text{(A-5)}$$

$$T_2 = 2D_2^2/(D_2^2 + D_3^2) \qquad \text{(A-6)}$$

where

T_1 = transmission factor applicable to stress wave movement from region 1 to region 2

T_2 = transmission factor applicable to stress wave movement from region 2 to region 3

D_1 = diameter of region 1

D_2 = diameter of region 2

D_3 = diameter of region 3

For the Rock Fracture Hammer (RFH), D_1 = 10.2 cm (4 in.), D_2 = 5.08 cm (2 in.), and D_3 = 2 cm (0.76 in.). Substituting these values into equations (A-5) and (A-6),

$T_1 = 1.60$

$T_2 = 1.75$

The maximum impact stress that reaches the impact bit can then be estimated by applying these transmission factors to equation (A-4). It should be noted that the stress developed statically between the impact bit and the rock surface is negligible and hence, is not considered in this estimation.

$$\sigma_m = T_1 T_2 (E/c)(2ah)^{0.5} \qquad \text{(A-7)}$$

where

σ_m = maximum stress developed at the impact bit

T_1, T_2, E, c, a, and h are as defined earlier.

The results of drop tests shown in Figure 7 conducted with the Rock Fracture Hammer (RFH) indicate that the

hammer reaches an acceleration of 9.81 m/s^2, which is the value of gravitational acceleration. Furthermore, for the steel used in building this device, c = 5100 m/s, $E = 2.07 \times 10^{11}$ N/m^2. Therefore,

$$\sigma_m = (1.6)(1.75)(2.07 \times 10^{11})(5100)^{-1}(2)(9.81)(h)^{0.5}$$

$$\sigma_m = 5.034 \times 10^{8} h^{0.5} \qquad \text{(A-8)}$$

When σ_m has MPa units and h is in meters, equation (A-9) can be used to estimate impact stress for any drop height. (Note that 1 MPa = 145 psi, and 1 m = 3.2808 ft.)

$$\sigma_m = 503.4 h^{0.5} \qquad \text{(A-9)}$$

Computations of σ_m for various drop heights, h, using equation (A-9) are shown in Table 2. In addition, σ_m can be read off directly for each drop height on Figure 8.

B. Impact Energy

The impact energy considered is the kinetic energy delivered to the top of the bit holder. From basic principles of dynamics,

$$E_o = 0.5 m V_f^2 \qquad \text{(A-10)}$$

where

E_o = impact energy delivered

m = mass of the impact hammer

V_f = velocity of hammer just before impact

Since the hammer is falling from a rest position, equation

(A-3) applies again. Therefore,

$$E_o = 0.5mah \qquad \text{(A-11)}$$

The hammer has a mass of 11.34 kg (25 lb). Substituting for m and a in equation (A-11), E_o can be directly calculated for each drop height, h.

$$E_o = (0.5)(11.34)(9.81)h$$

$$E_o = 55.62h \qquad \text{(A-12)}$$

It should be noted that E_o is in N.m (Joules) and h is in meters. (Note that 1 Joule = 0.738 ft.lb. force.) Computations of E_o for various h values are shown in Table 2. Figure 8 can also be used to read off E_o values directly for given values of h.

C. Relationship between Impact Stress and Impact Energy

From equation (A-11),

$$h = E_o/0.5ma \qquad \text{(A-13)}$$

From equation (A-7),

$$h = \sigma_m^2/T_1^2T_2^2 \ (E/c)^2 \ 2a \qquad \text{(A-14)}$$

Equating equations (A-13) and (A-14),

$$E_o/0.5 \ ma = \sigma_m^2/T_1^2T_2^2 \ (E/c)^2/m)^{0.5} \qquad \text{(A-15)}$$

$$\sigma_m = (4E_o \ T_1^2T_2^2 \ (E/c)^2/m)^{0.5} \qquad \text{(A-16)}$$

$$E_o = 0.5\sigma_m^2 ma/R_1^2 T_2^2 (E/c)^2 \; 2a \qquad \text{(A-17)}$$

$$E_o = \sigma_m^2 m/4T_1^2 T_2^2 (E/c)^2 \qquad \text{(A-18)}$$

When σ_m is in MPa and E_o is in Joules, substituting in T_1, T_2, m, E, and c values quoted earlier,

$$\sigma_m = 67.5\ E_o^{0.5} \qquad \text{(A-19)}$$

$$E_o = \sigma_m^2/4646.25 \qquad \text{(A-20)}$$